Synthesis and Characterization of Polymeric Sensing Materials for Detection of Gases in Energy Storage Devices

by

Shahrzad Ghodrati

A thesis

presented to the University of Waterloo

in fulfillment of the

thesis requirement for the degree of

Master of Applied Science

in

Chemical Engineering

Waterloo, Ontario, Canada, 2024

Author’s Declaration

I hereby declare that I am the sole author of this thesis. This is a true copy of the thesis, including any required final revisions, as accepted by my examiners.

I understand that my thesis may be made electronically available to the public.

Abstract

The increasing popularity of portable electronic devices, electric vehicles, and smart grids has created a need for energy storage systems including battery technology with lithium-ion batteries (LIBs) being one of the most common battery types. However, enhancing the safety of these LIBs remains a prominent aspect that requires advancements in battery technology as it has been shown that gas evolution occurs in LIBs. The identification and detection of these gases (which can be hazardous in different ways) are critical to protecting human and environmental health. Hence, there is an urgent need for gas-sensing devices (i.e., gas sensors) to minimize concerns regarding health, safety, and the environment.

This thesis presents an investigation on the design, evaluation, and characterization of polymeric gas sensing materials for the room-temperature detection of harmful gases (in ppm levels) generated in energy storage devices (e.g., lithium-ion batteries). The importance of gas sensing materials is well recognized as the sensing material is the ‘heart’ of a sensor that interacts with the target analyte, leading to a detection signal generated by the sensor. Four gases, namely, hydrogen (H_2), ethylene (C_2H_4), carbon monoxide (CO), and carbon dioxide (CO_2), were found to be the main gases released in LIBs and identified as target gases for detection.

Polymers modified/doped with metal oxides have displayed reasonable sensing behavior making them promising sensing materials in gas sensor applications. Polyaniline (PANI) doped with various concentrations of different metal oxide nanoparticles were synthesized and evaluated as sensing materials for target analytes, along with other polymeric materials like polypyrrole (PPy), polythiophene (PTh), and polyvinylpyrrolidone (PVP). Gas sorption characteristics were evaluated using formaldehyde as a "simulant" or "surrogate" due to safety concerns associated with testing target analytes in an academic environment.

The doped PANI materials, in particular, exhibited enhanced gas sorption properties, attributed to the synergistic effects of the dopants, which improved the interaction between the polymer matrix and gas molecules.

The effect of environmental factors (e.g., aging), on the sensing performance, related to the sensing material stability, was also evaluated for selected sensing materials. Other property characteristics of the sensing materials were also determined using different techniques such as scanning electron microscopy (SEM), transmission electron microscopy (TEM), energy dispersive X-rays (EDX), dynamic light scattering (DLS), and Brunauer-Emmett-Teller (BET) tests, to provide a more detailed explanation and additional confirmation of the sorption trends.

In the final step, optimal sensing materials were deposited on a MEMS (micro-electro-mechanical system) sensor, which is efficient, inexpensive, and of small size. The sensor as a whole was then evaluated for its sensing performance towards 50 ppm ethylene.

Acknowledgments

I am deeply grateful to my supervisor, Professor Alexander Penlidis, for his invaluable support and guidance throughout my MASc studies. His dedication to both my technical and personal growth has been truly inspiring and went far beyond my expectations. I always looked forward to our insightful discussions, which were not only technically/professionally enriching but also a source of inspiration that extended into various dimensions of my life. I feel very fortunate to have had his mentorship and supervision.

I would also like to express my heartfelt appreciation to Bhoomi Mavani, a senior PhD candidate in our group, who has generously shared her expertise and experience with me. Bhoomi's training helped me get on board with experimental work in the lab. Her patient responses to my countless questions and her mentorship have greatly enhanced my practical skills and understanding of our field.

I am thankful to Professor Eihab Abdel-Rahman and his PhD candidate, Yasser Shama, for their collaborations with the MEMS sensor testing. I also thank Professor Mekonnen for allowing the use of dynamic light scattering instrument in their lab. I am also grateful to Dr. Lena Ahmadi for her valuable advice at the onset of my research journey.

I am immensely grateful to my parents, Parviz and Rita, for their unwavering support. Their endless love and encouragement have been the source of strength through all the challenges and triumphs of this journey. I also extend my sincere thanks to my brothers, Afshin, Ashkan, and Ardalan, for their unrelenting support. Finally, a heartfelt thanks to all my friends, with a special mention to my lifelong friend, Niusha Shahbeik, for always being there for me.

Table of Contents

List of Figures

List of Tables

Chapter 1: Motivation, Objectives and Outline

1.1 Research Motivation and Objectives

Energy storage devices include fuel cells and batteries. Especially these days, lithium-ion batteries (LIBs) are becoming increasingly popular. They have high specific capacity and energy and promise a sufficiently long service life. Their widespread applications range from small-format batteries used in smartphones and e-notebooks, to large-format batteries used in electric vehicles and airplanes [1]. However, gas evolution during their cycling may pose a problem to safety because some gases released in lithium-ion batteries are flammable and might become an explosion hazard (such explosions have been reported in the press and literature [2], [3]). Therefore, there is an urgent need for the development of highly sensitive, selective, and stable gas sensors (and sensing materials) that can detect parts per million (ppm) levels of harmful gas concentrations. It has been shown that the largest portion of released gases in lithium-ion batteries consists of ethylene (C_2H_4), hydrogen (H_2), carbon dioxide (CO_2), carbon monoxide (CO), methane (CH_4), and ethane (C_2H_6) [1].

Hence, the objectives of this thesis are to indicate the most promising sensing materials after a comprehensive sweep of the literature, and subsequently synthesize such materials for testing and characterization. Testing and evaluation of sorption properties of these materials will take place using a simulant/surrogate gas, like formaldehyde, due to flammability and explosion concerns (safety concerns, in general, in a typical academic laboratory dealing with and storing hydrogen or ethylene, etc. cylinders). Characterization of properties of such materials will try to evaluate the most promising of these sensing materials, which can then be deposited on actual miniature MEMS (Micro-Electro-Mechanical Systems) sensors, which are efficient, inexpensive and are based on polymeric sensing materials (doped or undoped) operating at ambient conditions, as opposed to metal oxide (MO) sensors that currently exist but operate at elevated temperatures (150-500°C).

1.2 Thesis Outline

The first chapter serves as an introductory section to this thesis, outlining the research motivation and objectives. Furthermore, it provides an overview of the content that will be discussed in the following chapters.

The second chapter provides a comprehensive overview of the relevant literature background. The chapter starts with a discussion about the mechanisms of gas evolution in LIBs. Then, it delves into the topic of gas sensors, focusing on sensing materials that have been used in the literature for sensing the gas analytes of H_2, C_2H_4, CO_2, and CO. Furthermore, the chapter discusses important sensing characteristics, such as sensitivity and selectivity, along with different types of sensors.

The third chapter explains the experimental methodology from synthesis to sorption studies and characterization of the sensing materials. The chapter ends with a brief discussion of the experimental set-up used for evaluating sensing materials with the actual MEMS sensor (the final evaluation with the MEMS sensor was performed by our collaborating group in the Systems Design Engineering Department of the University of Waterloo, Professor Eihab Abdel-Rahman's laboratory).

Chapter 4 contains experimental results from gas sorption studies performed using a specialized test set-up including a sensitive gas chromatograph (GC). The results were analyzed using various methods of statistical analysis. The polymeric sensing materials were evaluated and compared for their sensitivity. In addition, this chapter contains the characterization results of the polymeric sensing materials in which an attempt was made to corroborate the sorption trends observed earlier with the results obtained from different characterization tests. The chapter wraps up with a brief discussion about the results of testing an actual MEMS sensor with ethylene, followed by an explanation of possible sensing mechanisms for detecting analytes.

Finally, Chapter 5 summarizes the concluding remarks, identifies the main contributions of this work, and includes (short- and long-term) recommendations for future work. Chapter 5 is followed

by the ‘Letters of Copyright Permission’ section, which includes the obtained copyright licenses and permissions for reproducing figures (obtained from the literature) throughout this thesis.

In addition, five technical appendices (A to E) at the end of this thesis provide additional (complementary) information. Appendices include extensive summary tables for sensing materials reported in the literature, a list of sensing materials evaluated in sorption studies, statistical analysis, and related equations and sample calculations.

Chapter 2: Literature Background

2.1 Energy Storage Devices

The rapid worldwide transition towards renewable energy is intensifying in response to environmental concerns (greenhouse gases, CO_2 emissions, etc.). Renewable energy systems have the potential to generate energy without emitting greenhouse gases, however, their reliance on unpredictable natural resources such as wind, sunlight, etc. results in intermittency and fluctuations. In other words, energy generation in these systems is dependent on weather, season, and daytime. To address this limitation, energy storage systems (ESSs) are recognized as the most pragmatic and effective approach which can store energy for consistent and controlled use in the future, thus ensuring proper energy management and preventing energy wastage [4].

ESSs gather energy from different sources, then transform and store it for later use in various applications. ESSs can be classified into five major categories based on the form of energy stored, namely, chemical, electrochemical, mechanical, electrical, and thermal energy storage. The most popular energy storage is electrochemical energy storage (EcES) with batteries as the key components. Among different battery types, lithium-ion batteries (LIBs) are extensively utilized in the electronics and transportation sectors (e.g., electrical vehicles) due to their superior charge density compared to other types of rechargeable batteries. However, lithium-ion batteries also involve the risk of bursting, among different safety risks, because of flammable and hazardous gases found in them [4].

2.2 Gas Evolution Mechanisms in LIBs

Reaction mechanisms occurring in lithium-ion batteries can be categorized into two groups. One group consists of reduction reactions occurring at the anode (negative electrode) which primarily result in the evolution of C_2H_4, H_2, and CO. The other group is oxidation reactions occurring at the cathode (positive electrode) which are responsible for CO_2 and CO evolution. Figure 2.1 shows a schematic overview of some commonly evolved gases (C_2H_4, CO, CO_2, and H_2) and their origin in lithium-ion batteries (LIBs).

Li-ion batteries have liquid electrolytes, a negative electrode (anode), and a positive electrode (cathode). The most common material used for the anode is graphite, and nickel manganese cobalt oxides (NMC) are one of the materials of interest for the cathode [5]. The liquid electrolytes are made of Li salt, an organic carbonate solvent, and different additives. One of the commonly used electrolyte solvents is ethylene carbonate (EC) which is known to decompose at the anode. The products of decomposition reactions become constituents of a solid electrolyte interface (SEI) formed on the anode [6]. One of the primary 'gassing' mechanisms is electrolyte reduction which results in the production of ethylene. Three reaction pathways have been proposed for ethylene evolution. Reactions 1 and 2 show ethylene evolution as a result of EC reduction, whereas reaction 3 shows ethylene evolution as a consequence of SEI decomposition [1].

$$2Li^+ + 2e^- + C_3H_4O_3(EC) \rightarrow C_2H_4 + Li_2CO_3 \quad (1)$$

$$2Li^+ + 2e^- + 2C_3H_4O_3(EC) \rightarrow C_2H_4 + (CH_2OCO_2Li)_2 \quad (2)$$

$$2Li + (CH_2OCO_2Li)_2 \rightarrow C_2H_4 + 2Li_2CO_3 \quad (3)$$

Another source of gas evolution caused by a reduction reaction on the anode is cell contaminants. The main contaminant in LIBs is water. Water contained in a battery electrolyte or insufficient drying can be two sources of water contamination (residual moisture) in LIBs. It is proposed that the reduction of water results in hydrogen release as shown in reaction 4 [5].

$$H_2O + e^- \rightarrow OH^- + \frac{1}{2}H_2 \quad (4)$$

The mechanisms of CO_2 and CO evolution in LIBs have also been investigated in earlier studies. It was shown that two reactions occurring at voltages higher than 4.0 V on the cathode are responsible for CO_2 generation. One proposed reaction is the oxidation of lithium carbonate (Li_2CO_3) on the cathode (reaction 5), which also leads to producing singlet oxygen. The other one is the electrolyte decomposition (oxidation of EC) shown in reaction 6, which also leads to CO evolution [5].

$$2Li_2CO_3 \rightarrow 4Li^+ + e^- + 2CO_2 + O_2^1 \quad (5)$$

$$2O_2^1 + C_3H_4O_3(EC) \rightarrow 2CO_2 + CO + H_2O \quad (6)$$

Another reaction pathway related to CO evolution, which occurs at the anode, has been proposed in the literature. Electrolyte (EC) decomposition at the anode may also lead to CO evolution (as per reaction 7) [5].

$$2Li^+ + 2e^- + C_3H_4O_3(EC) \rightarrow CO + (CH_2OLi)_2 \quad (7)$$

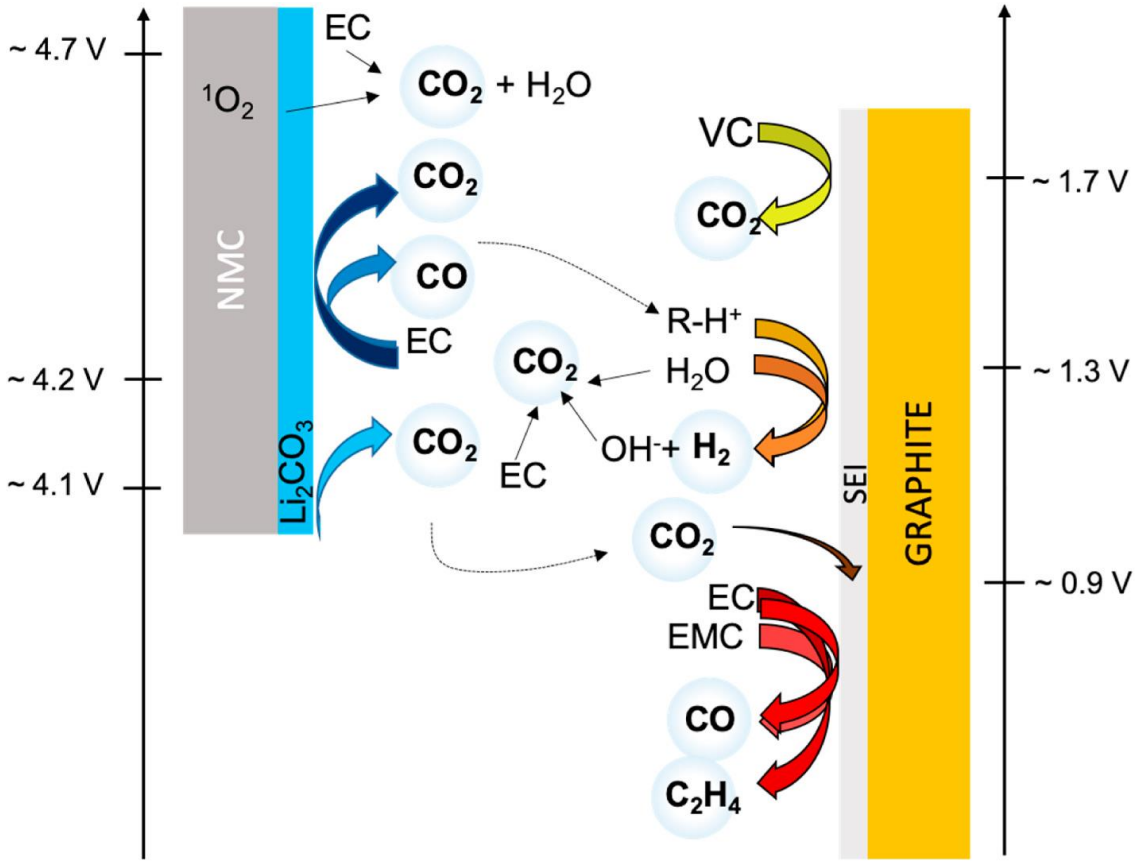

Figure 2.1: Schematic overview and proposed reactions for gas evolution observed in LIB. Reproduced with permission from [7].

2.3 Sensing Performance Characteristics

The performance of gas sensors can be evaluated based on important performance characteristics such as sensitivity, selectivity, and stability (sometimes referred to as three Ss), among which sensitivity is the most widely studied. Other sensing characteristics include operation temperature, detection range and limit of detection (LOD), response time and recovery time.

Sensitivity refers to the minimum detectable concentration of an analyte that a sensor or sensing material can detect. The sensitivity of a sensor increases as its ability to detect lower concentrations improves. In essence, sensitivity can be defined as a variation in response to a specific concentration of the target gas. In this thesis, sensitivity is evaluated based on the amount of gas sorption observed when a polymeric sensing material is exposed to the target gas. The higher the sorption amount is, the more sensitive the sensing material. Sorption is calculated by taking the difference between the total gas concentration in the source (baseline) and the residual gas concentration after the target gas comes into contact with a sensing material. Subsequently, sensitivity can be defined as the following (equation 8):

$$Sensitivity = \frac{(total\ gas\ concentration) - (residual\ gas\ concentration)}{(total\ gas\ concentration)} \qquad (8)$$

Selectivity refers to a sensing material's preference for a specific analyte over other gases in a mixture. Selectivity studies are important because the target analyte may come into contact with a sensing material while existing in a mixture of other gases, therefore, the presence of other gas(es) may interfere with detection of the target gas. A sensing material can be considered selective when the signal generated by the target analyte is significantly greater than the signal generated by an interfering substance. Selectivity can be measured by taking the ratio between the sorption amount of the target analyte and sorption value of interferent gases when a sensing material is exposed to a mixture of two or more gases. Note that selectivity is better when the ratio between the sorption of the target gas and that of an interferent gas is larger.

Stability is the other important characteristic of a sensing material which studies effectiveness of a sensing material with respect to different aspects (usually related to environmental effects) such as aging, temperature, humidity, etc. It is important for a sensing material to exhibit a relatively consistent and reproducible signal over a long-enough period or with varying environmental conditions because this is what determines how reusable a sensing material is.

This thesis is concerned with evaluating sensitivity and aging (stability characteristic) on sensing materials. Since sorption studies were conducted with only one gas analyte, only sensitivity and aging were investigated. This was so because the emphasis in the thesis was on testing different polymeric sensing materials; a parallel PhD study is investigating more details on selectivity.

2.4 Sensing of Hydrogen

Hydrogen (H_2) gas is colorless, odorless, tasteless, and highly flammable under normal conditions when released in air. It is flammable over a wide range of 4-75 vol% in air [8]. Hydrogen is a clean combustible energy source, and it is used as a fuel source in a variety of industries, including nuclear, fuel cell, petrochemical, automobile, and space. However, the explosive nature of hydrogen gas restricts its applications and causes safety concerns during its production, storage, transportation, and application process in case of any leakage. Therefore, development of highly sensitive, selective, and stable H_2 sensors is of great importance [9]. Various methods and materials for H_2 sensing have been studied in the literature. In the following paragraphs, a literature review of relatively recent studies related to this topic is presented.

Pippara et al. [10] reported the fabrication of a nanohybrid film based on tin oxide (SnO_2) nanosheets and polyaniline (PANI) doped with Pd for hydrogen sensing at room temperature and varying ppm levels of gas ranging from 50 to 400. A hydrothermal synthesis technique was used to prepare the films and interactions of H_2 gas molecules with SnO_2, SnO_2-Pd, PANI, PANI-SnO_2, and PANI-SnO_2-Pd nanocomposite were theoretically studied by density functional theory (DFT) calculations. Comparison between different films showed that SnO_2/Pd exhibited the highest sensitivity (540%) at 4000 ppm (0.4%) of H_2. However, the composite film of PANI-SnO_2-Pd

showed the highest performance factor, which was defined as the ratio of sensitivity to total cycle time, where total cycle time is the summation of response time and recovery time.

Arora et al. [9] developed a H_2 sensor based on PdO-PANI/indium tin oxide (ITO) film to improve the sensitivity of the sensor. Composites of PdO and PANI were synthesized via in-situ wet chemical polymerization process. The composite material was then deposited on sputtered Indium Tin oxide (ITO) layer-coated glass substrate to form a PdO-PANI/ITO heterojunction. The fabricated thin film was employed as a sensing material using direct metallic electrical contacts. This eliminated the need of expensive interdigitated electrodes (IDE).

In the study [9], the sensitivity responses of pristine PANI/ITO, 5 wt.% and 10 wt.% PdO-PANI/ ITO heterostructure-based sensors were studied at room temperature and at different concentrations of 1%, 3%, 10%, 20% of H_2 (Figure 2.2). The resistance of the sensor after exposure to the target gas increases as the percentage concentration of PdO increases from 5 wt.% to 10 wt.%. This is because the 10 wt.% PdO-PANI nanocomposite creates effectively large charge carrier separation and depletion as well as an increase in the potential barrier at ITO heterojunction. The base value of resistance (R_a) is when the sensor is exposed to dry N_2, and the R_a value decreased in PdO-PANI/ITO compared to pristine PANI. This reduction can be explained by an increase in the holes concentration of a p-type nanocomposite, which reduces the Schottky barrier of heterojunction, resulting in an increase in conductivity. Moreover, it has been observed that the sensitivity of PdO-PANI nanocomposites is twice as that of pristine PANI towards 1% (10,000 ppm) H_2 gas concentration [9].

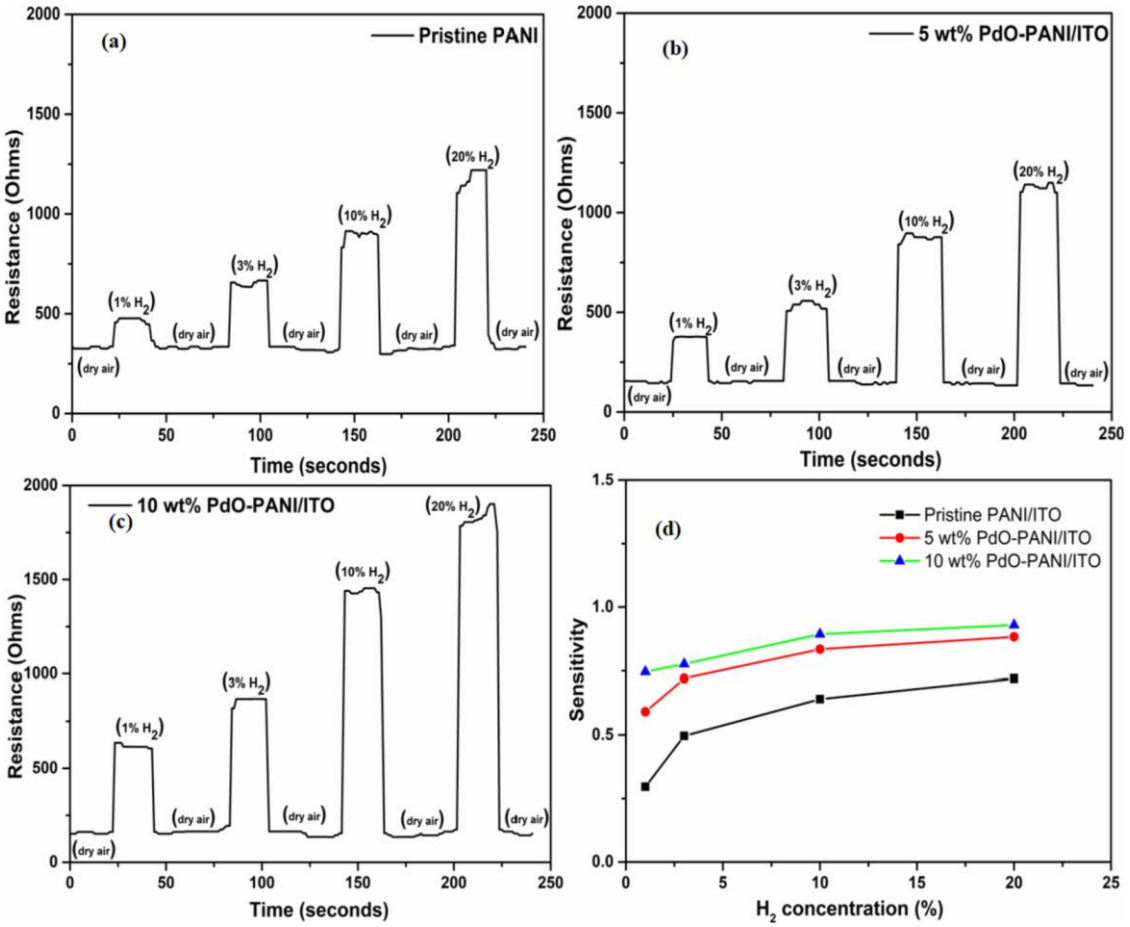

Figure 2.2: Sensing response (a) Pristine PANI/ITO, (b) 5 wt.% PdO-PANI/ITO, (c) 10 wt.% PdO-PANI/ITO and (d) Sensitivity comparison plot. Reproduced with permission from [9].

Table A1 in Appendix A summarizes recent studies on various sensing materials with possible applications as hydrogen gas sensors. Our target concentration for hydrogen is set to be in the range of 500-1000 ppm, which corresponds to 0.05%-0.1% of H_2 in the gas source. A short list of the most promising materials for detection of hydrogen is presented in Table 2.1. These materials have been selected based on our concentration range and significance of response upon exposure to hydrogen. In Table 2.1, RT stands for room temperature, and PANI for polyaniline.

Table 2.1: A shortlist of most promising sensing materials for the detection of hydrogen.

No.	Hybrid Sensing Material	Concentration (ppm)	Sensitivity/Sensing Response	Operating Temperature	Ref.
1	PANI+SnO_2+Pd	50 ppm 350 ppm	19.2% 353.7%	RT	[10]
2	PANI+SnO_2	6000 ppm	42%	30 ℃	[11]
3	PANI+SnO_2	1000 ppm	1.5	50 ℃	[12]
4	PANI+TiO_2:SnO_2	0.8% (8000 ppm)	1.25	27 ℃	[13]

Although the most promising sensing materials selected are not all in our target concentration range, they are the closest ones to our target (as reported in the literature). A few other literature publications reported hybrid polymeric materials detecting 50, 100, and 500 ppm of hydrogen, but they either work at elevated temperatures (e.g., 150-500℃) and/or include exotic (and more expensive) sensing elements such as polyvinylidene fluoride (PVDP) and carbon nanotubes, which are not in the scope of this research.

The proposed sensing mechanism in the literature is based on the formation of p-n heterojunction in SnO_2/PANI hybrid materials. PANI is a p-type molecule and SnO_2 is an n-type semiconductor. The n-type SnO_2 crystallites form a depletion region by destroying the holes of PANI molecules near the boundary. This makes the overall PANI matrix electrically more insulating. However, when the composite film is exposed to hydrogen, the H_2 molecules reach into the depletion region and act as a dielectric between the PANI and SnO_2 border. The depletion region field polarizes the hydrogen molecules, which in turn provide a positive charge to PANI molecules and become mobile upon their transfer to the central N atom of the PANI molecule. This process creates some free holes on PANI molecules, which make the composite film relatively more conducting electrically [12].

2.5 Sensing of Ethylene

Ethylene, also known as ethene, is the simplest molecule among all alkenes. It is widely used as raw material in the chemical manufacturing industry. Detection of ethylene gas finds several applications in various fields. Ethylene gas is a very important plant hormone that supports and accelerates ripening in fruits and vegetables. It is also a common pollutant released from automobile exhaust. It has recently been observed that ethylene gas is also generated and released in lithium-ion batteries. Ethylene gas is highly flammable and reactive. Moreover, it can affect the human body by creating headache, dizziness, fatigue, light-headedness, unconsciousness, and confusion. In case of breathing and skin-to-skin contact, irritation and frostbite may be caused, respectively [14]. Thus, it is important for many industries to have accurate and fast detection for ethylene to avoid the gas reaching dangerous toxic or flammability levels.

A recent review article has reported on different technologies and sensing materials for low-concentration ethylene gas detection [15]. According to this article, the most common classes of sensing materials for detection of ethylene are metal oxides. However, sensors based on metal oxides only are not always desirable since they operate at elevated temperatures. Our objective is to identify sensing materials that work at room temperature and are also relatively easy to synthesize. A short list of potential polymeric sensing materials working at room temperatures can be found in Table 2.2. The suggested sensing materials in this table have been ranked based on their limit of detection and sensitivity, i.e., sensing materials that show a larger response upon exposure to lower concentrations of ethylene come first in the table. Our target concentration for ethylene sensing is proposed to be 50 ppm or less.

Table 2.2: A shortlist of most promising sensing materials for the detection of ethylene at room temperature.

No.	Sensing Material	Concentration (ppm)	Sensitivity/Sensing Response	Sensing Range (% RH)	Ref.
1	PPy/Au nanoparticles (polypyrrole/gold)	5 ppm	1400 Hz/ppm frequency shift	0%	[16]
2	PVP/$AgBF_4$ (Polyvinylpyrrolidone/ Silver tetrafluoroborate)	7 ppm	51 Hz/ppm frequency shift	Not reported	[17]
3	PTh/ZrO_2 (polythiophene/zirconium oxide)	Not reported	9 ($\Delta I/I_0$) (Estimated value showing change in DC electrical conductivity)	~ 45%	[18]
4	PANI/MWCNT/SnO_2	10 ppm	2.42% (changes in resistance)	Not reported	[19]

Note: RH is relative humidity; MWCNT stands for multi-walled carbon nanotubes.

To the best of our knowledge, only a few studies in the literature have proposed an ethylene sensor based on a polymeric material. The majority of studies have focused on the use of metal oxides (at elevated temperatures), and some others have focused on the use of either carbon nanotubes or exotic sensing materials which conflict with our motivation to develop inexpensive and simple methods for detecting target gases.

According to a summary table in a recent review paper by Chen et al. [15], SnO_2 is one of the most common metal oxides studied in ethylene gas sensors. Therefore, one suggestion for our potential sensing material could be PANI with SnO_2. There is only one article in the literature that reports

on the use of SnO_2 with a polymer for detection of ethylene, however, multiwall carbon nanotubes (MWCNT) have also been incorporated in the hybrid sensing material to enhance the sensing performance of the sensor (case #4 in Table 2.2). Therefore, it may be proposed to remove MWCNT from the hybrid material (as to avoid exotic/expensive materials) and then study the sensing potential of the polymer and SnO_2 only.

ZnO and WO_3 are the other common metal oxides reported in the literature for sensing ethylene. In one approach, Sholehah et al. [20] reported an ethylene gas sensor using ZnO-Ag layer on a flexible PET-ITO (polyethylene terephthalate-indium tin oxide) substrate, which is the only study that reports a metal oxide-based sensor working at room temperature. In another study by Kathirvelan et al. [21], a composite of WO_3/TiO_2 has been reported for detection of ethylene. Krivec et al. [22] studied the sensitivity of two commercial ethylene sensors, one based on WO_3 and the other on SnO_2.

The first material proposed in Table 2.2 is PPy/Au nanoparticles used in Love SAW or L-SAW (surface acoustic wave) sensors in dry conditions. SAW sensors are a class of piezoelectric sensors which transduce mechanical vibrations to electrical signals. Frequency changes of the sensors have been observed towards various concentrations (2, 5, and 10 ppm) of ethylene. A negative frequency shift was observed during the exposure of L-SAW sensors to ethylene. This negative shift has been associated with the changes in the propagation path of the surface waves induced by the mass loading of the analytes at the sensing layer (PPy); mass loading refers to physical/chemical sorption of target gas molecules at the sensing layer. Overall, results suggested enhanced sensor performance for gold-modified PPy sensors compared to non-modified PPy-based sensors in dry conditions. However, it was shown that humidity negatively affects sensor response [16].

Another piezoelectric sensor has also been suggested in Table 2.2, based on a silver(I)/polymer composite on a quartz crystal microbalance (QCM). In this study [17], gas sensing properties have been investigated based again on a frequency shift. The oscillation frequency of the QCM was shown to decrease upon exposure to ethylene, which indicates an increase in the surface mass of

the crystal. Through a complexation reaction, silver ions in the composite bind with ethylene according to the following reaction:

$$C_2H_4 + Ag^+ \leftrightarrow C_2H_4 - Ag^+ \quad (9)$$

Husain et al. [18] suggested an ethylene sensor based on PTh/ZrO_2 synthesized via in-situ chemical oxidative polymerization. The variation in the DC (direct current) electrical conductivity on exposure to ethylene at room temperature (28 °C) and relative humidity of 45% was studied. PTh with 15% ZrO_2 showed the highest change in conductivity (i.e., maximum sensing response), which was about 19 times the sensing response in pristine PTh. This composite (PTh with 15% ZrO_2) also showed good selectivity over some saturated hydrocarbons such as n-hexane, dimethylbutane, and methyl pentane. In addition, stability of the samples was evaluated by comparing relative electrical conductivity versus time at different temperatures (ranging from 50 °C to 130 °C). The enhanced sensing performance of PTh/ZrO_2 nanocomposites was attributed to the interaction of lone pairs of sulfur of thiophene units with the d-orbitals of zirconium of ZrO_2.

In another study by the same authors (Husain et al.) [23], ZrO_2 was used with PPy and the sensing properties of the nanocomposite were reported for detection of ethylene at room temperature [23]. Similarly, the sensing response was calculated based on the change in DC electrical conductivity, and PPy with 20% ZrO_2 showed the best sensing properties. It was also observed that the sample could not regain its original conductivity after removing ethylene, however, the conductivity reached its original value after heating at 80 °C.

Appendix B summarizes additional recent studies on various sensing materials with possible applications as ethylene gas sensors.

2.6 Sensing of Carbon Oxides (CO_2 and CO)

Carbon dioxide (CO_2) is one of the greenhouse gases, which is odorless and colorless. It is released into the atmosphere from several sources such as combustion of fossil fuels, burning of trees, and

industrial processes. It is reported that exposure to CO_2 can cause health problems if its concentration is above 5000 ppm [8]. On the other hand, there is carbon monoxide (CO) which is produced by the incomplete combustion of fuels. CO is another odorless and colorless toxic gas, which can cause nausea, dizziness, headache, vomiting and unconsciousness at exposure levels much lower than CO_2 (the threshold limit value (TLV) for CO is 25 ppm) [24]. It has been shown that both CO_2 and CO are among the gases evolving in lithium-ion batteries, therefore causing safety concerns about the usage of lithium-ion batteries [1], [25][26][27]. This creates the need for developing gas sensors that can detect ppm levels of these gases.

2.6.1 Carbon Monoxide (CO)

Aranthady et al. [28] examined gas sensing performance of a hybrid composite based on Ta_2O_5-SnO_2-PANI (Ta stands for Tantalum) for sensing of CO at low concentrations and room temperature. The amount of polyaniline used was less than that of (Ta_2O_5-SnO_2) and it was found that a 1:0.5 weight ratio of TaSn:PANI showed the highest response to 10 ppm of CO, therefore, this was selected as the optimized composition. Sensing response was evaluated by measuring the change in the resistance of the hybrid composite and the resistance of the material was found to decrease upon exposure to CO gas. It was shown that the material is capable of sensing as low concentrations as 1 ppm of CO gas at room temperature. Selectivity studies with interferent gases such as H_2, CO_2 and CH_4 showed that the material is specifically sensitive to CO. Moreover, a stability study was done every 10 days for two months and the material did not show much loss of sensitivity over time. The sensor response was also evaluated at different relative humidity levels from 25% to 70% and no significant change in the sensitivity of the sensing material was observed. The authors proposed a gas-sensing mechanism that is based on the formation of a p-n heterojunction. Overall, the hybrid material showed improved CO gas sensing performance at room temperature.

Sen et al. [29] reported on the gas sensing capability of PANI/Co_3O_4 nanocomposites for room temperature detection of CO. PANI used in the nanocomposite was in its conductive form with a binary dopant of HCl and β-cyclodextrin (β-CD). The change in current was measured when the

nanocomposite was exposed to CO gas at ambient conditions (room temperature and RH of ~20%), and it appeared that PANI with 1 wt. % Co_3O_4 had the highest response towards 75 ppm of CO. This PANI/Co_3O_4 nanocomposite also showed high selectivity to CO in the presence of methane and liquefied petroleum gas (LPG). In addition, studying the effect of humidity revealed the high dependence of sensor response on RH, showing a significant drop in response on increasing RH from 20% to 75%. Suggested mechanism for gas sensing was explained due to the partial electron transfer between CO molecules and PANI.

Table 2.3 shows the short list of most promising sensing materials for CO detection at room temperature. Appendix C cites more related literature references for both CO_2 and CO.

Table 2.3: A short list of most promising sensing materials for the detection of CO.

No.	**Hybrid Sensing Material**	**Concentration (ppm)**	**Sensitivity/Sensing Response**	**Operating Temperature**	**Ref.**
1	PANI/Co_3O_4	50 & 75 ppm	81% (for 75 ppm) 20% (for 50 ppm)	RT	[29]
2	PANI/SnO_2/Pd	50-300 ppm	30–401%	RT	[30]
3	PANI/SnO_2 (45% PANI/55% SnO_2)	25-200 ppm	65% 53% (for 25 ppm)	30 °C	[31]

2.6.2 Carbon Dioxide (CO_2)

Nasirian [32] studied polyaniline/tin dioxide nanocomposites (PSNs) for CO_2 detection at room temperature under ultraviolet light illumination. Four PSN films with varying SnO_2 content of 10%, 20%, 30%, and 40% were made and denoted as PS1, PS2, PS3, and PS4. PS2 outperformed the others in low-light conditions and showed superior response and recovery times. In addition, it was observed that PS2 showed enhanced sensitivity and response/recovery time under UV light.

Another material reported for detecting CO_2 at room temperature is PANI with TiO_2 [33], [34]. Sonker et al. [33] fabricated a chemiresistive sensor based on PANI/TiO_2 thin film. They evaluated the gas sensing capabilities of the nanocomposite towards 1000 ppm of CO_2 and the sensor response (defined as the change in resistance) was found to be 53%. Nimkar et al. [34] studied the sensitivity of PANI/TiO_2 thin film in the range of 30-60℃ upon exposure to 1000 ppm CO_2. The sensitivity was determined to be 5% at 35℃ while decreasing to 1% at the higher operating temperature of 60℃. Table 2.4 lists the sensing capabilities of the most promising materials for detecting CO_2 at room temperature (see also Appendix C for more literature sources).

Table 2.4: A short list of most promising sensing materials for the detection of CO_2.

No.	**Hybrid Sensing Material**	**Concentration (ppm)**	**Sensitivity/Sensing Response**	**Operating Temperature**	**Ref.**
1	PANI-SnO_2	5000 ppm	47.4% (under UV)	RT	[32]
2	PANI-TiO_2	1000 ppm	53%	RT	[34]
3	PANI-NaO_2	4000 ppm	60%	RT	[35]

Pandey [36] has a good compendium of literature sources for PANI nanocomposites as sensing materials up to 2016, while Zegebreal et al. [37] and Verma et al. [38] have a more recent literature compendium of various polymer-based sensing materials for gas sensor applications.

2.7 Effects of Humidity on Analyte Sorption

Humidity refers to the amount of water vapor in the air. Two common methods for reporting and measuring humidity are absolute and relative humidity. Absolute humidity quantifies the amount of water vapor in a certain volume. Relative humidity (RH), on the other hand, is given as a ratio and involves comparing the current water vapor v

pressure with the water vapor pressure required for saturation at a specific temperature. Relative humidity is directly influenced by temperature [39].

Moisture is a prevalent and an inevitably interfering substance in gas sensor applications. Humidity can have an impact on sensing characteristics of gas sensors (e.g., sensitivity, etc.). The majority of studies do not study the effect of humidity in a systematic way and primarily report gas detection in the absence of humidity. Similarly, humidity detection is examined without the presence of other potentially interfering gases [37].

Cavallo et al. [40] studied the changes in electrical resistance of PANI films when they were exposed to volatile analytes. First, changes in resistance of the polymer were explained when water was used as a pure analyte, with no other interfering gas. Then, the effect of the presence of water vapor as an interfering agent was studied when PANI films were used for detecting other volatiles (e.g., ethanol and butanol). It was found that PANI resistance decreases when exposed to butanol at humidity levels lower than 40%, i.e., sensitivity increases. However, sensor resistance has an increasing trend when humidity is higher than 40%, meaning less sensitivity. Positive, negative, and nearly zero signal polarity obtained was attributed to the relative humidity value. Overall, humidity had a significant impact on the resistance (response) of PANI films to sensing butanol.

Nasirian [32] studied the sensing performance of a polyaniline/tin oxide nanocomposite for CO_2 detection at room temperature. The effect of relative humidity on the response of the proposed nanocomposite was studied and it was shown that the sensing response increased upon increasing the relative humidity from 30% to 90%. The observed increase in sensing response at higher relative humidity was attributed to the formation of hydrogen bonds between water molecules and the imine nitrogen of the polyaniline chains. This resulted in an increase in the p-type characteristics of the polymer network, leading to a greater number of active sites available for interacting with CO_2 molecules.

Sholehah et al. [20] fabricated an ethylene gas sensor using ZnO-Ag layer on a flexible PET-ITO substrate. The sensor responses were studied at different levels of humidity: 50% (low), 70% (middle level), and 80% (high humidity). Their humidity tests suggested that the responses increased as the relative humidity increased. The increasing response values is attributed to the

presence of water molecules on the surface of the ZnO-Ag0.6, which in turn contribute to an increase in conductivity and help to adsorb more ethylene to the surface.

Krivec et al. [22] studied the effect of humidity on two MOx-based chemiresistive sensors for ethylene sensing. One sensor (MiCS-5914) was based on tungsten oxide and the other (MQ-3) on tin oxide. Response and recovery measurements of MQ-3 sensor were carried out at four concentrations of ethylene (50, 40, 25, 10 ppm) in the resistivity mode, while MiCS-5914 sensor response was measured in the voltage mode. It was shown that relative humidity had a similar effect on both sensors, significantly reducing their sensitivity to ethylene. Table 2.5 gives a summary of observations from the literature.

Table 2.5: Summary of humidity effects on the performance of sensing materials.

Sensing response (sensitivity) behavior in the presence of RH	**Sensing material**	**Target gas**	**Ref.**
Decreases as RH increases.	- WO_3 and SnO_2 based sensors	- Ethylene	[22]
	- Au/PPy (1:2)	- Ethylene and Ammonia	[16]
	- PANI/Co_3O_4	- CO	[29]
	- PANI/ chloroaluminium phthalocyanine (ClAlPc)	- CO_2	[41]
Increases as RH increases.	- ZnO/Ag	- Ethylene	[20]
	- PANI/SnO_2	- CO_2	[32]
Conditional/bimodal behavior, i.e., it increases/decreases until a certain level of RH, but decreases/increases above that level.	- PANI	- Butanol	[40]
	- PANI	- CO_2	[41]
No change in sensor response.	- Ta_2O_5/SnO_2/PANI	- CO	[28]
	- Pd/Mg thin films	- H_2	[42]

2.7.1 Humidity Sensors

Manjunatha et al. [43] prepared TaS_2 (tantalum disulfide) encapsulated PANI composite and humidity sensing properties were studied in the range of 11–97% RH. The resistance showed a decreasing trend with an increase of relative humidity while the sensing response increased. The water molecules or moisture content existing in humidity chambers behave as electron donors resulting in donor doping and thus causing increased conductivity. This increased conductivity may also be linked to the mobility of dopant ions, which are attached loosely to the PANI chains by weak van der Waals forces. Table 2.6 gives a summary of humidity effects.

Table 2.6: Humidity sensing characteristics of various PANI-metal oxide composites [43].

Hybrid Material	**Response Time (s)**	**Recovery Time (s)**	**Sensing Response (%)**	**Sensing Range (%RH)**	**Ref.**
PANI/Pr_2O_3 (praseodymium oxide)	377	453	75%	15-95	[44]
PANI/Cr_2O_3	134	213	87%	20-95	[45]
PANI/TiO_2	50	122	84%	25-95	[46]
PANI/TaS_2-50% (tantalum disulfide)	36	49	97%	11-97	[43]

As shown in Table 2.6, the PANI/TaS_2 composite exhibited best humidity sensing characteristics among all of the cited efforts, which in turn makes it a promising material for the fabrication of humidity sensing devices.

Machappa et al. [47] suggested a humidity sensor based on polyaniline/magnesium chromate (PANI/$MgCrO_4$) composites. It was observed that resistance decreases with increasing relative humidity. This can be attributed to the conversion of the polymer complex into more of a p-type

material in nature due to absorption of water molecules. In other words, the hole concentration is increased by donation of the lone pair of electrons from the conducting complex towards the $MgCrO_4$ water molecules. These composites are sensitive to low humidity levels, ranging from 20–50 % of RH.

Mistry et al. [48] present a study on the performance of a zinc oxide (ZnO)-based microcantilever sensor designed for detecting low humidity levels. The microcantilever sensor demonstrates good sensitivity, particularly notable at low relative humidity levels. The peak sensitivity recorded is 23,649 ppm/% RH at 5.8% RH, which is substantially higher than those reported for other resonant humidity sensors in the literature. This high sensitivity is attributed to the low total mass of the ZnO cantilever and the ZnO capability to serve a dual function as both the structural and sensing layer. It is worth mentioning that this study [48] provides a list of frequency-shift (gravimetric-based) relative humidity sensors reported in the literature.

2.8 Polymers as Sensing Materials

One class of gas sensors is based on organic materials using polymers (often conductive) as their sensing materials. Polymers such as polypyrrole (PPy), polyaniline (PANI), polythiophene (PTh), poly (3,4-ethylene dioxythiophene) (PEDOT), polyacetylene (PA), and poly (phenylene vinylene) (PPV), have gained attention for gas sensing applications due to their favorable characteristics such as room-temperature operation, versatility, and tunable properties [38].

Polyaniline (PANI) is one of the most studied polymers in sensing applications since its discovery by MacDiarmid et al. [49]. It is a well-known conducting polymer with unique features of facile synthesis and high environmental stability. PANI exists in three different oxidation states, namely, leucoemeraldine, emeraldine, and pernigraniline. As illustrated in Figure 2.3, PANI is composed of ‘n’ reduced benzenoid diamine units and ‘m’ oxidized quinoid diamine repeating units, where nitrogen exists in either an amine or imine environment. The oxidation state of PANI is determined by the value of ‘m’. The most stable form of PANI is emeraldine, which has an equal number of oxidized and reduced units and is the insulating form with conductivity of ~ 10^{-5} S/cm. Emeraldine

salt (also known as metallic emeraldine) is the conductive form of PANI, which can be obtained by protonation of emeraldine base (i.e., doping with protonic acid (H^+)) or oxidative doping of leucoemeraldine base. Figure 2.3 also shows different salt (protonated) and base (unprotonated) forms of PANI in three redox forms [50].

Sensing performance of polymers can be improved by the addition of inorganic materials (e.g., metal and metal oxide nanoparticles), resulting in the formation of hybrid polymer/inorganic nanocomposites. The use of polymer/inorganic hybrid materials offers advantages compared to a single component due to possible synergistic (complementary) effects between polymer and metal oxide nanoparticles [37].

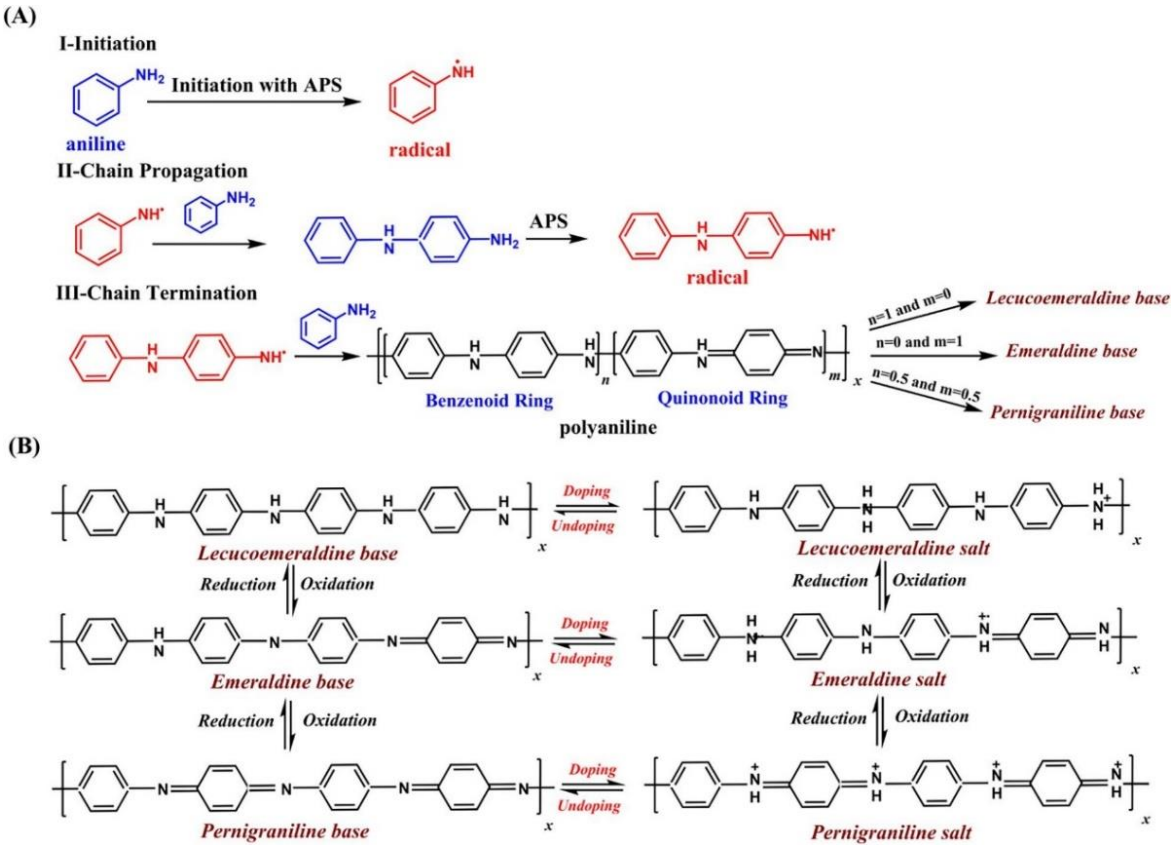

Figure 2.3: (A) Reaction mechanism for chemical oxidative polymerization of aniline, (B) different redox forms of PANI and their interconversion. Reproduced with permission from [50].

2.9 Doping

Although polymeric sensing materials have significant potential for gas detection at room temperature, their relatively low sensitivity often restricts their gas sensor applications. Among various techniques to improve sensing performance of polymers such as increasing surface area and appropriate functionalization, doping has been widely reported in the literature [38]. A dopant, in general, is a small amount of a substance that is incorporated into the polymer matrix, resulting in an improvement in sensing characteristics of the specific pristine polymer. Properties, such as resistance or conductivity of the polymer or polymer composite, are mostly controlled by the polymeric material because the concentration of dopant relative to the polymer typically falls within the range of 0.1% to (usually less than) 20% by weight. Choosing the appropriate type and amount of dopant enables the adjustment of electrical properties to an optimal level, leading to improved sensitivity [51]. The main assumption here is that there is a homogeneous dispersion of the dopant into the polymer matrix. If the dispersion is heterogeneous, then the dopant will likely have a negative effect via the disruption/fragmentation of the polymer matrix [52].

Doping affects the interactions between the polymeric sensing material and the gas analyte. Dopants often offer mechanical integrity, which is positive. If properly dispersed within the polymer, they may have other beneficial effects. Finally, dopants can be either electron donors or electron acceptors. Addition of an electron acceptor dopant to a polymer matrix creates positive charges (and holes allowing electron transfer) across the polymer chain. In other words, the polymer is oxidatively doped and becomes a p-type material. Contrarily, a negatively charged polymer can also be formed if an electron donor dopant is incorporated, resulting in the formation of a n-type material [38].

Metal oxides and metals are a well-known class of inorganic materials used as dopants in gas sensing applications. The catalytic potential of these materials encourages the interaction between polymer and gas analyte (depending on the temperature level employed) by breaking down the gas molecules and aiding in their bonding with oxygen-containing functional groups on the surfaces of polymers. This interaction leads to a strong sensitivity of these materials towards such gases

[8]. Some common n-type metal oxides include TiO_2, SnO_2, ZnO, and WO_3, while NiO, Co_3O_4, and CuO are among the p-type metal oxides [53].

2.10 Types of Sensors

Various sensors are used for gas sensing applications. Different types of sensors have different detection principles, transduction methods and different structures. In this section, different known types of sensors reported commonly in the literature are briefly discussed.

2.10.1 Chemiresistive Sensors

Chemiresistive sensors are renowned for their compact size, straightforward and inexpensive synthesis processes, and easy operation. Chemiresistive sensors typically include an array of electrodes covered with an active layer (sensing layer). The detection principle of this sensor is based on measuring the change in the resistance of a sensing material in the presence of a target gas. The electrical resistance of a sensing material changes upon its interaction with the target analyte. In other words, chemiresistive sensors translate chemical reactions into electrical signals (resistance or conductance) [54].

The sensor response is calculated based on resistance change measurement. It is commonly defined as a ratio between sensor resistance in air (R_a) and sensor resistance in the presence of target gas (R_g). For an n-type material and a reducing gas, the ratio is R_a/R_g, while for an n-type material and an oxidizing gas, the ratio changes to R_g/R_a. This situation is reversed for p-type materials. Table 2.7 gives a quick summary of the sensing response behavior in n-type and p-type materials. A comprehensive review of chemiresistive gas sensing materials can be found in Pandey [36] and Wong et al. [54].

Table 2.7: Summary of sensing response behavior to reducing and oxidizing gases (adopted from ref [54]).

Sensing response behavior	**n-type sensors**	**p-type sensors**
Reducing analytes (CO, H_2, CH_4, NH_4, H_2S, acetone, ethanol, etc.)	Resistance decreases	Resistance increases
Oxidizing analytes (CO_2, NO_x, SO_2, O_2, O_3, etc.)	Resistance increases	Resistance decreases
Dominant charge carrier	Electrons (e^-)	Holes (h^+)

2.10.2 Quartz Crystal Microbalances (QCMs)

Quartz crystal microbalances are mass-based detectors that exploit the piezoelectric effect to generate a signal. The detection principle of this sensor relies on frequency changes associated with mass changes on the surface of a piezoelectric material like quartz. Change in the mass of the crystal is a result of adsorption/binding of a target analyte to the crystal surface. Since the resonant frequency of the crystal depends on its mass (i.e., they are inversely proportional), this mass change will appear as a change in the resonant frequency of the crystal. QCMs are the most popular member of a broader family known as acoustic wave devices. Tolentino et al. [17] reported detection of ethylene based on a piezoelectric QCM. In addition, surface acoustic wave (SAW) sensors are another class of mass-based devices that employ a similar operation principle (as described for QCMs) but use a wave passing through the surface of a piezoelectric material. Šetka [16] studied the gas sensing properties of a SAW sensor in detection of ethylene and ammonia.

2.10.3 MEMS Sensors

Micro-electro-mechanical systems (MEMS) emerged during the 1990s, and they have found applications in detecting biomolecules, microorganisms, gaseous analytes, and other chemical compounds. As the name suggests, these sensors have dimensions in micrometers and involve a mechanical response (e.g., bending or deflection) when exposed to an analyte. This mechanical response will then be transformed into a measurable signal, like voltage, current or a frequency shift. A popular class of MEMS are microcantilever sensors [55].

Microcantilever sensors are mass-based sensors. They undergo bending (in the nanometer scale) because of molecular adsorption. This molecular adsorption results in a change in mass, causing a frequency shift, which can subsequently be quantified/measured by the sensor. Microcantilever-based sensors are extensively utilized in two operation modes for sensing applications: (a) static mode, and (b) dynamic mode (as shown in Figure 2.4). In the static mode, cantilever flexes due to an added mass or surface stress changes caused by gas molecules adsorption, and the deflection of the cantilever is measured. In the dynamic mode, shifts in the resonance frequency, which are again caused by mass change, are measured. The variation in resonance frequency is associated with the amount of mass added, and eventually to the concentration of analyte sorbed [56].

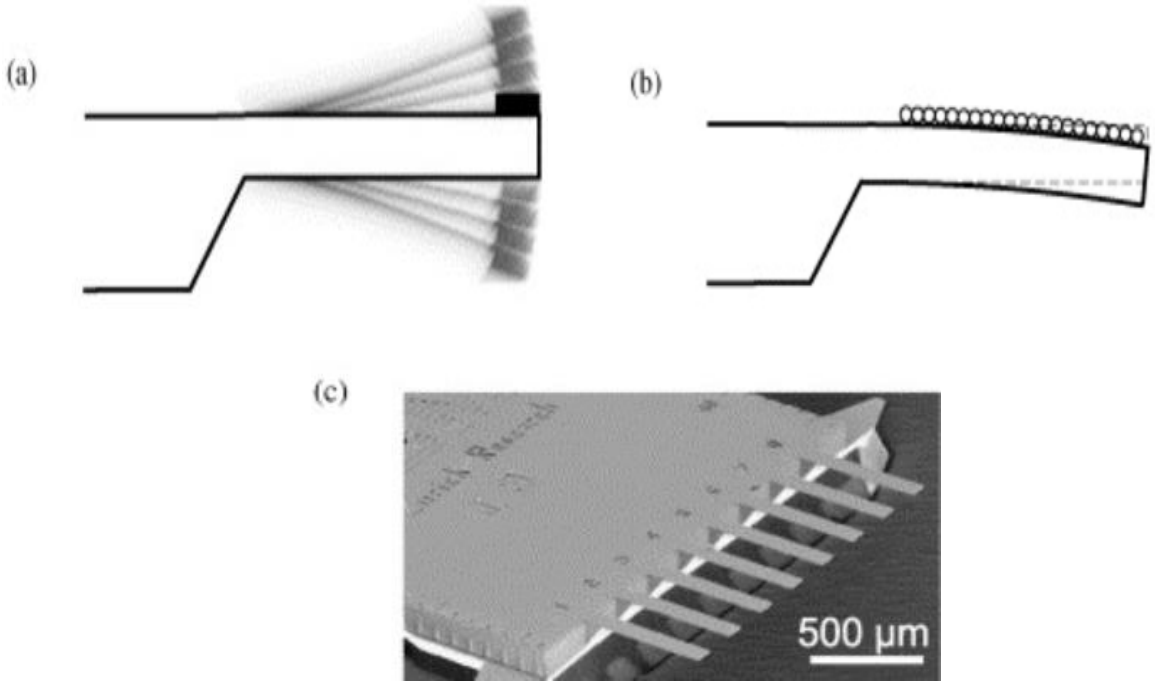

Figure 2.4: (a) Dynamic mode of microcantilever, (b) Static mode of microcantilever, (c) Scanning electron micrograph of a cantilever array. Reproduced with permission from [56].

The surface of a cantilever is coated with a thin layer of a sensing material (known as functionalized surface). The sensing material should be capable of identifying the target analytes by showing affinity for the analytes, leading to sorption of the analytes. It is important to understand the mechanisms through which target analytes interact with the functionalized surface, as the sensor's effectiveness relies on this interaction. Such interaction can manifest in chemical,

physical, or hybrid forms [57]. For example, palladium which is found suitable for sensing hydrogen can be coated over a microcantilever. Sorption of hydrogen gas molecules into the functionalized surface results in deflection of the cantilever, as shown in Figure 2.5 [58].

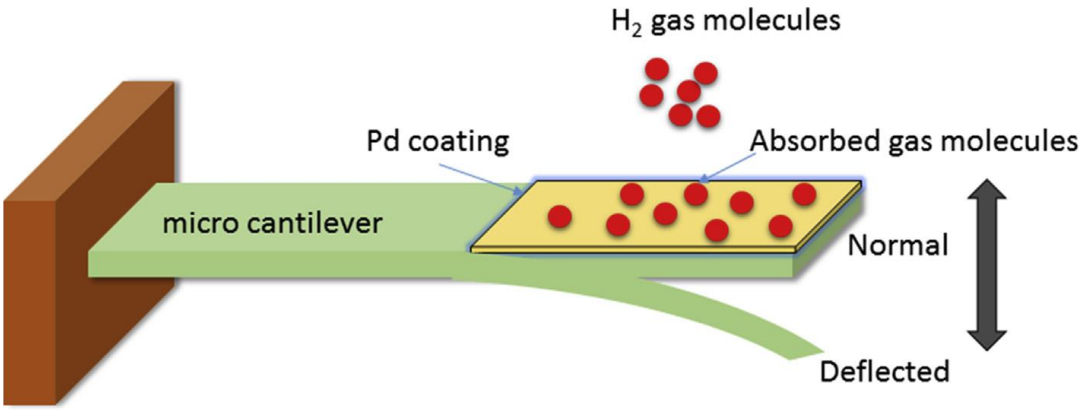

Figure 2.5: Schematic of a microcantilever sensor for sensing hydrogen gas. Reproduced with permission from [58].

Chapter 3: Experimental

3.1 Synthesis of Polymeric Sensing Materials

After a comprehensive literature review, short lists of top potential materials have been developed for the detection of our target analytes (see Chapter 2). Appendix D gives more details on polymeric materials tested, dates of experimental trials, and chemical formulas of the materials tested. Based on the short lists, pristine PANI and PANI doped with one or two metal oxides were selected and synthesized for further analysis. Note that some polymers (polypyrrole (PPy), polythiophene (PTh), and polyvinylpyrrolidone (PVP)) were available commercially (Sigma-Aldrich) and were tested as received.

3.1.1 Synthesis of Pristine PANI

For synthesis of pristine PANI, aniline was used as the monomer and ammonium persulfate (APS) was used as the initiator (both purchased from Sigma-Aldrich). In the case of preparing a doped PANI, metal oxide nanoparticles of tin (IV) oxide (SnO_2), titanium (IV) oxide (TiO_2), zinc oxide (ZnO), and cobalt (II, III) oxide (Co_3O_4) were purchased from Sigma-Aldrich and incorporated into the monomer during the synthesis procedure (see Table 3.1). Other chemicals used include deionized (DI) water and ethanol (ACS grade). DI water was used as the reaction medium, and for rinsing the synthesized polymer, and ethanol was used as received for additional washing and rinsing of the polymerization product.

Table 3.1: Summary of the metal oxides used with their particle sizes.

Metal Oxide	**Nanoparticle Size**
Tin (IV) oxide (SnO_2)	<100 nm
Titanium (IV) oxide (TiO_2)	21 nm
Zinc oxide (ZnO)	<100 nm
Cobalt (II, III) oxide (Co_3O_4)	<50 nm

The synthesis procedure of PANI followed the same recipe and proportions as stated in [59] Initially, 1 ml of aniline and 50 ml of DI water were added to a 100 ml round bottom flask and the flask was left in a sonicator for 30 minutes, which agitated monomer, water, and dopant (if present). The mixture was then put in a cooling bath at -1 ℃ for 30 minutes to ensure the mixture was cooled down before starting polymerization. Later, a solution containing 2.5 g of APS (initiator) and 12 ml of DI water was added to the flask containing the reaction mixture, and the flask was shaken for about one minute to ensure thorough mixing (when one could also observe that flask contents started to darken). The reaction mixture was again put back in the cooling bath to polymerize for 6 hours. The flask was introduced with a manual swirl every 15 minutes in the first hour, every 30 minutes for the next two hours, and subsequently every hour for the last two hours. After the 6-hour reaction period, the flask contents were transferred to a filter paper (Whatman#5) resting in a funnel. The polymer was first washed with DI water until the filtrate was colorless and then washed with ethanol three times. The polymer was left to dry in a fume hood for 24 hours or more. (If the polymer is not dry, then an oven can be used for further drying.) Finally, the polymer chunks/grains and powders were collected and transferred into a glass vial for storage.

3.1.2 Synthesis of Doped PANI

To synthesize doped PANI, the desired mass of metal oxide (MO) nanoparticles (not to exceed 20% by weight) was incorporated into the starting solution containing aniline monomer and DI water. For example, in the case of PANI with 5% tin (IV) oxide, the wt.% refers to the monomer mass; 5% SnO_2 (weight percent with respect to monomer), 95% (weight percent) aniline. The aniline and metal oxide amounts were dispersed in 50 ml of DI water (mixed in a 100 ml flask); the water volume was kept the same for all experiments. The rest of the polymerization procedure followed the same steps as described above for undoped or pristine PANI.

3.2 Gas Sorption/Sensing Set-up

Prospective sensing materials were evaluated in a test system incorporating a specialized gas chromatograph. The GC is able to measure the concentration of gas analytes used. The test set-up for gas sorption studies has been previously discussed in reference [60] and a schematic of the test system is shown in Figure 3.1. The general principle to evaluate a sensing material is based on determining the amount of a gas analyte sorbed on the sensing material. A sensing material that sorbs a higher concentration of a gas analyte is more sensitive to that gas analyte. It is worth mentioning that all the experiments were performed at room temperature and roughly 15 psi (atmospheric pressure).

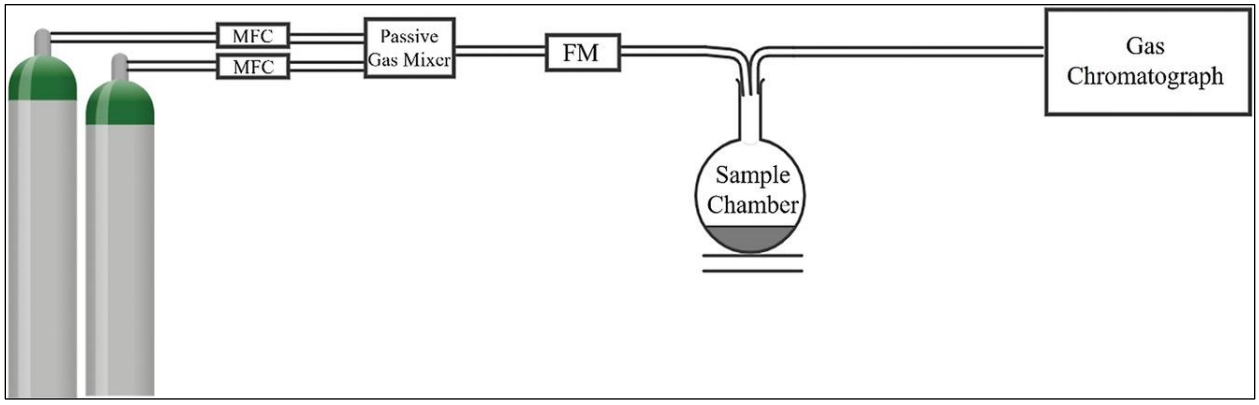

Figure 3.1: Gas sorption test set-up. Note: MFC= Mass Flow Controller, FM= Flowmeter. Reproduced with permission from [61].

To perform sorption studies, 0.1 g of a sensing material (e.g., PANI with or without dopants) was taken and transferred to a 100 ml flask with about 5 ml of ethanol. The flask was given a swirl and left in the fume hood until the ethanol evaporated and the polymer sample was dried out. Before exposing a polymer sample to a gas analyte, all the samples were purged with nitrogen for 30 minutes to ensure no other residual analytes were present in the sample.

In the next step, a known concentration of gas analyte was made to pass through an empty flask on its way to the specialized gas chromatograph (GC) to determine the initial gas concentration. This was done to obtain a (reference) baseline for the day. The concentration readings from the

GC (with an empty flask) were expected to be very close to the concentration of gas in the source cylinder, which will be henceforth referred to as ‘blanks’. Then, a sensing material was exposed to the gas analyte by replacing the empty flask with a flask containing the sensing material and passing the gas stream over the sample chamber. GC measured the concentration of gas that did not sorb onto the sample. The difference between the concentration of gas in the blanks trial and the trial with a sensing material was taken as the amount of gas sorbed onto the sensing material.

The GC used in experiments is a Scion 436 gas chromatograph purchased from Scion Instruments located in Edmonton, Alberta, Canada. It has a Varian CP-Sil 5 CB capillary column capable of separating compounds that are very similar in chemical nature. Additionally, the GC is equipped with a highly sensitive photon discharge helium ionization detector (PDHID) that measures gas concentrations. The GC can accurately record concentrations as low as parts per billion (ppb) ranges.

3.3 Gas Analyte Tested

As mentioned earlier in section 1.1, exploiting the specific target analytes for evaluation of sorption properties was avoided due to safety concerns (explosivity and/or toxicity issues attributed to H_2, C_2H_4, CO, CO_2,). Therefore, formaldehyde was used as a surrogate/simulant gas analyte for all the gas sorption studies performed using the specialized GC test set-up described in section 3.2.

Formaldehyde (F) gas used for sorption evaluation was of standard grade and contained 11.1 ppm (parts-per-million) of F in nitrogen balance (purchased from Praxair located in Mississauga, Ontario, Canada). Pure nitrogen was also purchased from Praxair (5.0 grade) to purge samples before being exposed for F sensing. It is worth noting that for the final test using the actual MEMS sensor, ethylene (one of the target gases, but in a much smaller cylinder for safety reasons) was directly used within a specially designed chamber enclosure (in collaboration with the Department of Systems Design Engineering, Professor Eihab Abdel-Rahman’s group). Note that the ethylene

cylinder was ~5 times smaller in height and ~3 times smaller in volume than the regular F cylinder, which has a typical height of 122 cm and a volume of 30 L.

3.4 Sensing Material Characterization

3.4.1 Scanning Electron Microscopy (SEM)

Scanning Electron Microscopy (SEM) is a powerful technique used for imaging the surface of solid materials at high magnifications. In SEM, a focused beam of electrons scans the specimen, and the interactions between the electrons and the sample produce various signals that can be detected and processed to create an image, revealing details about the surface morphology and composition of a sample.

Selected samples were analyzed for their surface morphology using a Zeiss Ultra Plus FESEM at the WATLAB facility located at University of Waterloo. Sample preparation was performed using carbon tape and SEM stubs. A small piece of carbon tape was stuck on a stub. The polymeric sample suspended in ethanol was then transferred on the carbon tape using a pipette, and the SEM stub was left at room temperature for the ethanol to evaporate. Note that SEM imaging for some samples was also performed (for independent corroborations) at a different facility (Quantum-Nano Fabrication and Characterization, QNFC, University of Waterloo) using a JEOL JSM-7200F machine.

3.4.2 Energy Dispersive X-Ray Spectrometry (EDX)

Energy Dispersive X-ray Spectrometry (EDX) is an analytical technique used in parallel with electron microscopy to analyze the elemental composition of materials. By analyzing the characteristic X-rays emitted from a sample, EDX provides a rapid and comprehensive identification of the elemental composition present. EDX fires a high-energy electron beam at a sample. This beam knocks inner-shell electrons out of atoms, and as outer-shell electrons rush to fill the gaps, they emit characteristic X-rays (i.e., unique fingerprints of each element). An X-ray detector captures these fingerprints, and software translates them into a spectrum with peaks

corresponding to the elements present. By analyzing these peaks, one can identify the elements in the sample, their relative amounts, and even create elemental maps showing their distribution across the sample surface.

EDX is often paired with a Scanning or Transmission Electron Microscope. Therefore, EDX analysis was performed on the same equipment used for SEM/TEM analysis (as mentioned in sections 3.4.1 and 3.4.3).

3.4.3 Transmission Electron Microscopy (TEM)

Transmission Electron Microscopy (TEM) is another microscopy technique that uses a beam of electrons to image the internal structure of thin specimens at a very high resolution. It is also capable of determining the size and shape of nanoparticles and nanowires. TEM equipment operates based on the principles of electron optics and imaging.

Transmission Electron Microscopy (TEM) utilizes electron beams like light beams, but with much higher resolution due to their tiny characteristic wavelength. TEM fires electrons from a heated filament, shapes them with electromagnetic lenses, and guides them through an incredibly thin sample mounted on a special grid inside a vacuum chamber. As the electrons travel through the sample, some pass straight through, some scatter, and some interact with the material itself. By capturing these interactions with a detector, TEM translates them into a detailed image, allowing one to observe a material's structure down to the atomic level. Additionally, TEM can be equipped with various detectors to analyze the elemental compositions of a sample.

TEM images of selected samples were taken using a JEOL JEM-F200 transmission electron microscope at the Quantum-Nano Fabrication and Characterization (QNFC) Facility at the University of Waterloo. The machine was also equipped with a JEOL 100 mm^2 silicon drift detector (SDD) for EDX analysis. Hence, the samples were analyzed with EDX on the same equipment. Note that TEM imaging for selective samples was also performed at the Biology Department, University of Waterloo, using a Philips CM10 transmission electron microscope (again for the sake of independent corroborations).

3.4.4 Dynamic Light Scattering (DLS)

Dynamic light scattering (DLS), sometimes referred to as quasi-elastic light scattering (QELS), is a non-invasive technique for measuring particle size and size distribution. DLS is based on the Brownian motion of dispersed particles which causes laser light to be scattered at different intensities. The relation between the speed of particles and the particle size is given by the Stokes-Einstein equation $\left(D = \frac{K_B\, T}{6\, \pi\, \eta\, R_H}\right)$, where D is the translational diffusion coefficient (related to the speed of particles), K_B is the Boltzmann constant, T is temperature, η is viscosity, and R_H is the particle hydrodynamic radius. DLS determines the diffusion coefficient (D) from which the sizes of particles in solution (hydrodynamic radius R_H) may be estimated [62].

The size of the synthesized PANI materials was evaluated by Zetasizer Nano ZS from Malvern Instruments (Herrenberg, Germany) in Professor. T. Mekonnen's lab (E6-5007, Chemical Engineering Department, University of Waterloo). The machine is equipped with a 633 nm He-Ne laser and operates at 173° angle using dynamic light scattering (DLS). Dilute solutions of 0.4 mg of PANI material in 20 ml of N-methyl pyrrolidone (NMP) were prepared before evaluating them using the Zetasizer analyzer. The evaluation was carried out under ambient conditions.

3.4.5 Brunauer-Emmett-Teller (BET) Technique

The Brunauer–Emmett–Teller or BET test is particularly useful for calculating the specific surface area of materials. The process involves adsorbing a layer of gas molecules (adsorbate) on the surface of the material under investigation (adsorbent) and using the adsorption data to calculate the surface area. The adsorbate gas used in this technique is usually an inert gas like nitrogen (N_2), krypton (Kr), and argon (Ar). The surface area determination should be carried out at a constant temperature yielding the so-called adsorption isotherm.

Surface area analysis involved analyzing about 0.1g of polymeric samples at different degassing conditions under vacuum. Nitrogen (N_2) gas was used as an adsorbate for surface area and pore analysis of all polymeric materials. The analysis was performed at two different facilities in order

to check reproducibility. Some trials were conducted in the Chemistry Characterization lab at McGill University (Department of Chemistry), whereas some others were conducted using the Gemini® VII 2390 surface area analyzer, located in the Analytical lab, Department of Chemical Engineering, University of Waterloo.

3.5 MEMS Sensor Chamber

A brief overview of the MEMS sensor was provided in section 2.10.3. Final evaluation of optimal sensing materials was performed using a MEMS sensor and with ethylene gas at 50 ppm. This final gas detection test was performed in collaboration with Yasser Shama (Ph.D. candidate in the research group of Professor Eihab Abdel-Rahman, Department of Systems Design Engineering, University of Waterloo). The sensor consists of a sensing plate supported by two cantilever beams and two electrodes, namely, an actuating electrode and a landing electrode. Figure 3.2-a provides a top view of the sensor showing its dimensions. Sensor functionalization starts with depositing a sensing material on its sensing plates. Since the sensing materials were in powder form, a suspension of material powder in ethylene glycol (as a carrying medium) was prepared and transported to its target location on the sensor using a semi-automated deposition process as explained in [63]. Ethylene glycol was then allowed to evaporate, leaving the sense-plate surface with an even coating of the sensing material. Figure 3.2-b shows the SEM image of a functionalized senor after deposition of the detector material.

a) b)

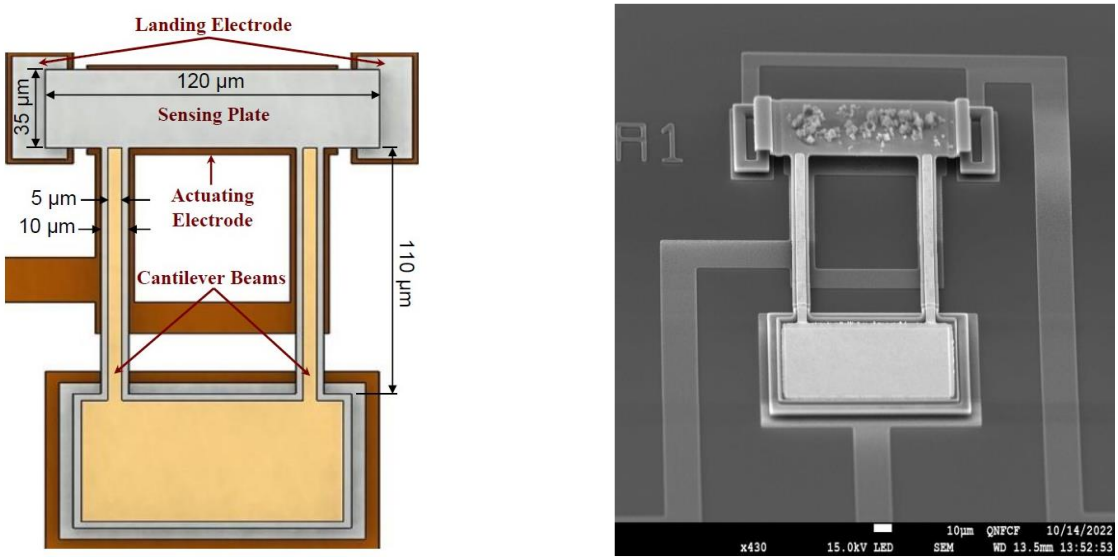

Figure 3.2: (a) Schematic of a MEMS sensor, (b) SEM image of the sensor with sensing material deposited on the sense-plate. Reproduced with permission from [64]-[65] (open access).

Once the sensor is functionalized (i.e., with a sensing material deposited), it is placed in an enclosed test chamber. The experimental gas test set-up is shown in Figure 3.3, again curtesy of our collaborators in the Department of Systems Design Engineering. The gas flows from the cylinders at the very left corner of the experimental setup, and it is introduced to the test chamber through a mass flow control (MFC) to obtain the sensor response in the presence of the target gas.

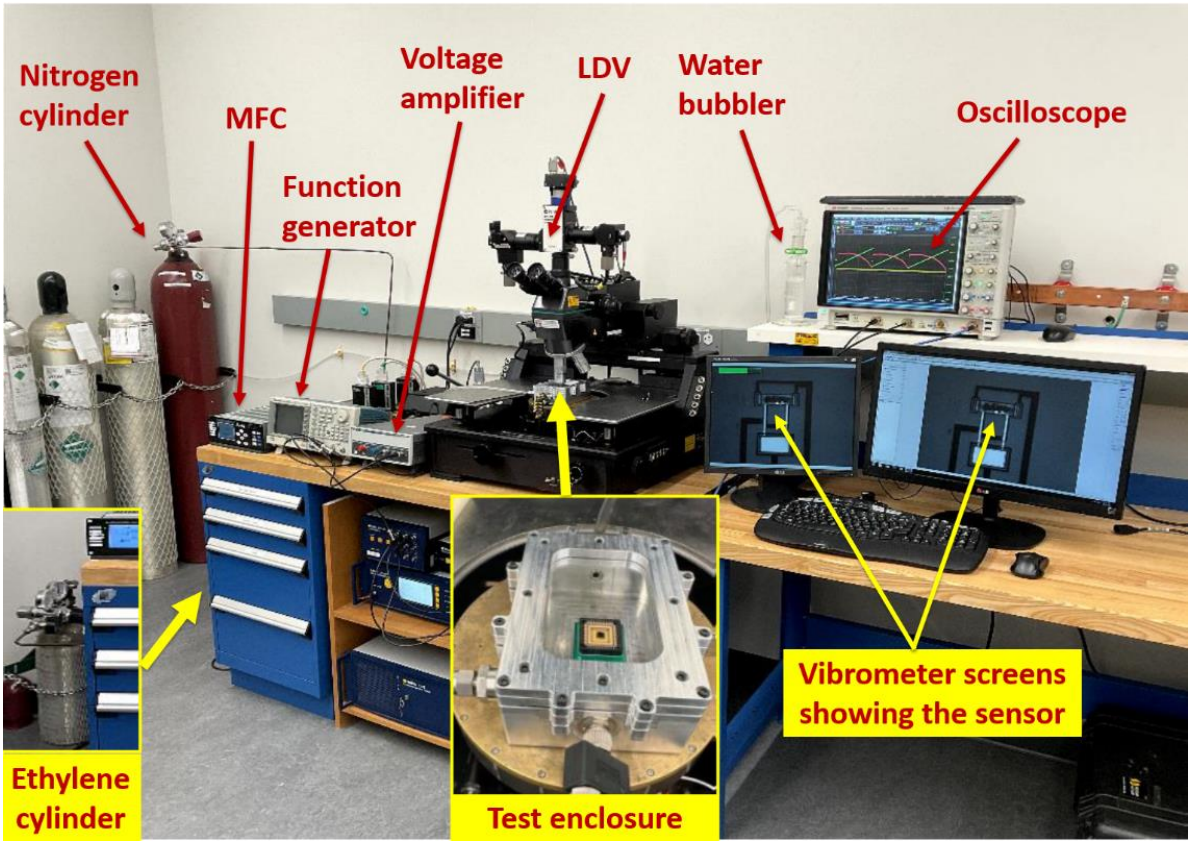

Figure 3.3: The experimental set-up for ethylene testing (MFC: Mass Flow Control, LDV: Laser Doppler Vibrometer). Image adopted from references [64]-[65] (open access), and modified by the author.

Chapter 4: Results and Discussion

4.1 Formaldehyde (F) Sorption Studies

Potential polymeric materials for sensing analytes targeted in this thesis, which include hydrogen, ethylene, carbon monoxide, and carbon dioxide, were evaluated for their sorption capabilities. Experimentation with these gases is not the easiest in an academic environment, primarily due to health/safety concerns, and hence a simulant (surrogate) gas was chosen for sorption trials. Each sample was exposed to a source of 11.1 ppm of formaldehyde (F) as the surrogate gas, and the amount of formaldehyde sorbed was measured. The experimental steps for sorption studies have been described in section 3.2. Appendix D gives a summary of the polymeric materials tested during the formaldehyde sorption studies (along with additional information on the chemical formulas of the different polymeric materials used).

Considering again Tables 2.1 to 2.4, one can see that the top sensing materials for detecting hydrogen, ethylene and carbon oxides have polyaniline (PANI) as the most common polymer, followed by polypyrrole (PPy), polythiophene (PTh) and polyvinylpyrrolidone (PVP), and PANI composites along with tin, titanium, zinc and cobalt oxides. That was the justification for the decision to evaluate the sorption sensitivity of these materials with formaldehyde as the surrogate gas. It should also be mentioned from the outset that the main interest was to detect the amount/mass of the sorbed gas molecules (the interest was in mass-based sensors and not in sensing that uses resistance or conductivity properties). The obtained results are discussed herein (related to the sorption of formaldehyde), and they culminate with confirmation tests of the actual MEMS sensor for the detection of ethylene.

4.1.1 Comparison of Pristine Polymers

First, the sorption performance of four different undoped polymer backbones was examined to see which polymer could be selected for potential modification, i.e., doping with metal oxides. Polyaniline (PANI) is one of the most widely used sensing materials because of its facile synthesis procedure and ability to interact/detect a wide range of gases and vapors. Moreover (see Chapter

2), polypyrrole (PPy), usually with a dopant, has been reported in the literature for the detection of H_2, C_2H_4, and CO_2. Also, polythiophene (PTh) and polyvinylpyrrolidone (PVP) are potential sensing materials for the detection of ethylene. Therefore, these pristine polymers were evaluated for their sorption ability towards formaldehyde (F).

Figure 4.1 shows the experimental sorption data for the four pristine polymers, namely, PANI, PPy, PTh, and PVP. It can be observed that PPy, PTh, and PVP do not seem to sorb formaldehyde, with average sorption levels ranging from 1 - 2.5%, while pristine PANI sorbs relatively much more formaldehyde with an average sorption of 14%.

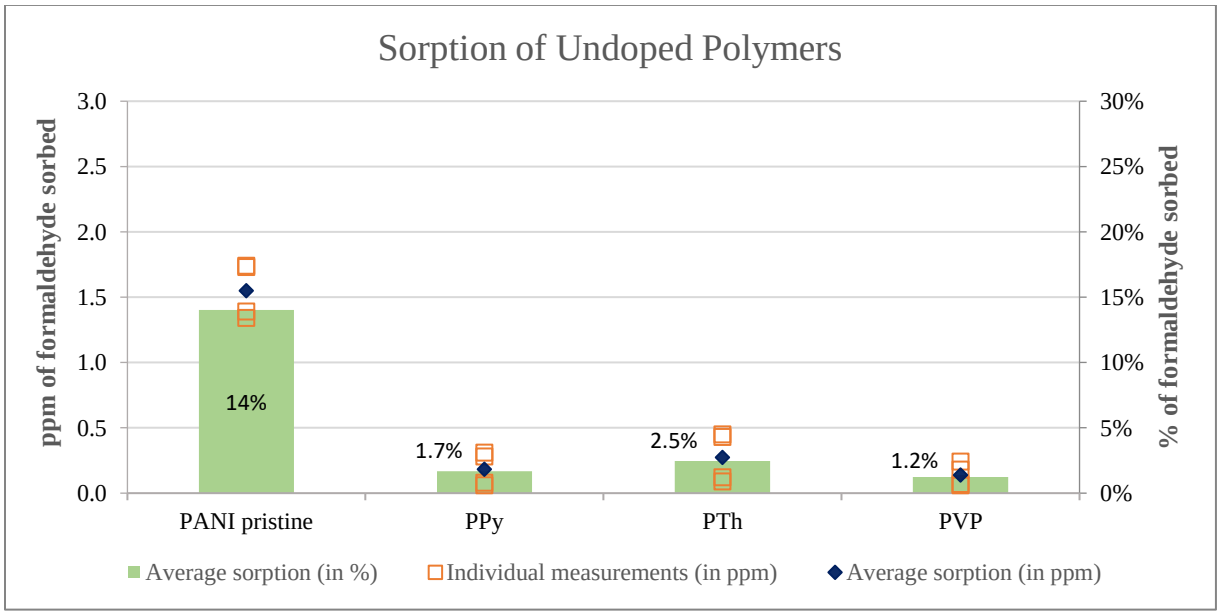

Figure 4.1: Formaldehyde sorption for various pristine polymers; (Source: F 11.1 ppm).

Figure 4.1 shows average sorption values, estimation of standard error (se) and 95% confidence interval (CI) ranges for the pristine polymers evaluated. Performing 95% confidence intervals on individual polymers also confirms that the sorption for PPy and PTh is almost zero, whereas PVP shows negligible (insignificant) levels of sorption. Note that all sorption measurements listed throughout this chapter were independently replicated (minimum two independent replicates).

Table 4.1: Average sorption values (in ppm) for undoped polymers.

Sensing Material	**Average Sorption ± se**	**Average Sorption ± 95% CI [Upper limit, Lower limit]**
PANI pristine	1.55 ± 0.215 ppm of F	1.55 ± 0.342 ppm of F [1.208, 1.892]
PPy	0.18 ± 0.131 ppm of F	0.18 ± 0.208 ppm of F [-0.028, 0.388]
PTh	0.27 ± 0.194 ppm of F	0.27 ± 0.309 ppm of F [-0.039, 0.579]
PVP	0.14 ± 0.069 ppm of F	0.14 ± 0.072 ppm of F [0.068, 0.212]

Note: Values following the ± sign indicate the estimate of one standard error (se) for the average sorption values; CI stands for confidence interval.

4.1.2 PANI Doped with Metal Oxides (MO)

Based on the results in Figure 4.1 and Table 4.1, PANI seems to be superior to other pristine polymers, therefore, it was chosen as a candidate polymer to be modified with metal oxides. It is suggested that metal oxides may enhance the gas sensing performance due to their larger surface areas and other synergistic effects between inorganic materials (metal oxides) and organic components (polymers) [59]. They can certainly improve the mechanical integrity of the material, however, they may also have adverse effects depending on their content, if they disrupt the polymer backbone structure [61], [66]. Therefore, several MO dopants (again, MOs that were considered more promising as per Chapter 2) were incorporated into PANI to see if the sorption of formaldehyde could be enhanced.

In what follows, PANI materials doped with different levels of metal oxides (based on previous use in the literature for detection of our target analytes) will be discussed and compared in terms

of their sorption sensitivity (once more, the emphasis in this thesis is to evaluate different polymeric materials, hence sensitivity). Note that the sorption behavior of pristine PANI is included in every section that follows so one can make a direct comparison between MO-doped PANI and pristine PANI as the 'base case' material. The metal oxide dopants used for sorption studies are SnO_2 (tin oxide), TiO_2 (titanium oxide), ZnO (zinc oxide), and Co_3O_4 (tricobalt tetraoxide). The MO dopant levels mentioned below are all in wt.% (see Chapter 3).

4.1.3 PANI Doped with ZnO

PANI materials doped with two dopant levels of 2.5% and 5% of ZnO were tested for sorption towards 11.1 ppm of formaldehyde in the source. Figure 4.2 and Table 4.2 show the sorption values of pristine PANI and modified PANI with ZnO. It can be seen that the sensitivity of PANI towards F seems to increase by decreasing the weight percent of ZnO. This trend is in agreement with the results obtained by Kim [67]. As also observed earlier, ZnO nanoparticles tend to form aggregates, therefore, higher concentrations of ZnO could induce heterogeneities in the polymer matrix that can hinder the sorption capabilities of the polymeric material. Overall, PANI with 2.5% ZnO seems to have a better sorption performance among other materials in this series with an average sorption of 2.09 ppm. However, given the aggregation characteristics of metal oxides, the optimal loading of ZnO could eventually be found to be less than 2.5%.

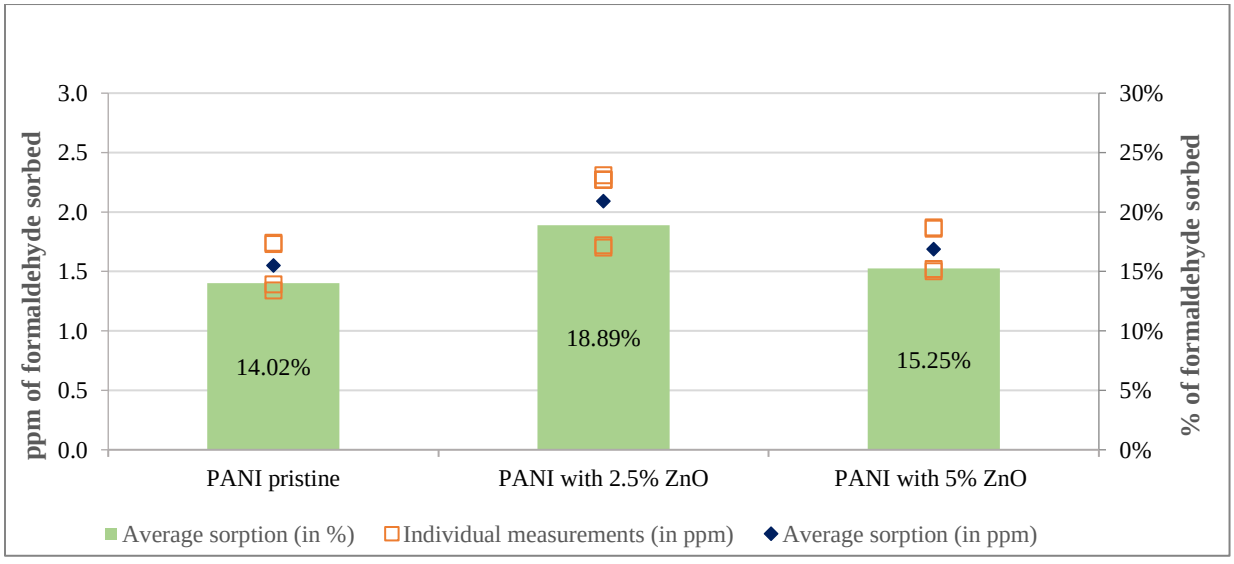

Figure 4.2: Formaldehyde sorption for PANI and PANI doped with ZnO; (Source: F 11.1 ppm).

Table 4.2: Average sorption values (in ppm) for PANI and PANI doped with ZnO.

Sensing Material	**Average sorption values ± se**	**Average sorption values ± 95% CI, [Upper limit, Lower limit]**
PANI pristine	1.55 ± 0.215 ppm of F	1.55 ± 0.342 ppm of F [1.208, 1.892]
PANI with 2.5% ZnO	2.09 ± 0.295 ppm of F	2.09 ± 0.309 ppm of F [1.781, 2.399]
PANI with 5% ZnO	1.69 ± 0.205 ppm of F	1.69 ± 0.326 ppm of F [1.364, 2.016]

Note: (1) Values following the ± sign indicate the estimate of one standard error (se) for the average sorption values; CI stands for confidence interval. (2) The coefficient of variation (defined as the ratio of standard deviation and mean) was calculated to be ~13% (on average) for this table.

4.1.4 PANI Doped with SnO_2 and TiO_2

First, PANI polymers doped with 5% SnO_2 (tin oxide) and 5% TiO_2 (titanium oxide) were evaluated for their sorption of F. Figure 4.3 shows individual and average sorption values measured in each sample. It can be seen that the addition of 5% SnO_2 improved the sorption of formaldehyde when compared to undoped PANI. However, there was no significant difference between the amounts of formaldehyde sorbed for undoped PANI compared to PANI with 5% TiO_2, meaning that doping PANI with 5% TiO_2 (during synthesis) does not seem to improve sorption. More detailed data analysis in section 4.4 also confirms that undoped PANI and PANI with 5% TiO_2 do not show statistically significant difference in formaldehyde sorption.

Since PANI with lower amounts of ZnO was observed to have better sorption, PANI samples with 2.5% of SnO_2 and TiO_2 were also evaluated to see if the same trend would be observed with SnO_2 and TiO_2, i.e., more sorption with decreasing the amount of metal oxide. As can be seen in Figure 4.3, sorption does not seem to improve with decreasing the amount of SnO_2 from 5% to 2.5%,

unlike what was observed for PANI with ZnO. PANI with 2.5% TiO_2 shows little improvement in formaldehyde sorption compared to its counterpart with 5% TiO_2.

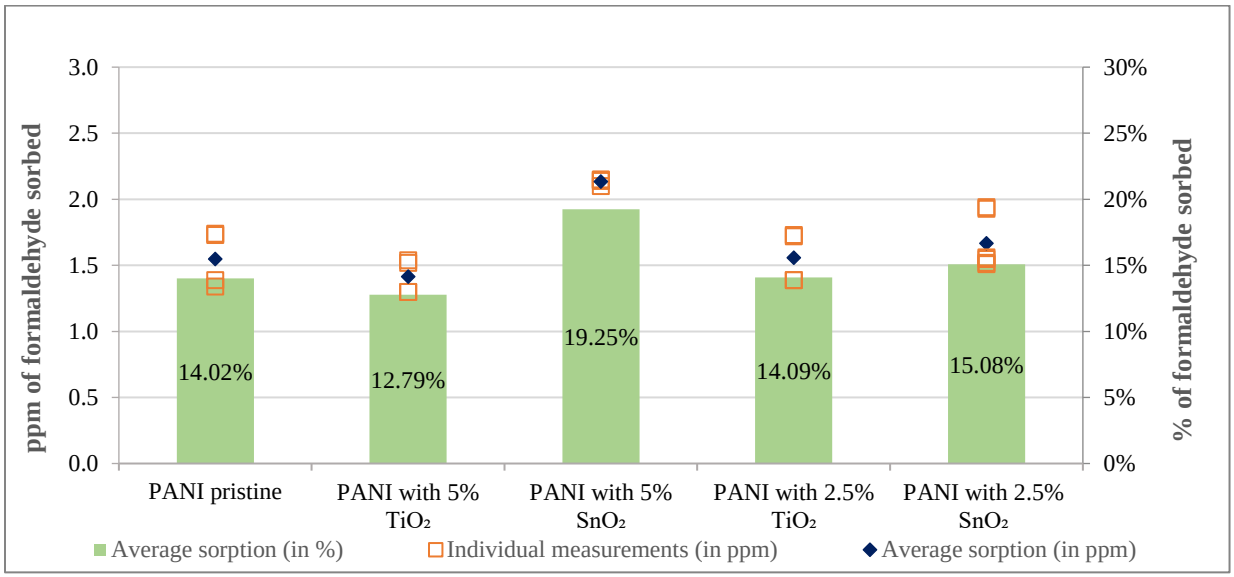

Figure 4.3: Formaldehyde sorption for PANI and PANI doped with SnO_2 and TiO_2; (Source: F 11.1 ppm).

Average sorption values and estimation of standard errors (se values) for each sample are listed in Table 4.3. Average values and confidence intervals have been calculated considering the last two readings (upon convergence) in each sample sequence in the GC trials. In other words, two consecutive sorption observations were taken from the GC in each sample trial to ensure the sorption had reached equilibrium. The third column in this table shows the values for 95% confidence intervals (CI) for each sample. Values of standard error are consistently quite low.

Table 4.3: Average sorption values (in ppm) for PANI and PANI doped with SnO_2 and TiO_2.

Sensing Material	**Average sorption values ± se**	**Average sorption values ± 95% CI, [Upper limit, Lower limit]**
PANI pristine	1.55 ± 0.215 ppm of F	1.55 ± 0.342 ppm of F [1.208, 1.892]
PANI with 5% TiO_2	1.415 ± 0.1330 ppm of F	1.415 ± 0.212 ppm of F [1.203, 1.627]
PANI with 5% SnO_2	2.135 ± 0.0238 ppm of F	2.135 ± 0.038 ppm of F [2.097, 2.173]
PANI with 2.5% TiO_2	1.56 ± 0.1935 ppm of F	1.56 ± 0.308 ppm of F [1.252, 1.868]
PANI with 2.5% SnO_2	1.67 ± 0.207 ppm of F	1.67 ± 0.218 ppm of F [1.452, 1.888]

Note: (1) Values following the ± sign indicate the estimate of one standard error (se) for the average sorption values; CI stands for confidence interval. (2) The coefficient of variation (defined as the ratio of standard deviation and mean) was calculated to be ~10% (on average) for this table.

4.1.5 PANI Doped with Combinations of SnO_2 and TiO_2

Both SnO_2 and TiO_2 have been observed commonly in the literature for sensing H_2, CO_2, and CO. Nasirian and Moghaddam [13] reported PANI doped with a combination of TiO_2 and SnO_2 for sensing hydrogen. In their work, three different 2:1 (wt.%) ratios of TiO_2:SnO_2 were studied, and it was observed that PANI with 30% TiO_2 and 15% SnO_2 had the highest response and lowest recovery time, although its response time was not the best (i.e., the lowest). Based on the same analogy, we decided to test PANI doped with a combination of metal oxides of TiO_2 and SnO_2 for its sorption towards formaldehyde. Therefore, two combinations of TiO_2 and SnO_2 were chosen to be incorporated into PANI:

1) PANI with (5% TiO_2 + 2.5% SnO_2): Since we had evaluated PANI with 5% TiO_2 before, it was interesting to see if adding a bit of tin oxide improves the sorption of PANI with titanium oxide.

2) PANI with (2.5% TiO_2 + 5% SnO_2): Here, we used the reverse analogy, i.e., to see if adding a bit of titanium oxide to PANI with 5% SnO_2 could improve the sorption.

Note that both cases still follow a 2:1 ratio of metal oxides, yet we do not exceed 20 wt.% of dopants in total.

Figure 4.4 depicts the sorption results of PANI with metal oxides of TiO_2 and SnO_2 as dopants; the green columns represent the percentage sorption of formaldehyde (according to the vertical axis on the right-hand side of the graph), while the symbols show the sorption values in ppm (vertical axis on the left-hand side). Comparing PANI with a single metal oxide and PANI with a combination of metal oxides, one can see that PANI with a dual metal oxide of TiO_2 and SnO_2 does not seem to improve sorption. In fact, adding 2.5% of TiO_2 to the composite of PANI with 5% SnO_2 negatively affects sorption, reducing it from 19% to 12%. Moreover, it seems that PANI with 5% TiO_2 does a better sorption job (even if slightly) than its counterpart with an extra ingredient of 2.5% SnO_2.

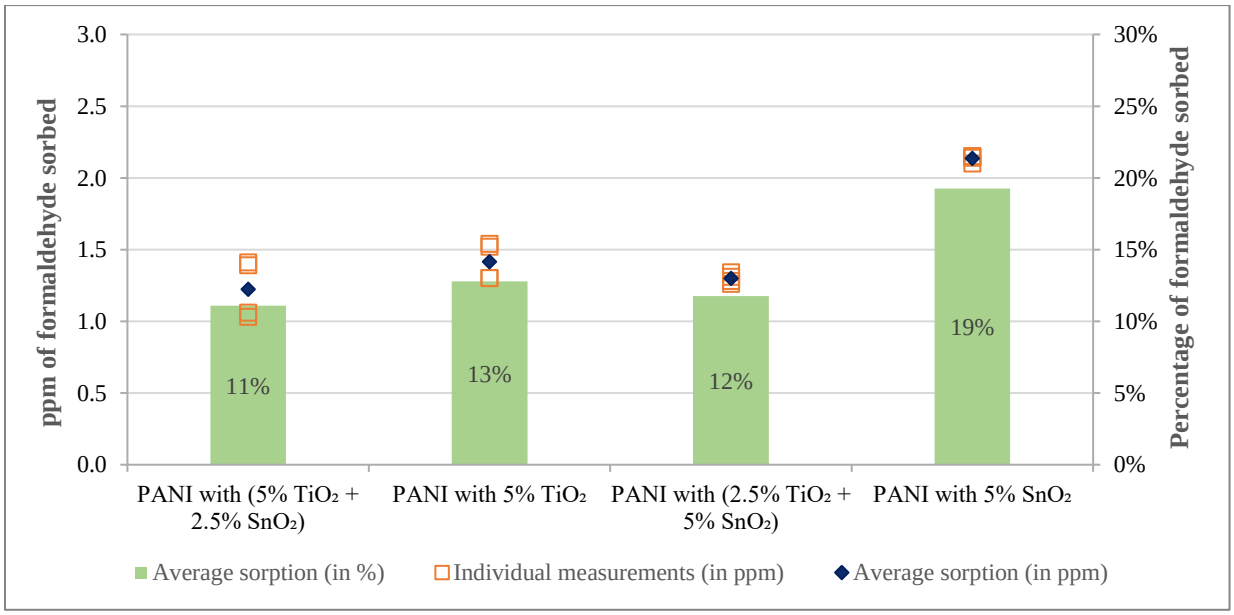

Figure 4.4: Formaldehyde sorption for PANI doped with metal oxides of SnO_2 and TiO_2; (Source: F 11.1 ppm).

Table 4.4 represents the average sorption values and the estimation of standard errors (se values) for each sample. One can observe that the CI's for the first three sensing materials do overlap, but the fourth material sticks out (as in Figure 4.4).

Table 4.4: Average sorption values (in ppm) for PANI with metal oxides of TiO_2 and SnO_2.

Sensing Material	**Average Sorption**	**Average Sorption ± 95% CI [Upper limit, Lower limit]**
PANI with (5% TiO_2 + 2.5% SnO_2)	1.2225 ± 0.2055 ppm of F	1.2225 ± 0.3270 ppm of F [0.8955, 1.5495]
PANI with 5% TiO_2	1.415 ± 0.133 ppm of F	1.415 ± 0.212 ppm of F [1.203, 1.627]
PANI with (2.5% TiO_2 + 5% SnO_2)	1.2975 ± 0.0350 ppm of F	1.2975 ± 0.0557 ppm of F [1.2418, 1.3532]
PANI with 5% SnO_2	2.135 ± 0.024 ppm of F	2.135 ± 0.038 ppm of F [2.097, 2.173]

Note: (1) Values following the ± sign indicate the estimate of one standard error (se) for the average sorption values; CI stands for confidence interval. (2) The coefficient of variation (defined as the ratio of standard deviation and mean) was calculated to be ~8% (on average) for this table.

4.1.6 PANI Doped with Co_3O_4

PANI with tricobalt tetraoxide, Co_3O_4, (with 1, 2 and 3 wt.% of Co_3O_4) has been reported in the literature for CO detection [29]. Cobalt (II, III) oxide is one of the most active catalysts among semiconductor oxides for carbon monoxide oxidation. Its performance in CO oxidation is comparable to that of noble metals [68]. Therefore, PANI was doped with varying amounts of Co_3O_4 to investigate the potential for enhancing sensitivity/sorption. Since sorption experimentation towards CO was avoided because of safety concerns, evaluation of PANI doped with Co_3O_4 was performed again with formaldehyde as the simulant. Both CO and F are polar molecules, leading to the speculation that there may be some similar interactions happening in both gases.

Figure 4.5 and Table 4.5 summarize sorption data for PANI and PANI doped with Co_3O_4. One can see that PANI with 1% Co_3O_4 seems to sorb the same amount of formaldehyde as pristine PANI. It is evident from Table 4.5 that the sorption range for PANI doped with 1% Co_3O_4 falls within the 95% CI range of pristine PANI, i.e., they overlap. Therefore, it may be suggested that no significant amount of Co_3O_4 was present in the case of PANI with 1% Co_3O_4 (see also Table 4.14), explaining the similar sorption of PANI and PANI with 1% Co_3O_4. By increasing the amount of Co_3O_4 from 1% to 2%, the material seems to show higher sorption probably because of the higher incorporation of cobalt into the polymer matrix. Sorption of the materials seems to maintain the increasing trend with further increasing the wt.% of Co_3O_4 as one can see that PANI with 5% Co_3O_4 shows the highest sorption among all the other dopant levels of Co_3O_4. It is interesting to note that values of standard errors for the average sorption of PANI materials doped with Co_3O_4 are acceptably and consistently low, which gives us more confidence in the validity of our experimental results.

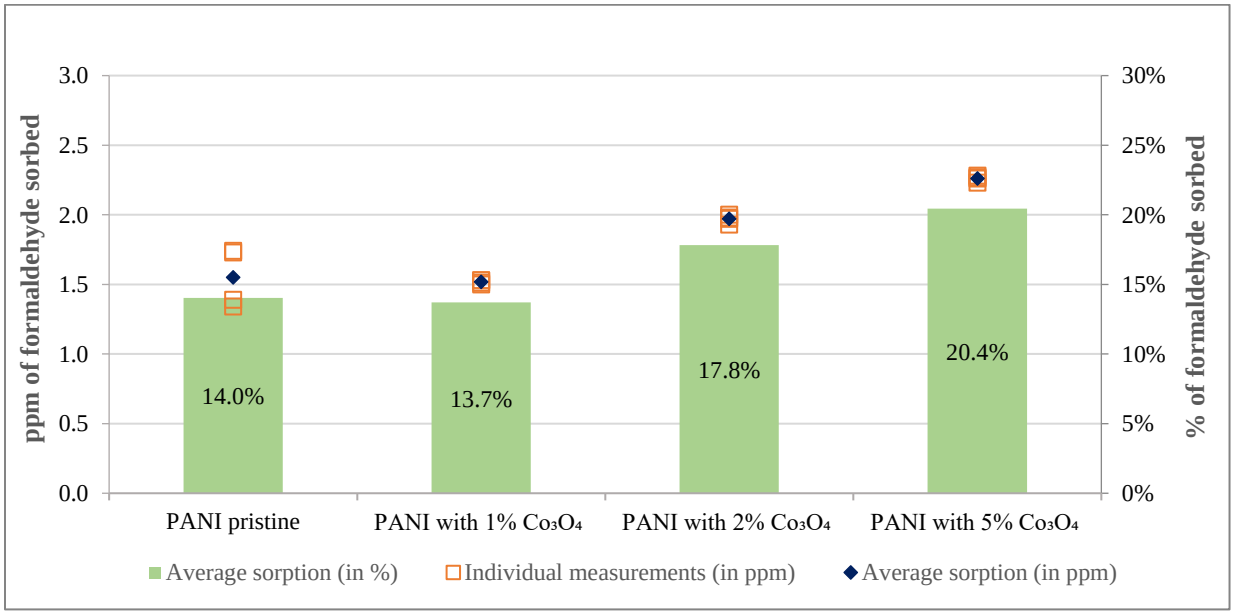

Figure 4.5: Formaldehyde sorption for PANI and PANI doped with Co_3O_4; (Source: F 11.1 ppm).

Table 4.5: Average sorption values (in ppm) for PANI doped with Co_3O_4.

Sensing Material	**Average Sorption ± se**	**Average Sorption ± 95% CI [Upper limit, Lower limit]**
PANI pristine	1.55 ± 0.215 ppm of F	1.55 ± 0.342 ppm of F [1.208, 1.892]
PANI with 1% Co_3O_4	1.52 ± 0.015 ppm of F	1.52 ± 0.024 ppm of F [1.496, 1.544]
PANI with 2% Co_3O_4	1.97 ± 0.029 ppm of F	1.97 ± 0.047 ppm of F [1.923, 2.017]
PANI with 5% Co_3O_4	2.26 ± 0.022 ppm of F	2.26 ± 0.034 ppm of F [2.226, 2.294]

Note: (1) Values following the ± sign indicate the estimate of one standard error (se) for the average sorption values; CI stands for confidence interval. (2) The coefficient of variation (defined as the ratio of standard deviation and mean) was calculated to be ~4% (on average) for this table.

4.1.7 Evaluation of PANI Materials with 5% of Metal Oxides

The results for the sorption behavior of PANI materials with four different metal oxides of SnO_2, TiO_2, Co_3O_4, and ZnO (at different dopant levels) have been discussed earlier. This section provides a comparison between all PANI materials with a dopant level of 5%.

As can be seen in Figure 4.6, PANI with 5% Co_3O_4 sorbs the highest amount of gas analyte (20.4%), followed by PANI with 5% SnO_2 with 19.3% sorption. If a metal oxide is added into the polymer backbone in situ, one hopes that the dispersion and aggregation of the metal oxide are going to enhance diffusion of the gas analyte. Not all metal oxides do that. In this case, the rectangular prism (tetragonal structure) of SnO_2 and the tetra- and octa-hedral interstices formed by Co_3O_4 seem to enhance sorption compared to the other materials. Incorporation of 5% ZnO into PANI improved sorption of the undoped PANI by only 1% (almost negligible change), while TiO_2 dopant showed an adverse effect, reducing the sorption by ~1%.

Based on the discussion above, both SnO_2 and Co_3O_4 seem to be promising dopants. The improvement in sorption behavior could be attributed to the effect of these dopants on the morphology of PANI, which will be discussed in more detail in Section 4.5.

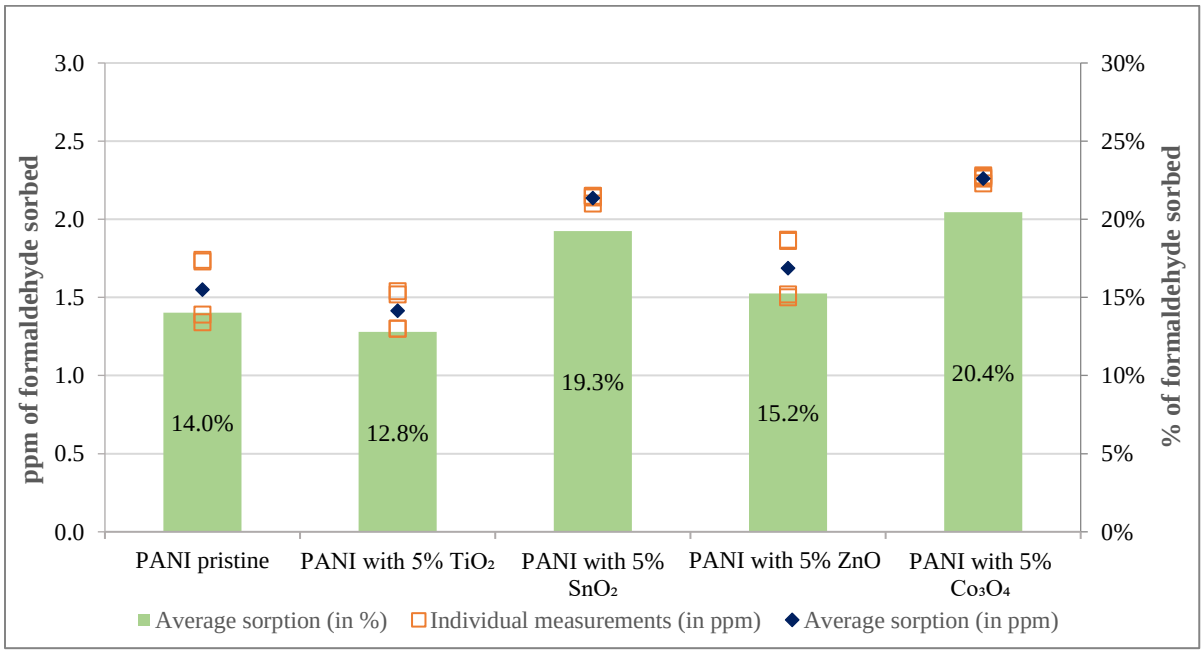

Figure 4.6: Formaldehyde sorption for PANI materials at 5% dopant level; (Source: F 11.1 ppm).

4.1.8 Evaluation of PANI Materials with 2.5% (or less) of Metal Oxides

In a way similar to the summary figure in section 4.1.7, Figure 4.7 compares formaldehyde sorption levels of PANI materials with 2.5% of different metal oxides. Figure 4.7 suggests that PANI with ZnO seems to have the highest sorption followed by PANI with Co_3O_4.

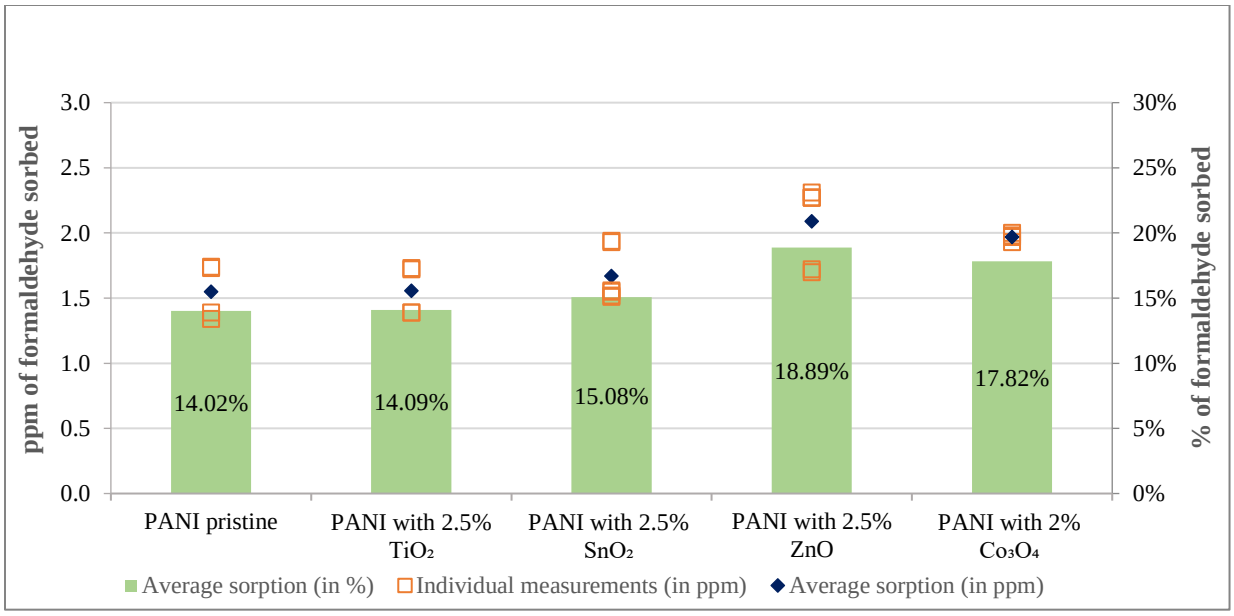

Figure 4.7: Formaldehyde sorption for PANI materials at dopant level of 2.5% (or less); (Source: F 11.1 ppm).

4.2 Stability Studies

Stability of a sensing material (and eventually of the final sensor) is another essential factor for evaluating the effectiveness of a sensing material for detection of an analyte. Sensor stability is described as the ability to exhibit a relatively consistent and reproducible signal over a long-enough period [69]. Stability studies may involve the effect of the testing environment (e.g., temperature, humidity, etc.) and aging on the performance of the sensing materials, and how to control the effect of these interferences. Stability is not frequently investigated in literature publications.

4.2.1 Effect of Aging

Given the luxury of long-term research, aging effects were studied for PANI, PANI with 5% SnO_2, and PANI with 5% TiO_2 to evaluate the stability of sensing materials. All the sensing materials were synthesized using the same recipe but by different operators. Sorption tests were also performed following the same procedure and by different operators in the lab, and also at different times. It can be seen from Figure 4.8 that PANI shows an average sorption of ~1.6 ppm over 8

months, PANI with 5% SnO_2 has an average sorption of ~2.1 ppm over 4 months, while PANI with 5% TiO_2 shows an average sorption of ~1.48 ppm over 7 months. We can say that the materials synthesized and tested have shown consistent performance over a period of six months. This observation is consistent with aging experimental data reported by Mavani and Penlidis [61] even over a much longer period (5 and 10 years).

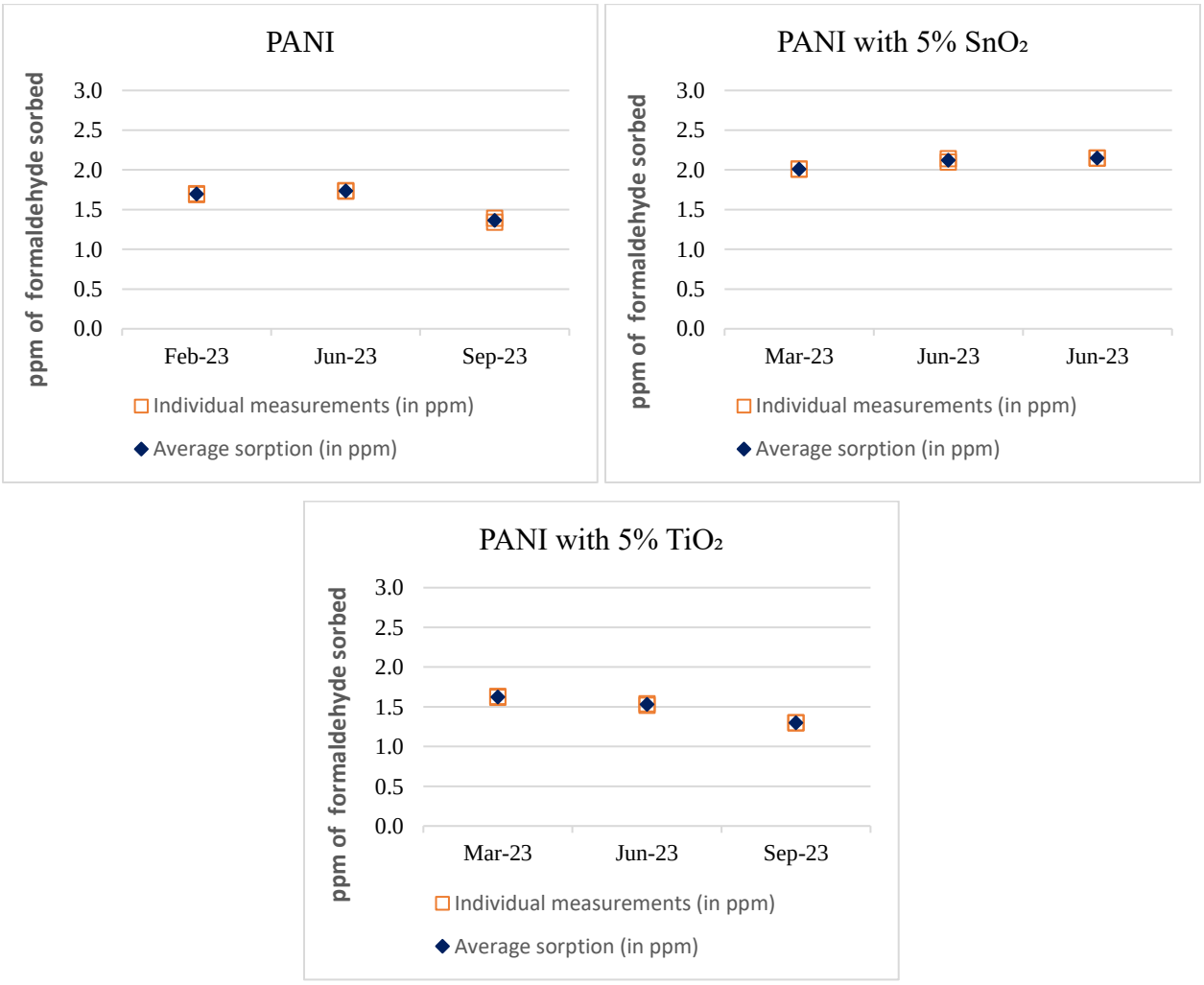

Figure 4.8: Sorption results from experiments performed in different months.

4.3 Raw Data Trends

Each GC sorption trial (run) with formaldehyde takes anywhere from 60 to 90 minutes, in sampling intervals of 12 minutes (see Figure 4.9 for plots of the raw data points, as measured and recorded by the GC set-up). The data points in Figure 4.9 for PANI with 5% SnO_2 came from the first sample of the day to be tested after 'blanks'. Trials with 'blanks' are conducted as the second step each day of experimentation. The first step each day is to purge the whole system with nitrogen for about 30 minutes. During blanks, F flows from the F cylinder (which is accurately calibrated and of known content) through the system but without passing the F stream over a sensing material. Hence, the GC records F in ppm as a check of the calibration curve, and this is taken as the baseline for the day.

In the first run of the day (right after blanks, with F flowing over the sensing material), the F level starts high and then approaches the final value, after having been given sufficient time to equilibrate. In other words, the F level with 5% SnO_2 starts at a high concentration very close to that of blanks (or source gas), close to 11 ppm, and decreases until it stabilizes after about 60 minutes. To evaluate the reproducibility of our results, a replicate run of PANI with 5% SnO_2 was performed at the end of the day when the concentration of formaldehyde starts from a lower concentration (again an echo from the previous sample/trial), but now with an increasing trend until it reaches steady state. These trends are evident in Figure 4.9, and they also confirm the very good reproducibility of our trials. Similar trends were obtained selectively for all GC trials, but not shown here for the sake of brevity.

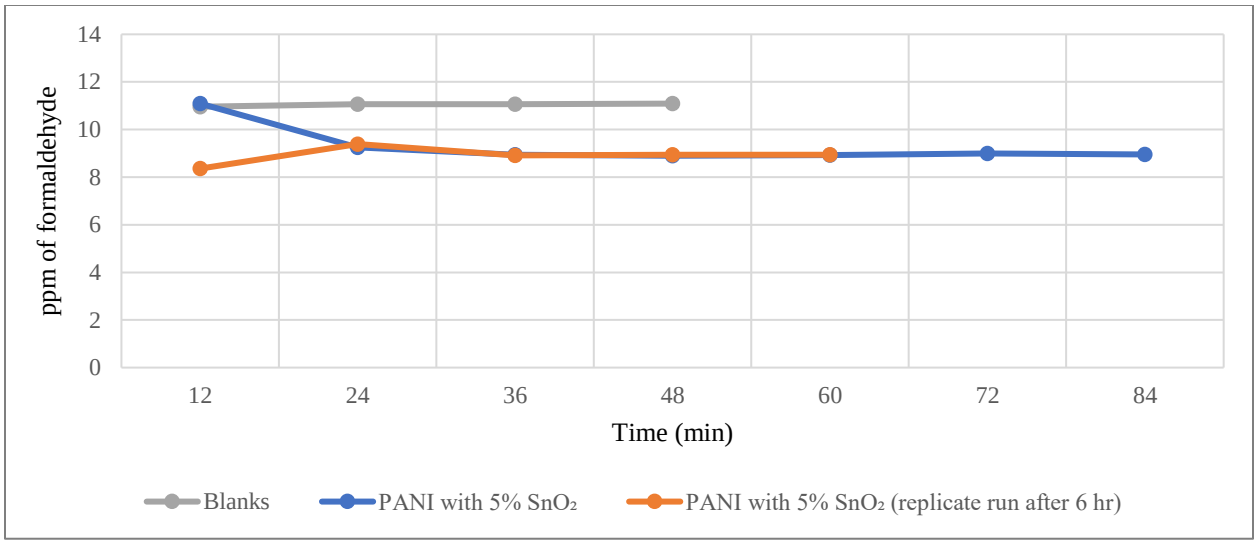

Figure 4.9: Raw data trends from F sorption runs of PANI with 5% SnO_2 and its replicate (about 6 hours difference between replicate runs); (Source: F 11.1 ppm).

4.4 Statistical Analysis

4.4.1 Analysis of Variance (ANOVA)

Analysis of variance (ANOVA) can be used to determine whether a statistically significant difference exists among the means (μ) of two or more samples. Thus, ANOVA was employed to compare means of gas concentrations (collected from GC) over different materials to determine if the variation between different types of polymeric materials is significantly larger than the variation within each polymeric material (variation 'within' represents typical background (inherent) error). ANOVA determines if at least one sample mean is different from the others.

In ANOVA tables, the value of $F_{observed}$ (denoted as $F_{obs.}$) is calculated and will be compared with the value of $F_{critical}$ (denoted as $F_{crit.}$) extracted from the corresponding F-table at a preselected significance level α (typically $\alpha = 0.05$). If $F_{obs.}$ is greater than $F_{crit.}$, then one is located in the rejection region of the null hypothesis, which states that there is no difference between treatments. Hence, it can then be concluded that there is a statistically significant difference between treatments. However, ANOVA cannot detect how different the treatments are (i.e., which treatments are different). For this to happen, another test has to complement the ANOVA analysis

(see Section 4.4.2). In the following sections, ANOVA analysis is presented for some representative cases.

4.4.1.1 ANOVA for PANI with 5% SnO_2 and its replicate

The analysis below is representative of the methodology adopted when analyzing our data and justifying comparisons. In this specific case, the analysis was done to show that there is no difference between the two trials plotted in Figure 4.9, and that the two data sets are actually coming from the same 'process'. Table 4.6 cites the collected data, whereas Table 4.7 shows the ANOVA results.

Table 4.6: Raw data points for PANI with 5% SnO_2 and its replicate, as plotted in Figure 4.9.

Time (min)	12	24	36	48	60	72	84	Total
Raw data (ppm of F) for PANI with 5% SnO_2	11.09	9.25	8.94	8.90	8.93	8.99	8.95	n = 7
Raw data (ppm of F) for PANI with 5% SnO_2 replicate	8.36	9.39	8.92	8.94	8.94			n = 5

Table 4.7: ANOVA table for the comparison of data sets in Table 4.6.

Source	**SS (Sum of Squares)**	**df (degrees of freedom)**	**MS (Mean Square)**	**Comparison of F values**
Between the treatments	0.42752381	2-1=1	0.427524	$F_{obs.} = 0.97471474$
Within the treatments	4.386142857	11-1=10	0.438614	$F_{1,10,0.05} = 4.96$
Total	4.813666667	12-1=11		$F_{obs.} < F_{1,10,0.05}$

From Table 4.7, one can see that $F_{observed}$ is less than $F_{critical}$ (from F-table at significance level of $\alpha = 0.05$). Therefore, there is no significant difference between the means in the two trials. This is in agreement with the visual representation of the two trials in Figure 4.9. Given the data in Table 4.6, equations for calculating the ANOVA table entries for SS, df and MS are shown in Appendix E (section E2). Note that all the ANOVA tables throughout the thesis were constructed following the procedure and sample calculations presented in Appendix E (section E2).

4.4.1.2 ANOVA for undoped PANI and PANI with 5% TiO_2

Table 4.8 sites the raw data for this comparison. Table 4.9 contains the ANOVA comparison results. Since $F_{observed}$ is less than $F_{critical}$, the concluding remark here is that the two materials sorb about the same amount, as per the discussion around Figure 4.3 and Table 4.3.

Table 4.8: Raw data points for undoped PANI and PANI with 5% TiO_2.

Time (min)	12	24	36	48	60	72	84	96	Total
Raw data (ppm of F) for PANI with 5% TiO_2	8.53	9.34	9.41	9.45	9.47	9.47	9.55	9.57	n = 8
Raw data (ppm of F) for undoped PANI	8.74	9.33	9.22	9.30	9.33	9.35	9.36		n = 7

Table 4.9: ANOVA table for data sets in Table 4.8.

Source	**SS (Sum of Squares)**	**df (degrees of freedom)**	**MS (Mean Square)**	**Comparison of F values**
Between treatments	0.05014	2-1=1	0.05014	$F_{obs} = 0.59280$
Within treatments	1.09963	14-1=13	0.08459	$F_{1,13,0.05} = 4.67$
Total	1.14977	15-1=14		$F_{obs} < F_{1,13,0.05}$

4.4.2 Multiple Comparison Using Fisher's Least Significant Difference (LSD)

A very useful tool for multiple comparisons is Fisher's least significant difference (LSD). It is a more rigorous test for evaluating the difference between polymers (treatments), which can be specially performed when the ANOVA analysis reveals that there are statistically significant differences between treatments. As mentioned earlier, ANOVA only determines if there is a significant difference between the means of at least one pair of treatments, but it cannot distinguish which pairs/treatments are different from one another. Therefore, the LSD test was performed to determine which pairs of means show a difference and quantify that difference. LSD represents the value at which the difference between two means becomes significant. If the difference between two means (of two polymers/treatments) exceeds the value of LSD, then there is a

significant difference between the two polymers/treatments. The equations used for the LSD test are also listed in Appendix E (section E3).

Sorption results of PANI materials with dopant content of 2.5% (or less) and 5% (i.e., all the doped polymers discussed in sections 4.1.7 and 4.1.8) were analyzed using ANOVA and Fisher's LSD, and the analysis results are presented in the following tables. First, the 8 doped polymers (see Table 4.11) were analyzed by ANOVA to determine whether there was a statistically significant difference between polymers (see Table 4.10). ANOVA revealed that there was a statistically significant difference between at least one pair of the means ($F_{obs.} > F_{crit.}$). Therefore, the Fisher's LSD test was then employed to identify which means were different (see Table 4.12). Highlighted rows (in yellow) are those polymers whose average sorptions are significantly different. In other words, given the measured data and the inherent underlying error, we can distinguish between them. Since the calculated LSD in Table 4.12 is about 0.4, any difference between the different pairs (or among all processes/treatments compared) that exceeds the LSD is detectably significant.

Table 4.10: ANOVA comparing formaldehyde sorption on PANI doped with different metal oxides.

Source of Variation	**SS**	**df**	**MS**	**$F_{obs.}$**	**$F_{crit.}$ ($F_{7,28,0.05}$)**
Between Polymers	2.8032	8-1= 7	0.4005	11.8399	2.3593
Within Polymers	0.9470	35-7= 28	0.0338		
Total	3.7502	36-1= 35		**$F_{obs.} > F_{crit.}$**	

Table 4.11: Summary of polymer designations, their averages, and standard errors.

	Polymer	**# of Readings**	**Average (ppm)**	**Standard Deviation**
A	PANI 5% TiO_2	4	1.415	0.1330
B	PANI 5% SnO_2	4	2.135	0.0238
C	PANI 5% ZnO	4	1.6875	0.2052
D	PANI 5% Co_3O_4	4	2.26	0.0216
E	PANI 2.5% TiO_2	4	1.5575	0.1935
F	PANI 2.5% SnO_2	6	1.6683	0.2074
G	PANI 2.5% ZnO	6	2.09	0.2948
H	PANI 2% Co_3O_4	4	1.97	0.0294

Table 4.12: Multiple comparisons using Fisher's LSD related to Table 4.11.

Mean Comparison				Steps towards LSD Calculation	
A-B= 0.72	B-D= 0.125	C-G= 0.4025	E-H= 0.4125	[k(k-1)]/2	28
A-C= 0.2725	B-E= 0.5775	C-H= 0.2825	F-G= 0.4217	α	0.0018
A-D= 0.845	B-F= 0.4667	D-E= 0.7025	F-H= 0.3017	α/2	0.0009
A-E= 0.1425	B-G= 0.045	D-F= 0.5917	G-H= 0.12	s.e.	0.1226
A-F= 0.2533	B-H= 0.165	D-G= 0.17		t (α/2, df_w)	3.453
A-G= 0.675	C-D= 0.5725	D-H= 0.29		**LSD**	**0.4234**
A-H= 0.555	C-E= 0.13	E-F= 0.1108			
B-C= 0.4475	C-F= 0.0192	E-G= 0.5325			

Note: Highlighted rows indicate polymers that have means significantly different from one another; df_w is degrees of freedom 'within' polymers.

4.5 Characterization of Sensing Materials

After evaluating the sorption characteristics of different polymeric materials, the pristine polymers of PANI, PPy, PTh, and PVP, along with PANI nanocomposites doped with SnO_2, Co_3O_4 and a combination of TiO_2 and SnO_2, were characterized using different techniques. SEM and TEM were used to study morphology and 'locate' metal oxide dopants in nanocomposites, whereas the incorporation of metal oxides into the polymer matrix was analyzed using EDX. Pristine PANI was further characterized BET technique to analyze the polymer surface area. Dynamic light scattering (DLS) was also used to measure the particle size of both undoped and doped PANI.

4.5.1 Surface Morphology and Dopant Incorporation (SEM/EDX/TEM)

4.5.1.1 Pristine Polymers

All the pristine polymers compared in section 4.1.1 were characterized by SEM imaging to explore their surface morphology. As seen in Figure 4.10-a, pristine PANI shows a fibrous structure with filaments intertwined with each other. This morphology likely creates sufficient free volume (interstitial space) that is required for analyte diffusion and helps with analyte 'entrapment' within the interstices, which in its turn promotes potential interactions between a sensing material (i.e., the active sites or 'hot spots' of a sensing material) and an analyte. PPy, on the other hand, reveals

a globular structure (see Figure 4.10-b) that may possess a smaller surface area than the fibrillar structure of PANI. Therefore, there may be less active surface area (hence, fewer active/sorption sites) available for possible interactions of the polymer and the target analyte, which may explain the poor sorption of PPy towards formaldehyde.

However, one must note that material with enough interstitial space may still show poor sorption towards a specific analyte, alluding to the point that even if an analyte manages to diffuse and move into a material's interstitial space, no sorption will be detected unless there is sufficient interaction (affinity) taking place between the polymer functional groups and those of the analyte. For example, PPy was shown to have a higher sorption towards acetone than PANI [70], suggesting that favorable interactions between PPy and acetone were taking place that could help physisorption. Therefore, it can be suggested that the presence of interstitial space (pores and cavities) is necessary for analyte diffusion, but it is not necessary and sufficient for sorption.

The SEM image of PTh indicates flat and short rods that have formed irregular "starfish-like" shapes at some spots (see Figure 4.10-c). The morphology seems to be quite compact, suggesting that there is not enough free volume for the analyte to diffuse into the core of the sensing material. On the other hand, the surface of PVP (Figure 4.10-d) consists of what looks like 'polished/smooth stones' with almost no interstices, which supports its limited sorption capability.

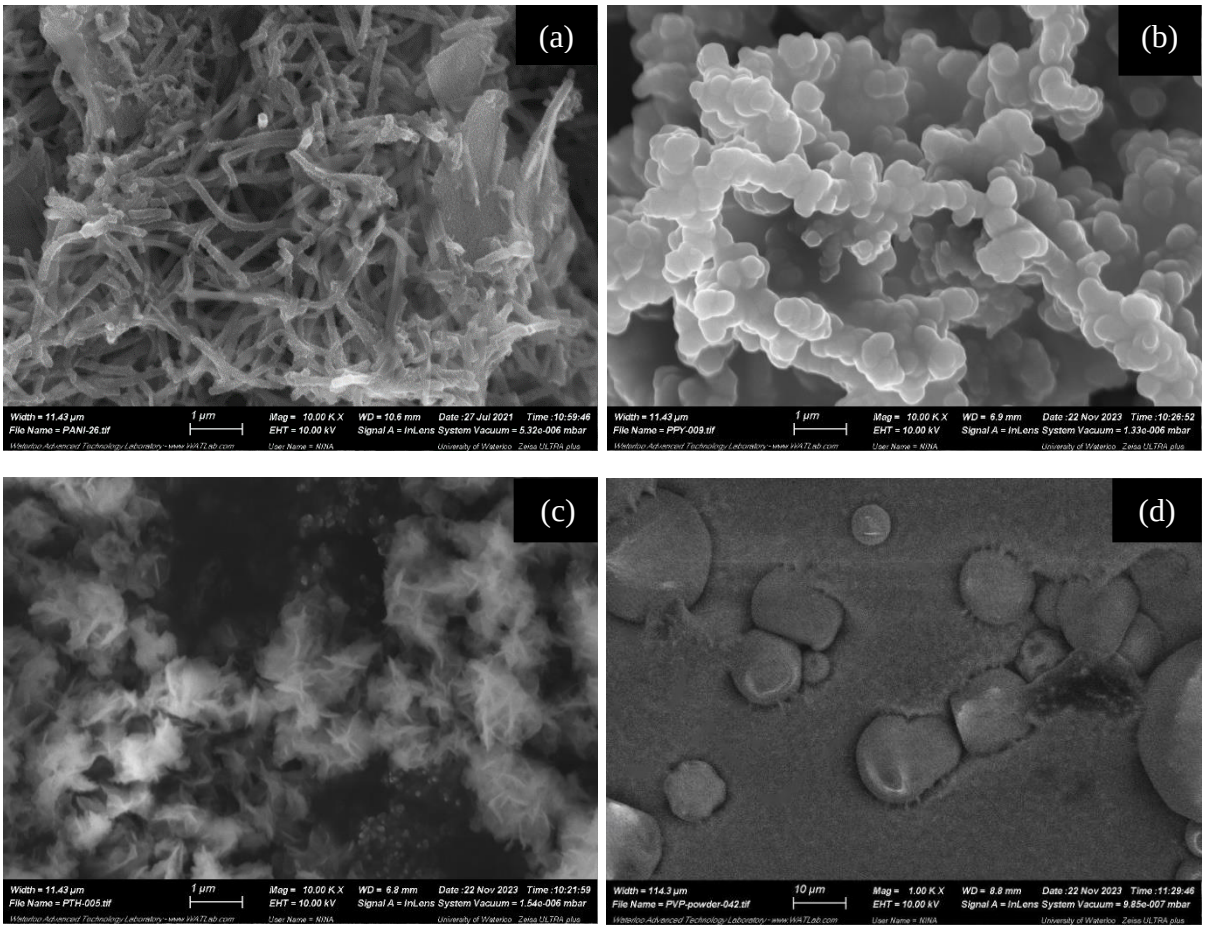

Figure 4.10: SEM images of (a) pristine PANI, (b) PPy, (c) PTh, (d) PVP; Note: (a, b, c) at 10000X magnification, (d) at 1000X magnification.

PANI (as the reference 'base case' material) and PPy were chosen for further morphology characterization by TEM. Figure 4.11 and Figure 4.12 show TEM images of PANI and PPy, respectively. From the images presented in Figure 4.11 (a and b), one can see a fibrous network with fibers stacked together in some spots, while the fibrous structure in images c-f (Figure 4.11) is mostly evident from spikes on the edges of the sample. This fiber-like morphology was also observed earlier in the SEM images of PANI (Figure 4.10-a). Moreover, comparing TEM and SEM images of PPy further confirms the globular/spherical morphology of PPy (see Figure 4.12).

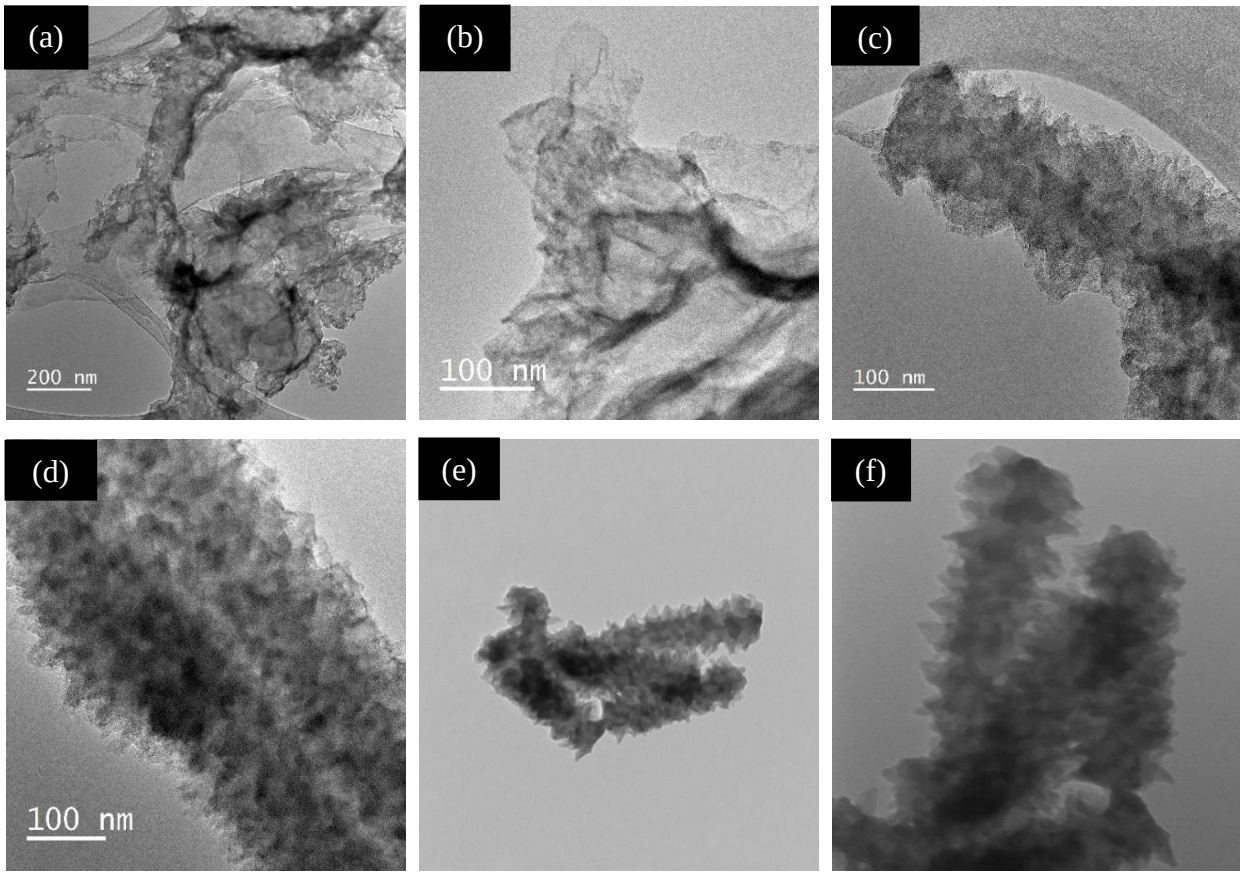

Figure 4.11: TEM images of PANI at different magnifications.

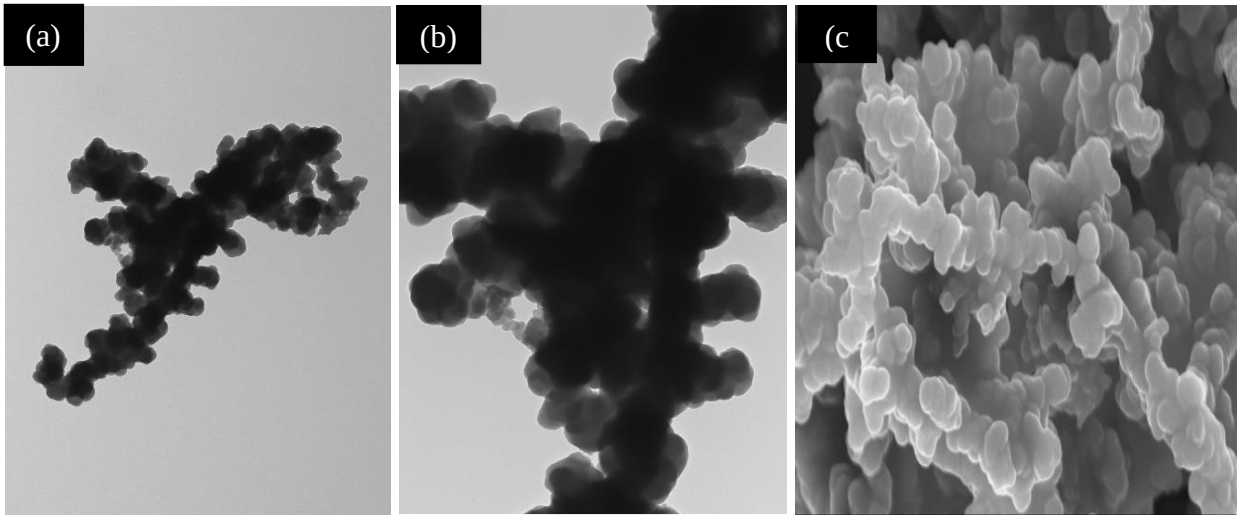

Figure 4.12: (a) and (b) TEM images of PPy, (c) SEM image of PPy.

4.5.1.2 PANI Doped with SnO_2 and TiO_2

Three samples of PANI polymers with 5% SnO_2, 5% TiO_2 and (5% SnO_2+2.5% TiO_2) were compared and analyzed with respect to their surface morphology and metal oxide incorporation. These concentrations of dopants reflect the amount of metal oxide added during synthesis, with respect to the total polymer weight (e.g., PANI with 5% SnO_2 indicates the presence of 5% SnO_2 and 95% of aniline monomer). The actual amount of metal oxide incorporated into the polymer matrix was determined using EDX analysis for further verifications and the data obtained have been summarized in Table 4.13. The results of incorporation analysis appear to be acceptable. Note that the wt.% of the metal oxide measured by EDX is usually lower than the amount specified in the recipe due to experimental errors in the dispersion of metal oxide during synthesis (perfect integration of metal oxide into polymer matrix cannot be always expected) and detection limitations of EDX analysis.

Table 4.13: Summary of EDX analysis for PANI with metal oxides of SnO_2 and TiO_2.

Polymer nanocomposite showing wt.% of metal oxides used during synthesis	**Actual wt.% of metal oxide incorporated measured by EDX**
PANI with 5% SnO_2	SnO_2 = 5.32%
PANI with 5% TiO_2	TiO_2 = 4.59%
PANI with (5% SnO_2+2.5% TiO_2)	SnO_2 = 4.14%, TiO_2 = 1.51%

Figure 4.13 represents SEM images of the samples presented in Table 4.13 while also including pristine PANI as a base material for comparison. The addition of SnO_2 nanoparticles seems to have changed the morphology of PANI (Figure 4.13-a) from a totally entangled fibrous structure to a mixture of flaky and 'spongy' segments (sometimes with serrated edges), while having shorter and fewer filaments compared to undoped PANI. This morphology formed a more porous surface and thus created more interstitial space for the diffusion of analyte molecules to sensing sites available. This morphology modification explains the better sorption performance of PANI with 5% SnO_2 (see Figure 4.4).

Figure 4.13-b is a representative image of PANI with 5% TiO_2. The distinct fibrous structure of undoped PANI with long and entangled filaments is no longer present, suggesting that the surface area has decreased. On the other hand, the morphology does not seem to be as porous as PANI with 5% SnO_2, thus supporting the poor gas sorption capabilities of TiO_2-doped PANI (see Figure 4.3).

When PANI is doped with a mixture of 5% SnO_2 and 2.5% TiO_2 (Figure 4.13-c), the morphology seems to have evolved to more densely packed and highly agglomerated particles (again with no fibrous network). The surface of particles (clusters) seems to be smooth and quite polished. Therefore, it is suggested that there is not enough free volume and pores available for the gas molecules to move freely through the material and bond with active sites. Hence, it may be suggested that the addition of 2.5% TiO_2 to the composite of PANI with 5% SnO_2 hampered the gas sorption performance (see section 4.1.5) via (undesirable) morphology deterioration.

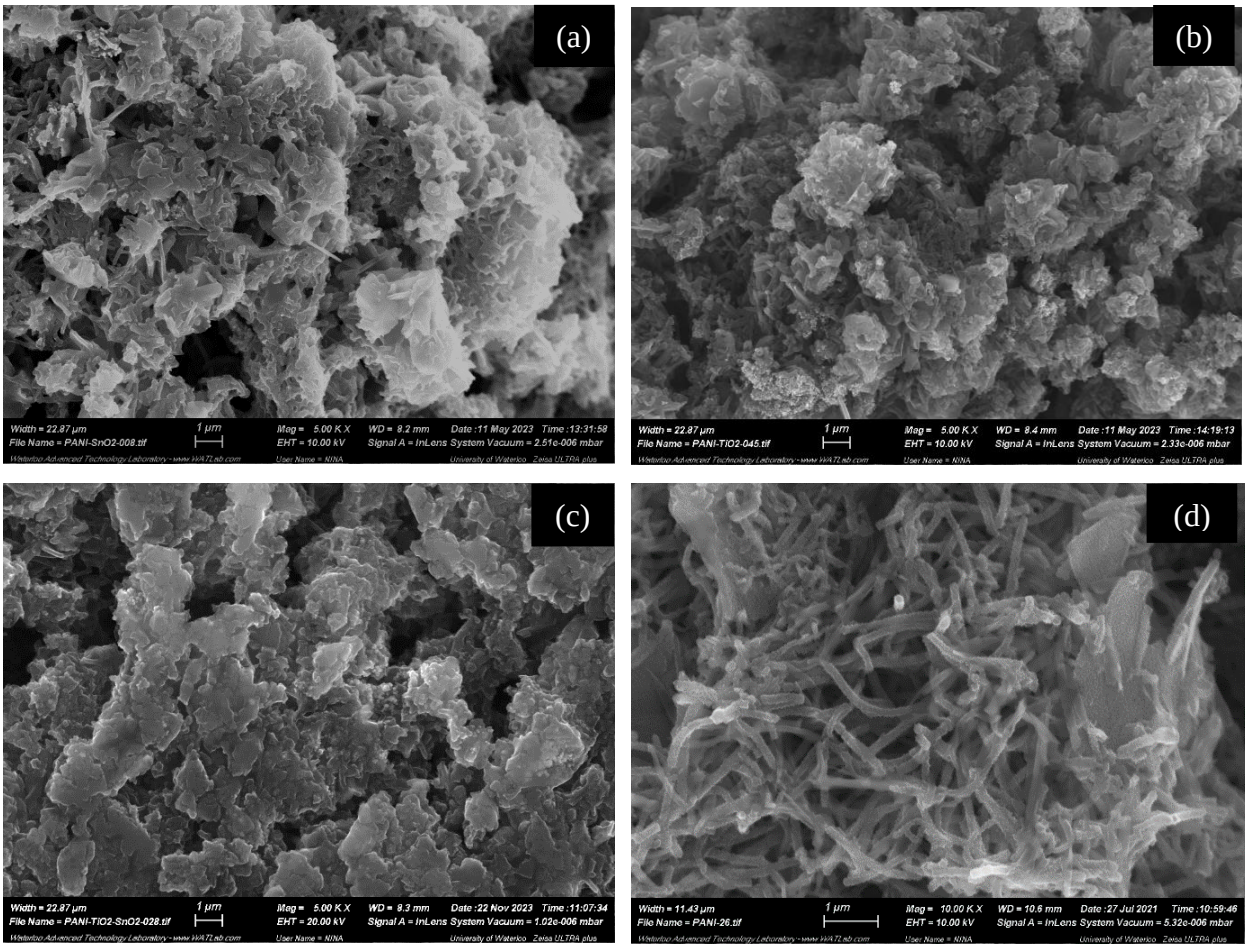

Figure 4.13: SEM images of (a) PANI with 5% SnO_2, (b) PANI with 5% TiO_2, (c) PANI with (5% SnO_2+2.5% TiO_2), (d) pristine PANI. Note: (a), (b), and (c) at 5000X magnification; (d) at 10000X magnification.

Among the materials in Figure 4.13, PANI with 5% SnO_2 was selected for further imaging using TEM to see if the presence of metal oxide could be captured and spotted in the nanocomposite. Figure 4.14 shows distinct darker (black) regions in the polymer matrix which can be attributed to SnO_2 nanoparticles. While some images show the encapsulation of SnO_2 by PANI (Figure 4.14-a, c, d), other images (Figure 4.14-b, e, f) depict the presence of SnO_2 on the edges of the PANI network. It may be speculated that when SnO_2 is encased by PANI, the lack of possible contact of the metal oxide with the analyte may result in no sorption enhancement. Therefore, improved sorption capabilities possibly result from those spots where SnO_2 nanoparticles can come in contact with the analyte and interact with it. Such an enclosed structure has also been reported by many researchers in the literature [71] [72]. SnO_2 exhibits the so-called rutile structure (like a

rectangular prism), which leaves a lot of space for gas molecules to move through the structure and coordinate with the hydrogen and oxygen atoms of formaldehyde. Moreover, a "millipede-like" structure can be seen in images (b), (e), and (f) (Figure 4.14), which is similar to what was observed earlier in the TEM images of pristine PANI (see Figure 4.11-c, d, f), confirming the presence of PANI as the base component in the nanocomposite.

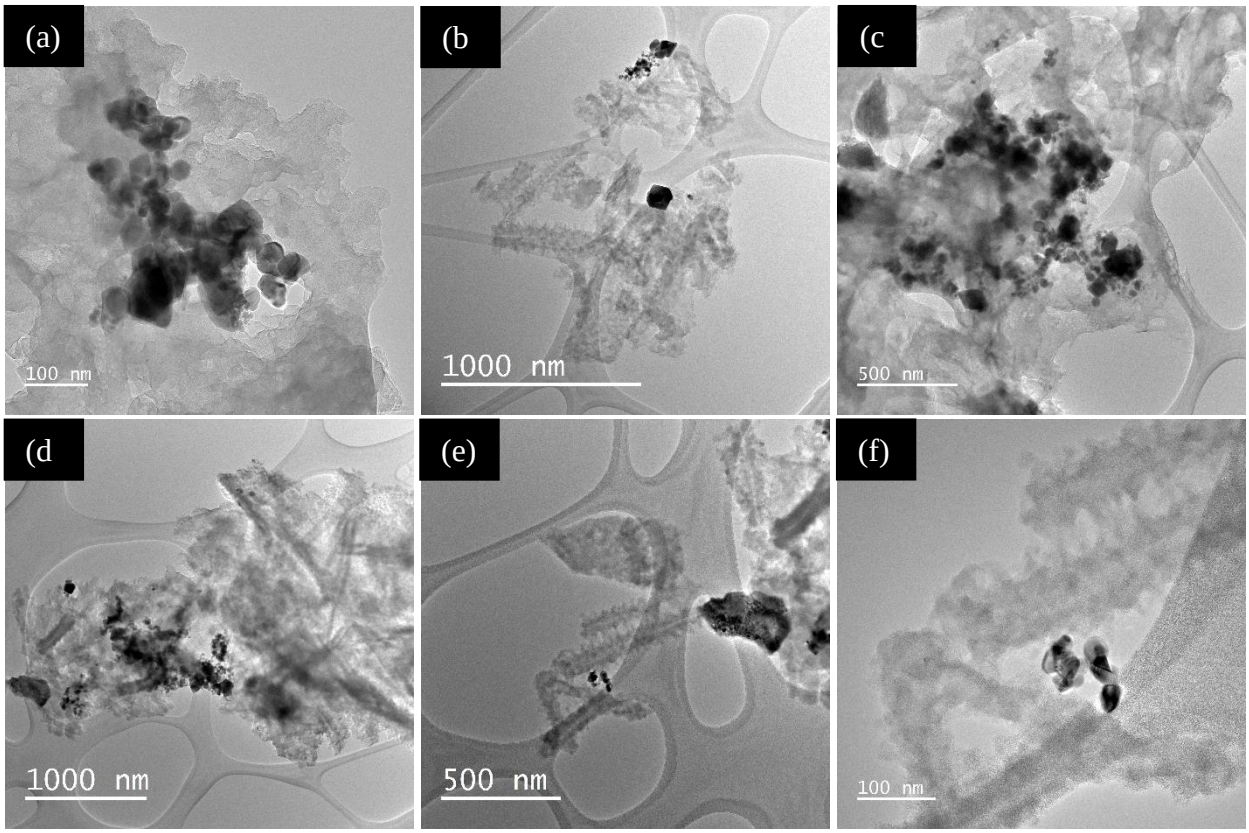

Figure 4.14: TEM images of PANI with 5% SnO_2 at different sections of the sample.

4.5.1.3 PANI Doped with Co_3O_4

Figure 4.15 includes SEM images of pristine PANI and PANI with 2% Co_3O_4. As seen in Figure 4.15-a, pristine PANI shows fibrous structures entangled in each other, which are sometimes located in between twisted sheets, forming cavities and interstitial space. It can be seen that the incorporation of Co_3O_4 into PANI has affected the surface morphology. Figure 4.15-b (lower magnification) shows the presence of filament-like structures to a lesser extent (maybe because the filaments look thicker and shorter), while having some "cauliflower-type" clusters. The higher

magnification image (Figure 4.15-c) reveals a distinct “rose-shaped” spot and a “valley-shaped” region formed by two twisted sheets/plates. This open structure observed in the morphology of PANI with 2% Co_3O_4 is probably creating more ‘holes’ and cavities (also seen in Figure 4.15-d), which is favorable for the diffusion of analyte molecules within the microstructure of the sensing material in their attempt to find the so-called “hot spots” (active sites for sorption). Therefore, the higher sorption of PANI with 2% Co_3O_4 (see Figure 4.5) may be corroborated by the corresponding SEM images.

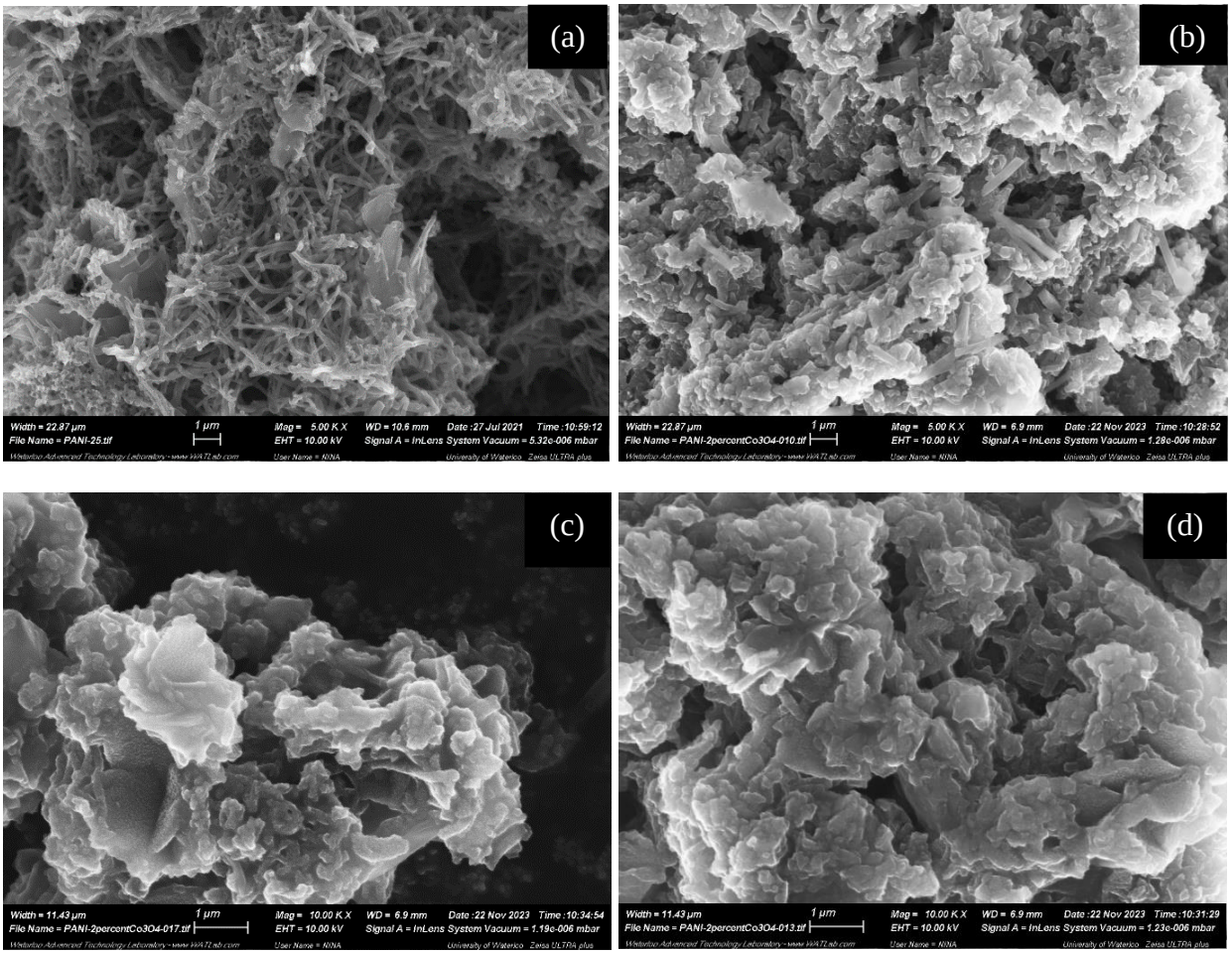

Figure 4.15: SEM images of (a) pristine PANI, (b) PANI with 2% Co_3O_4 at 5000X magnification; (c) & (d) PANI with 2% Co_3O_4 at 10000X magnification.

SEM images of PANI with 5% Co_3O_4 are shown in Figure 4.16. Increasing the Co_3O_4 content from 2% to 5% has interestingly affected the morphology. One can see that a fibrillar morphology

is dominating in the composite containing 5% Co_3O_4, suggesting that higher amounts of Co_3O_4 nanoparticles have an influence on 'guiding' the formation of PANI nanofibers. Similar information about morphology of PANI containing Co_3O_4 can also be found in the literature [29]. The interconnectivity and porosity within a fibrillar structure contribute to a higher surface area and facilitation in diffusion of gas molecules, which may support superior gas sorption of PANI with 5% Co_3O_4 (as in Figure 4.5).

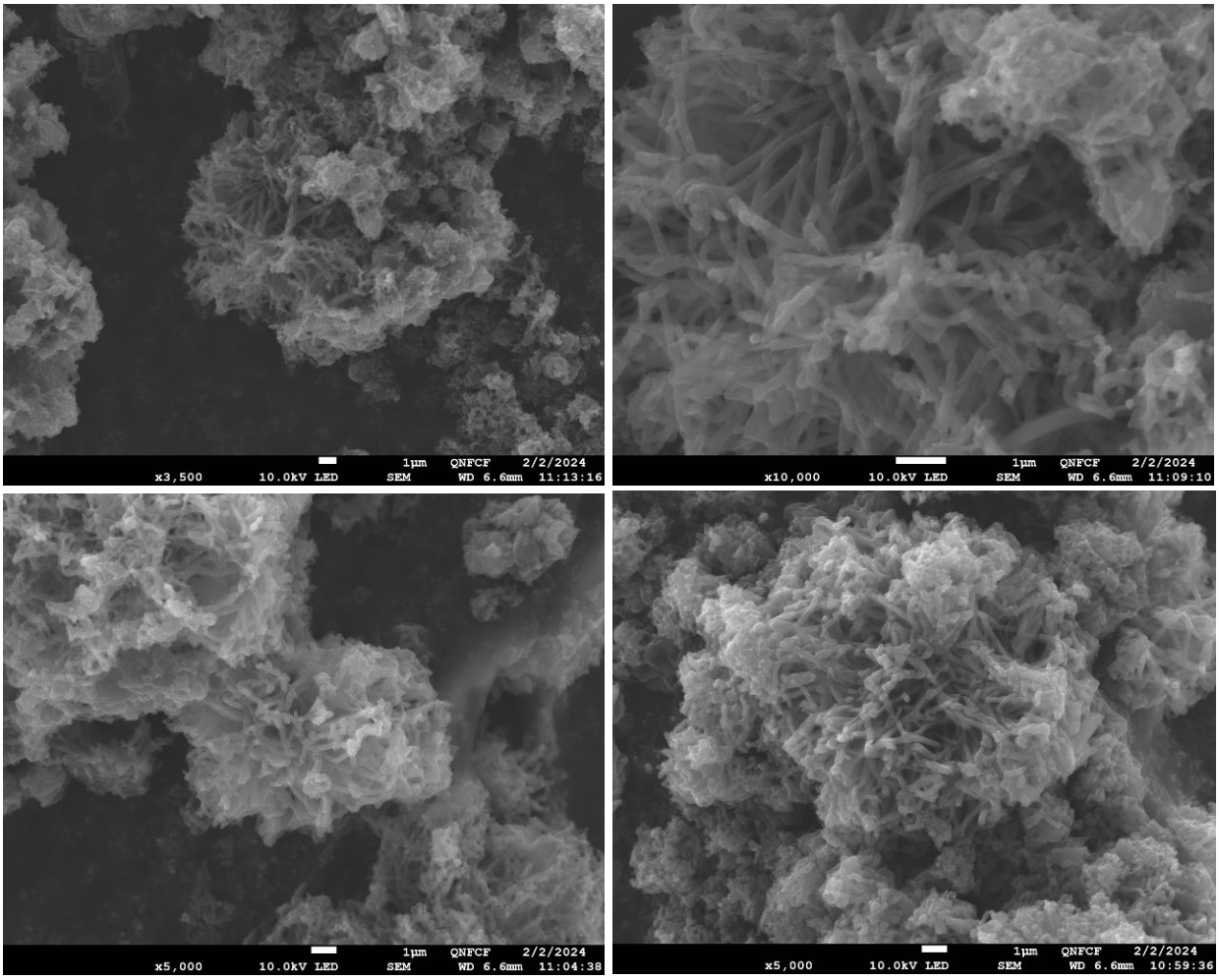

Figure 4.16: SEM images of PANI doped with 5% Co_3O_4 at different magnifications.

The presence of Co_3O_4 nanoparticles in the PANI matrix was confirmed by EDX analysis (see Table 4.14). When 2% Co_3O_4 was used during synthesis, EDX analysis detected 0.78% of Co_3O_4 in the sample. However, for PANI with 5% Co_3O_4, the incorporation measurement was a bit higher

than the amount available during synthesis. One may argue that metal oxide content cannot be higher than what was originally present in the synthesis recipe, but one should note that EDX usually analyzes a sample based on localized composition measurements without necessarily including the surrounding matrix material, potentially introducing an inherent error in EDX analysis. This is especially more evident in heterogeneous samples where the metal oxide is not evenly distributed in the polymer matrix. More discussion on heterogeneity of the sample is presented when analyzing the TEM images of PANI with 5% Co_3O_4 (as per Figure 4.17).

Table 4.14: Summary of EDX analysis for PANI with Co_3O_4.

Polymer nanocomposite showing wt.% of metal oxide used during synthesis	**Actual wt.% of metal oxide incorporated measured by EDX**
PANI with 2% Co_3O_4	Co_3O_4 = 0.78%
PANI with 5% Co_3O_4	Co_3O_4 = 7.34%

The TEM images of PANI with 5% Co_3O_4 captured the presence of Co_3O_4 in the polymer matrix. The black granules evident in Figure 4.17 (a-f) are indicating Co_3O_4 nanoparticles surrounded by PANI. Note that images a-c and images d-f are showing two different regions of the sample at different magnifications. Moreover, the 'millipede-like' or 'worm-like' structure seen earlier in TEM images of pristine PANI can also be observed in Figure 4.17 (see especially images (a), (b), and (g-i)). Co_3O_4 nanoparticles seem to have a particle size ≤50 nm in the polymer matrix, which is in agreement with data provided by the commercial supplier of the metal oxide.

Figure 4.17 (especially images (a) and (d)) also shows that the metal oxide does not look evenly dispersed in the polymer matrix. Tendency of the metal oxide nanoparticles to form agglomerates and/or aggregates when dispersed in aqueous media during the synthesis of PANI is apparent in images of the first and second rows of Figure 4.17, giving the final polymeric material a heterogeneous property. On the other hand, there seem to be no metal oxide nanoparticles in images (g-i), again suggesting that composites may suffer from uneven (vs. even or good) distribution of metal oxide nanoparticles.

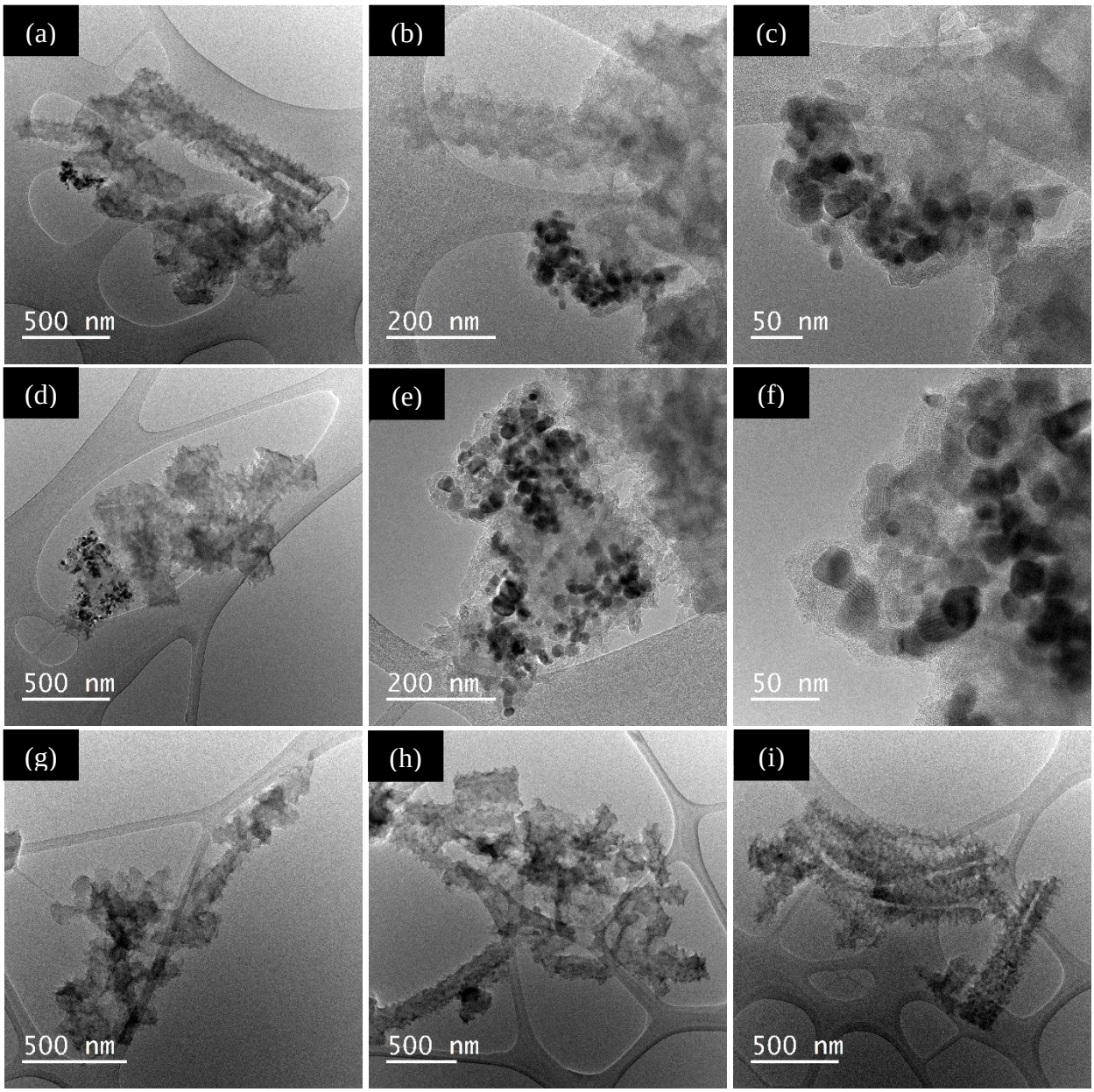

Figure 4.17: TEM images of PANI with 5% Co_3O_4 taken form different sections of the sample.

4.5.2 Particle Size Analysis (DLS)

Dynamic light scattering (DLS) was performed to find the sizes of selected polymers, and the results obtained have been summarized in Table 4.15 and Table 4.16. PANI sample in NMP (N-methyl-2-pyrrolidone) solvent was shown to have smaller size with an average of ~356 nm, followed by PANI in water and THF with size averages of ~574 nm and ~957 nm, respectively. The differences in size of PANI when different solvents were used can be explained by sample

aggregation. PANI in water and THF (Tetrahydrofuran) seem to form aggregates after a while in the cuvette inserted in the DLS machine, therefore, larger size values for polymeric nanoparticles were determined by DLS. As suggested earlier in [66], NMP is the 'best' solvent for PANI, hence, it makes sense that PANI in NMP is showing better dispersion and a smaller particle size.

Table 4.15: Summary of particle size measurements for PANI in different solvents.

Sample Name	Solvent	Diameter (in nm)		
		Measurement 1	**Measurement 2**	**Measurement 3**
PANI	NMP	359.7	331.7	378.2
PANI	Water	572.1	566.8	582.3
PANI	THF	617.9	1072	1180

Note: NMP= N-methyl-2-pyrrolidone, THF= Tetrahydrofuran.

Incorporation of tin oxide (as a dopant) into polyaniline results in a polymer nanocomposite with a smaller particle size as measured by DLS (see Table 4.16). The presence of tin oxide particles within the polyaniline matrix can lead to steric hindrance, which can prevent the agglomeration of polyaniline chains, leading to smaller particle sizes. The other potential reason for the observed reduction in particle size is that tin oxide can serve as nucleation centers during the polymerization process of aniline. The presence of these centers can lead to a higher nucleation rate, which results in the formation of more, but smaller, polymer particles compared to a system without such centers.

Particle size of a commercial PPy sample (bought from Sigma Aldrich) was also evaluated using DLS. The analysis revealed an average particle size of ~1047 nm. This large particle size measured is again attributed to aggregation in the polymeric solution (PPy in NMP), therefore, it may be suggested that NMP was not the best solvent for PPy.

Table 4.16: Summary of particle size measurements for different polymers, all in NMP solvent.

Sample Name	Solvent	Diameter (in nm)		
		Measurement 1	**Measurement 2**	**Measurement 3**
PANI	NMP	359.7	331.7	378.2
PANI with 5% SnO_2	NMP	287.4	262.8	275.3
PPy (commercially bought sample)	NMP	1080	1079	982.4

4.5.3 Surface Area Analysis (BET)

As described earlier in 3.4.5, the BET test is commonly used in experimental characterization of surface areas because it only requires knowledge of the adsorption isotherm. The adsorption isotherm describes the relationship between the amount of gas adsorbed (in mol/g) and the equilibrium relative pressure (p/p^{o}) at a constant temperature. The equilibrium relative pressure is the ratio of the pressure (p) to the saturation pressure (p^{o}) of the pure adsorptive gas at the operational temperature [73]. By analyzing the adsorption data at different relative pressures, the BET method allows for the calculation of the monolayer coverage of gas molecules on the material's surface.

Among different polymer backbones tested, PANI exhibited superior sorption capability to formaldehyde (see section 4.1.1), hence, pristine PANI was analyzed for the BET surface area. In addition, PANI with 1.25% In_2O_3 was selected for BET analysis as a metal oxide-doped polymer as it was observed to have a good formaldehyde sorption [61]. This enabled us to compare the BET surface area of pristine PANI with that of a doped PANI.

Table 4.17 consists of the average BET surface area, one standard error and 95% confidence intervals [74]. Pristine PANI seems to have a higher BET surface area than its doped counterpart. The reduction in the surface area in a doped/modified polymer may be attributed to the smaller metal oxide particles blocking the polymer substrate pores [75] or metal oxide agglomeration [76]. Therefore, it is important to note that enhancement in gas sorption performance of a polymeric sensing material when metal oxides are incorporated into the polymer matrix cannot be exclusively linked to available surface area. We may again come to the same conclusion that although accessible surface area and sorption capability are related, other influential factors like the interaction between the analyte and active sites of the polymeric material may be dominating in shaping the sorption characteristics of these materials (see also section 4.5.1.1).

Table 4.17: Summary of BET surface area analysis for PANI and PANI doped with of In_2O_3 [74].

Sample Name	**Average BET surface area ± se (m^2/g)**	**95% Confidence Interval (m^2/g)**
PANI	37.14 ± 9.19	[28.64, 45.64]
PANI with 1.25% In_2O_3	29.17 ± 5.56	[27.27, 36.08]

4.6 MEMS Sensor Testing for Ethylene

After identifying, synthesizing, and characterizing the most promising sensing materials for gas detection applications, the final step of evaluation takes place with an actual MEMS sensor. For this purpose, six potential materials (as presented in Table 4.18) for sensing ethylene were prepared and provided to our collaborators in the Department of Systems Design Engineering for testing the detector materials with the actual MEMS sensor in a specifically designed testing chamber. Note that trials with some sensing materials failed (at the deposition stage) due to adhesion issues in the deposition process; in such cases, the sensing materials have been specified with an X in Table 4.18.

Table 4.18: Shortlisted sensing materials for MEMS sensor application for ethylene.

Sample name	**Adhesion to sensor**
PANI with 5% SnO_2	Yes
PANI with 5% ZnO	Yes
PPy	Yes
PANI pristine	X
PVP	X
PTh	X

The data of sensor testing was collected from Yasser Shama (Ph.D. candidate at the Department of Systems Design Engineering) and sensor responses have been summarized in Table 4.19. Note that the time period from synthesis of the polymeric materials to polymer deposition to testing the MEMS sensor is substantial; the effort may take anywhere from 8 to 12 months (depending on prior experience with deposition). The representative frequency-response curves of two sensors functionalized with sensing materials of PANI with 5% SnO_2 and PPy can also be seen in Figure

4.18 and Figure 4.19, respectively. One can see that PPy exhibits a larger frequency shift upon exposure to 50 ppm ethylene. The frequency shifts observed in PANI with 5% SnO_2 and PANI with 5% ZnO were close to each other. The larger frequency shift means a larger sensor signal resulting from higher gas sorption in the sensing material. Therefore, one can say that PPy sorbed the highest amount of ethylene, hence, it seems to be more sensitive towards ethylene.

Table 4.19: MEMS sensor response to 50 ppm ethylene for different sensing materials.

Sample Name	**Frequency Shift (in Hz)**
PANI with 5% SnO_2	39
PANI with 5% ZnO	34
PPy	67

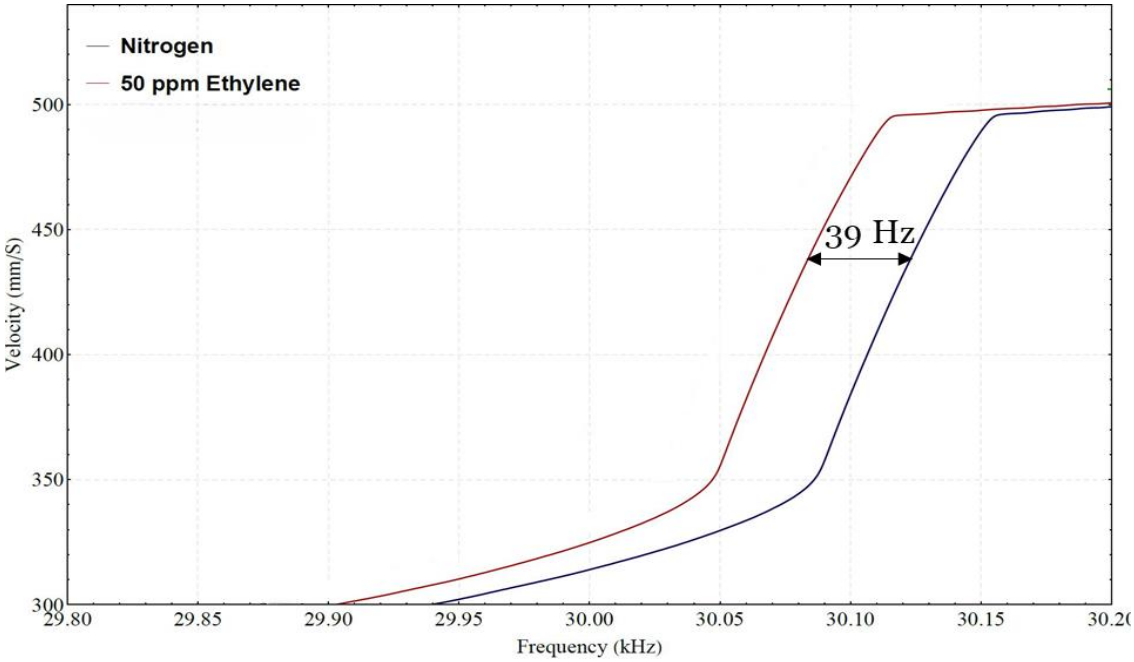

Figure 4.18: Sensor response of PANI with 5% SnO_2 before and after ethylene exposure.

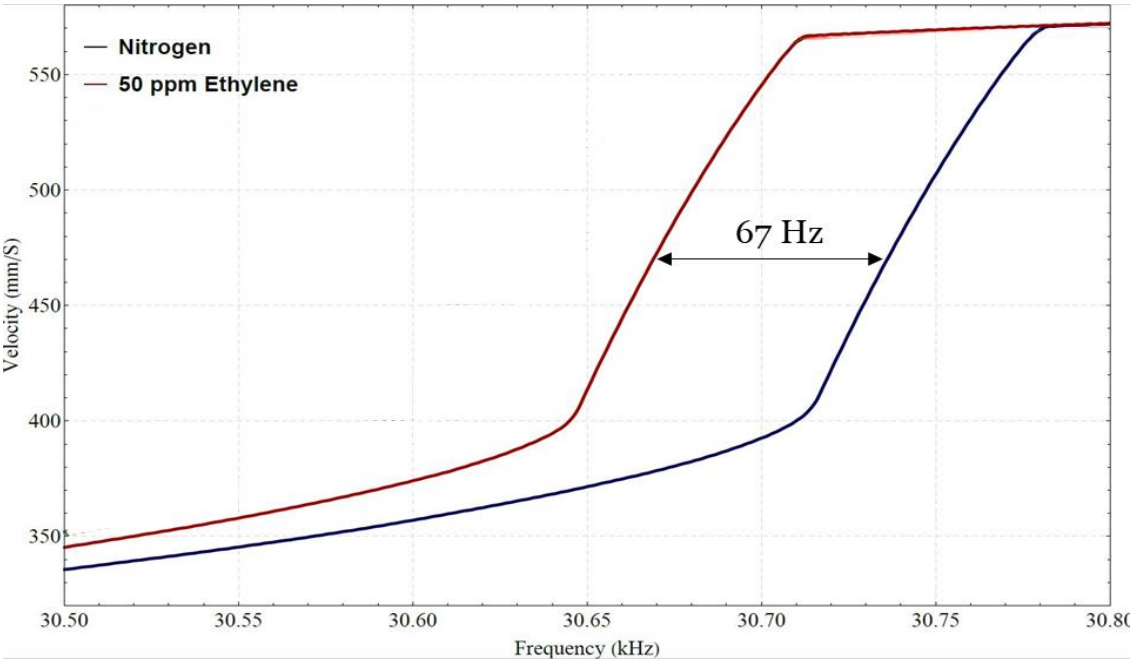

Figure 4.19: Sensor response of PPy before and after ethylene exposure.

4.7 Why Do Some Materials Sense?

Sensing capabilities of materials are attributed to their ability to interact with analytes, leading to detectable responses. The interactions between sensing materials and analytes can be described by potential sensing mechanisms. This interaction is influenced by various factors such as the chemical composition/nature of both the sensing material and analyte, particularly the functional groups, the surface properties including surface area, morphology (shape and arrangement of molecules), and porosity (presence and size of pores). Materials with specific surface functionalities or a higher surface area provide more potential binding sites, leading to increased sensitivity.

Possible mechanisms governing the interactions between polymeric sensing materials and analytes can be categorized into two groups: primary and secondary mechanisms [52]. Primary mechanisms describe electrostatic forces/effects governing the attraction or repulsion between an analyte and a sensing material. Secondary mechanisms, on the other hand, refer to additional effects that only take place when the analyte is close to the sensing material, i.e., when the analyte is absorbed into

the sensing material (a polymer in our case). A notable secondary effect is swelling, which refers to an increase in the polymer's overall volume as a result of analyte absorption into the polymer.

Primary mechanisms based on attractive forces include polarity (and hydrogen bonding), Lewis's acid-base interactions, and metal coordination. On the other hand, there is a repulsive force that pushes the analyte away from a sensing material, known as steric hindrance.

Understanding the principles of these potential mechanisms enables us to identify the dominant sensing mechanism(s) responsible for the interaction and affinity between the analyte and sensing material, which consequently explains why the analyte is sorbing or not sorbing onto the sensing material. To this end, a brief overview follows of the primary mechanisms described in Stewart and Penlidis [52]. In addition, an attempt will be made to relate the sorption behavior of the polymeric sensing materials (evaluated in Chapter 4) with the most suitable mechanism(s).

Polarity and hydrogen bonding- Polarity arises from certain atoms within the molecule attracting electron density towards themselves. Atoms with high electronegativities draw electron density from less electronegative atoms and become even more negative, resulting in an overall charge distribution known as a dipole moment. When the target analyte is polar, then a polar sensing material will attract the analyte. The more polar both the analyte and the sensing material, the stronger the attraction between them. Hydrogen bonding is a special case of polarity, which is the formation of weak (and physical) bonds between hydrogen and the electronegative atom in another molecule.

For example, the interaction of PANI and polar target analytes such as formaldehyde (our surrogate gas) and CO (our actual target analyte) is likely due to the hydrogen bonding between the hydrogen in the amine (NH) group of PANI and oxygen on formaldehyde (or CO). Note that the amine functional group in PANI is polar and capable of hydrogen bonding. In terms of repulsive forces, both formaldehyde and CO are small molecules, meaning they are less sterically hindered, and therefore, are able to diffuse into even smaller interstitial spaces of PANI. Hence, the observed formaldehyde sorption for PANI could be corroborated.

Lewis's acid-base interactions- This interaction results in a weak physical bond between a Lewis acid (an electron-deficient atom) and a Lewis base (a nucleophile with at least one lone pair of electrons). Analytes such as formaldehyde and CO have lone pairs of electrons, therefore can act as a Lewis base. These Lewis bases can interact with PANI which can act as a weak Lewis acid. However, between the two interactions, the dominant mechanism is more likely to be hydrogen bonding.

Metal coordination- This mechanism relies on the presence of metal oxides within the sensing material. The metal oxide acts essentially as a 'catalyst', facilitating an oxidation reaction, i.e., breaking down the target analyte. This basic catalysis occurs via coordination between the analyte and a metal oxide. Metal oxides should be selected in such a way that ensures the analyte is attracted to the metal and is able to coordinate well with it. The important consideration here is that coordination occurs once the molecules are close enough to the metal to coordinate.

The metal should also be able to coordinate with the polymer. When a metal or metal oxide is added to a polymer, a change in the conformation of the polymeric chain (also referred to as formation of 'kinks') takes place because the polymeric backbone tries to coordinate around the metal and bind with it. On the other hand, polymer/metal coordination may reduce the available spots for analyte coordination with the metal, consequently resulting in the formation of 'cavities' known to enhance the sorption of the analyte on the polymer.

Therefore, different metal oxides were incorporated into the polymeric backbone for potential improvement in the sorption of analyte either via utilizing the catalytic properties of metal oxides to degrade the analyte or influencing the morphology and geometry for better diffusion. The careful consideration here was to avoid adding too much metal oxide dopant as the polymer chain may not be able to withstand the strain caused by conforming around the metal oxide, therefore, the polymer may fail to actually coordinate well with the metal oxide and begin to break, which reduces the benefit of adding metal oxide dopants. Typical levels of metal oxide addition in polymers are usually below 20%.

An example of this mechanism (metal coordination) was clearly seen in PANI doped with Co_3O_4 (as discussed in sections 4.1.6 and 4.5.1.3), in which sorption improvement in the metal-oxide doped PANI may be speculated to be related to the catalytic properties of Co_3O_4 to oxidize formaldehyde, as well as the morphology modification caused by adding Co_3O_4.

Finally, a graphical schematic for the mechanism of potential interactions between gas analytes and a polymeric sensing material on a sensor is illustrated in Figure 4.20**.** The figure was a collaborative effort between the author of this thesis and a PhD colleague (B. Mavani). The figure depicts three levels of the mechanism. In the first stage, the gas analyte (formaldehyde in this case) is introduced into the sensor chamber after functionalizing the sensor (microcantilever-based sensor in our case) with the polymeric sensing material. See stage 1 in Figure 4.20.

Assuming that there are no external resistances, the gas molecules reach the surface of the polymeric material (stage 2). That is when diffusion of the gas molecules into the bulk of the polymeric material starts to happen. Gas molecules move through the polymeric material to reach pores and interstices, where they get 'trapped' and can engage and interact with 'hot spots'/active sites (depicted as yellow spheres in the magnified image) of the polymeric material. Note that the formaldehyde gas molecules are depicted as clusters of atoms with red (oxygen), white (hydrogen), and grey (carbon) spheres. The (analyte) gas molecules temporarily 'adhere' (sorb) to the active sites of the polymeric material. This sorption is most likely of the physisorption kind (rather than chemisorption, i.e., formation of chemical bonds). This sorption process is reversible, meaning that the gas molecules and active sites/sorption sites will disengage when the gas flow from the source is removed. The added mass due to the sorbed gas molecules results in the cantilever deflection (which is detected as a frequency shift).

In stage 3, the gas analyte flow is removed, and the sensor chamber is purged with nitrogen gas. Due to the physisorption nature of interactions between gas analytes and the polymeric sensing material, gas molecules leave the sensor chamber (desorption) upon purging, and consequently, the cantilever returns to its original position. Therefore, the sensor/sensing material is ready to be

used again for another cycle of gas analyte exposure (underlying the reusability of the sensing material).

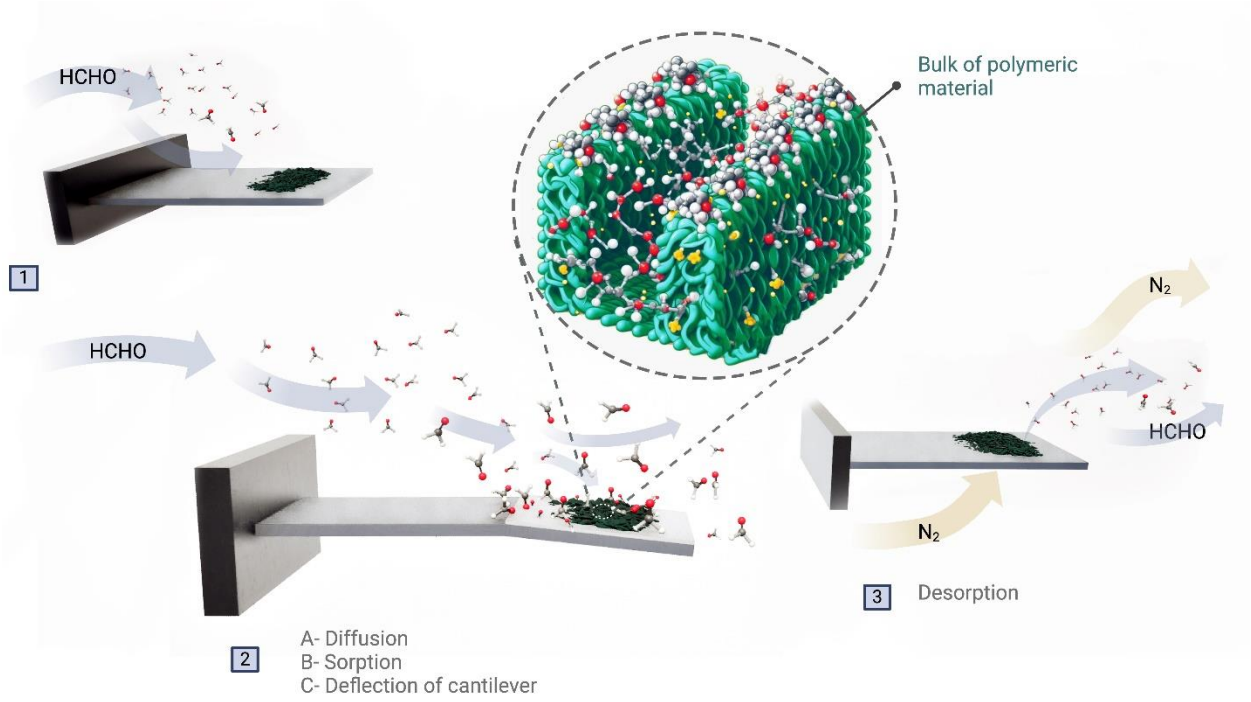

Figure 4.20: Graphical schematic of the mechanism of interactions between gas analyte molecules and a polymeric sensing material in a microcantilever sensor.
Note: The inset image was generated with the aid of ChatGPT.

Chapter 5: Concluding Remarks, Contributions and Future Recommendations

5.1 Concluding Remarks

In total, 13 polymeric materials were synthesized and evaluated for their sensitivity towards formaldehyde (surrogate gas). In addition, 3 other commercially available polymers were also evaluated as potential sensing materials (see Appendix D for a complete list of polymeric materials evaluated). Sorption studies on pristine polymers revealed that PANI was superior in terms of sensitivity to formaldehyde. Moreover, on comparing metal oxide doped polymers, it was found that PANI with 5% Co_3O_4 had the highest sensitivity to formaldehyde, followed by PANI with 5% SnO_2. It was suggested that the good sorption capability of PANI can be attributed to its surface morphology, showing more interstitial space (compared to other pristine polymers), which is necessary for analyte diffusion to the sensing material.

Surface area analysis via the BET technique revealed pristine PANI poses a larger surface area than its metal oxide doped counterpart although the metal oxide doped PANI was observed to have a better gas sorption behavior. Based on this observation, three conclusions can be made: (a) Enhanced gas sorption is not a sole function of a change in the surface area of a sensing material, (b) Incorporation of metal oxide into pristine polymers does not necessarily result in an increase in the surface area of modified polymers, (c) Materials with comparable surface area measurements might display divergent sorption behaviors based on the presence or absence of chemical/electronic interactions (affinity) between the analyte and the polymer matrix.

The final step of sensing material evaluation took place in an actual MEMS sensor chamber upon exposure to 50 ppm of ethylene (the actual target analyte), and the results revealed a frequency shift in PANI with 5% SnO_2, PANI with 5% ZnO, and PPy, indicating sensitivity of these materials to ethylene. It is worth noting that the largest frequency shift (i.e., largest signal) upon exposure to ethylene was observed with PPy.

5.2 Contributions

The overall objectives of this thesis were to: (a) identify polymeric sensing materials for detection of gases evolving in energy storage devices through a comprehensive literature survey, (b) synthesize and modify these polymers through doping with metal oxides, (c) evaluate the sorption properties of the synthesized and potential commercially available polymers using a simulant gas (e.g., formaldehyde), (d) characterize the most promising materials using various analytical techniques to corroborate and explain the trends observed in the gas sorption experiments, (e) apply the most promising materials onto a MEMS sensor platforms to test sensing performance in the presence of the target gas.

All the research objectives mentioned above were met, and the main contributions of this thesis can be summarized as follows:

- PANI materials doped with combination of metal oxides (TiO_2 and SnO_2) were synthesized, and the combined effect of incorporating two metal oxides on sorption capabilities was studied. This does not happen frequently in the open literature.

- Sorption properties of several doped and undoped polymeric materials towards formaldehyde were tested and sensitivity of these materials was reported in terms of actual ppm of gas analyte sorbed, unlike most literature studies which only report sensitivity based on resistance/conductivity change and do not report changes in the electrical property measured (e.g., resistance, conductivity, or frequency) versus actual ppm levels. In addition, experimental error was clearly quantified via independent replication.

- Comprehensive summary tables on sensing materials for the detection of the target gases were provided in Appendices A to C. These tables are a very good starting point for the novice for future work.

- The actual MEMS sensor was tested and demonstrated for detecting ethylene, a flammable gas released in lithium-ion batteries. It is worth mentioning that testing the MEMS sensor showed promising results at room temperature (~22-25℃), unlike the metal oxide sensors that operate at much higher temperatures of 150-500℃. This also represented the 'full circle', from polymer synthesis to evaluating promising polymeric sensing materials, all the way to testing the final MEMS sensor.

5.3 Future Recommendations

5.3.1 Short-term Recommendations

Sorption behavior at higher wt.% of Co_3O_4: It was found that formaldehyde sorption of PANI with Co_3O_4 increased with increasing the amount of metal oxide from 1% to 2% and 2% to 5% in PANI matrix (see section 4.1.6). Therefore, it is worth evaluating higher wt.% of Co_3O_4 (e.g., 10 wt.%) to determine if the same trend would be observed (i.e., enhanced sorption on further increasing the Co_3O_4 content).

Different combination/mixture of metal oxides: Two different combinations of TiO_2 and SnO_2 in the PANI matrix were evaluated (see section 4.1.5) but did not seem to improve sorption of pristine PANI. Hence, it would be worth doping PANI with other combinations of TiO_2 and SnO_2 to investigate an optimal level for this metal oxide combination. In addition, SnO_2 and Co_3O_4 on their own were found to enhance the sorption performance of PANI, therefore, one can evaluate different combinations of SnO_2 and Co_3O_4 in PANI to see if a reinforced effect on sorption performance could be observed with this combination of metal oxides.

5.3.2 Long-term Recommendations

Modify PPy with different dopants: MEMS sensor testing with ethylene revealed that PPy was sensitive to 50 ppm of ethylene. Hence, it is worthwhile to modify PPy with different metal oxides like SnO_2 and ZnO to investigate sorption properties of doped PPy.

Incorporate ZrO_2 into PPy and/or PANI: Application of ZrO_2 (zirconium dioxide, also known as zirconia) for detection of ethylene has been reported in some studies [18], [23]. Zirconia is a transition metal oxide used in a variety of applications such as adsorbents, catalysts and catalyst carriers [77]. Therefore, it is worth evaluating the sorption capabilities of composites of PANI/ ZrO_2 and PPy/ZrO_2, and eventually testing their gas sensing potential in an actual MEMS sensor.

Study humidity effects: Humidity is pervasive, making it an important factor to account for when designing sensing materials. Humidity can affect the sensing performance in different ways. Therefore, understanding the main trends of humidity effects is important and helpful in evaluating sensing materials.

Letters of Copyright Permission

License agreement for Figure 2.1

ELSEVIER LICENSE
TERMS AND CONDITIONS

Jun 17, 2024

This Agreement between Shahrzad Ghodrati ("You") and Elsevier ("Elsevier") consists of your license details and the terms and conditions provided by Elsevier and Copyright Clearance Center.

License Number	5811420821687
License date	Jun 17, 2024
Licensed Content Publisher	Elsevier
Licensed Content Publication	Journal of Power Sources
Licensed Content Title	Gas evolution in commercial Li-ion battery cells measured by on-line mass spectrometry – Effects of C-rate and cell voltage
Licensed Content Author	Ulriika Mattinen,Matilda Klett,Göran Lindbergh,Rakel Wreland Lindström
Licensed Content Date	Nov 30, 2020
Licensed Content Volume	477
Licensed Content Issue	n/a
Licensed Content Pages	1
Start Page	228968
End Page	0

Type of Use	reuse in a thesis/dissertation
Portion	figures/tables/illustrations
Number of figures/tables/illustrations	1
Format	both print and electronic
Are you the author of this Elsevier article?	No
Will you be translating?	No
Title of new work	Synthesis and Characterization of Polymeric Sensing Materials for Detection of Gases in Energy Storage Devices
Institution name	University of Waterloo
Expected presentation date	Jun 2024
Portions	Figure 1 on page 2
The Requesting Person / Organization to Appear on the License	Shahrzad Ghodrati
Requestor Location	University of Waterloo 200 University Ave West Waterloo, ON N2L 3G1 Canada Attn: University of Waterloo
Publisher Tax ID	GB 494 6272 12
Total	0.00 USD

License agreement for Figure 2.2

ELSEVIER LICENSE
TERMS AND CONDITIONS

Jun 17, 2024

This Agreement between Shahrzad Ghodrati ("You") and Elsevier ("Elsevier") consists of your license details and the terms and conditions provided by Elsevier and Copyright Clearance Center.

License Number	5811440012450
License date	Jun 17, 2024
Licensed Content Publisher	Elsevier
Licensed Content Publication	Materials Chemistry and Physics
Licensed Content Title	Chemiresistive sensing platform based on PdO-PANI/ITO heterostructure for room temperature hydrogen detection
Licensed Content Author	Kamal Arora,Nitin K. Puri
Licensed Content Date	Jun 1, 2020
Licensed Content Volume	247
Licensed Content Issue	n/a
Licensed Content Pages	1
Start Page	122850
End Page	0

Type of Use	reuse in a thesis/dissertation
Portion	figures/tables/illustrations
Number of figures/tables/illustrations	1
Format	both print and electronic
Are you the author of this Elsevier article?	No
Will you be translating?	No
Title of new work	Synthesis and Characterization of Polymeric Sensing Materials for Detection of Gases in Energy Storage Devices
Institution name	University of Waterloo
Expected presentation date	Jun 2024
Portions	Figure 9 on Page 7
The Requesting Person / Organization to Appear on the License	Shahrzad Ghodrati
Requestor Location	University of Waterloo 200 University Ave West Waterloo, ON N2L 3G1 Canada Attn: University of Waterloo
Publisher Tax ID	GB 494 6272 12
Total	0.00 USD

License agreement for Figure 2.3

ELSEVIER LICENSE
TERMS AND CONDITIONS

Jun 17, 2024

This Agreement between Shahrzad Ghodrati ("You") and Elsevier ("Elsevier") consists of your license details and the terms and conditions provided by Elsevier and Copyright Clearance Center.

License Number	5811440773769
License date	Jun 17, 2024
Licensed Content Publisher	Elsevier
Licensed Content Publication	Chemical Engineering Journal
Licensed Content Title	Polyaniline-based adsorbents for aqueous pollutants removal: A review
Licensed Content Author	Akbar Samadi,Ming Xie,Jingliang Li,Hokyong Shon,Chunmiao Zheng,Shuaifei Zhao
Licensed Content Date	Aug 15, 2021
Licensed Content Volume	418
Licensed Content Issue	n/a
Licensed Content Pages	1
Start Page	129425
End Page	0

Type of Use	reuse in a thesis/dissertation
Portion	figures/tables/illustrations
Number of figures/tables/illustrations	1
Format	both print and electronic
Are you the author of this Elsevier article?	No
Will you be translating?	No
Title of new work	Synthesis and Characterization of Polymeric Sensing Materials for Detection of Gases in Energy Storage Devices
Institution name	University of Waterloo
Expected presentation date	Jun 2024
Portions	Figure 2 on Page 3
The Requesting Person / Organization to Appear on the License	Shahrzad Ghodrati
Requestor Location	University of Waterloo 200 University Ave West Waterloo, ON N2L 3G1 Canada Attn: University of Waterloo
Publisher Tax ID	GB 494 6272 12
Total	0.00 USD

License agreement for Figure 2.4

ELSEVIER LICENSE
TERMS AND CONDITIONS

Jun 17, 2024

This Agreement between Shahrzad Ghodrati ("You") and Elsevier ("Elsevier") consists of your license details and the terms and conditions provided by Elsevier and Copyright Clearance Center.

License Number	5811441246098
License date	Jun 17, 2024
Licensed Content Publisher	Elsevier
Licensed Content Publication	Sensors and Actuators B: Chemical
Licensed Content Title	A chemical sensor based on a microfabricated cantilever array with simultaneous resonance-frequency and bending readout
Licensed Content Author	F.M Battiston,J.-P Ramseyer,H.P Lang,M.K Baller,Ch Gerber,J.K Gimzewski,E Meyer,H.-J Güntherodt
Licensed Content Date	Jun 15, 2001
Licensed Content Volume	77
Licensed Content Issue	1-2
Licensed Content Pages	10
Start Page	122

End Page	131
Type of Use	reuse in a thesis/dissertation
Portion	figures/tables/illustrations
Number of figures/tables/illustrations	1
Format	both print and electronic
Are you the author of this Elsevier article?	No
Will you be translating?	No
Title of new work	Synthesis and Characterization of Polymeric Sensing Materials for Detection of Gases in Energy Storage Devices
Institution name	University of Waterloo
Expected presentation date	Jun 2024
Portions	Figure 1 on Page 123
The Requesting Person / Organization to Appear on the License	Shahrzad Ghodrati
Requestor Location	University of Waterloo 200 University Ave West Waterloo, ON N2L 3G1 Canada Attn: University of Waterloo
Publisher Tax ID	GB 494 6272 12

License agreement for Figure 2.5

ELSEVIER LICENSE
TERMS AND CONDITIONS

Jun 17, 2024

This Agreement between Shahrzad Ghodrati ("You") and Elsevier ("Elsevier") consists of your license details and the terms and conditions provided by Elsevier and Copyright Clearance Center.

License Number	5811450180924
License date	Jun 17, 2024
Licensed Content Publisher	Elsevier
Licensed Content Publication	International Journal of Hydrogen Energy
Licensed Content Title	Hydrogen gas sensing methods, materials, and approach to achieve parts per billion level detection: A review
Licensed Content Author	Pankaj Singh Chauhan,Shantanu Bhattacharya
Licensed Content Date	Oct 4, 2019
Licensed Content Volume	44
Licensed Content Issue	47
Licensed Content Pages	24
Start Page	26076
End Page	26099

Type of Use	reuse in a thesis/dissertation
Portion	figures/tables/illustrations
Number of figures/tables/illustrations	1
Format	both print and electronic
Are you the author of this Elsevier article?	No
Will you be translating?	No
Title of new work	Synthesis and Characterization of Polymeric Sensing Materials for Detection of Gases in Energy Storage Devices
Institution name	University of Waterloo
Expected presentation date	Jun 2024
Portions	Figure 4 on Page 26082
The Requesting Person / Organization to Appear on the License	Shahrzad Ghodrati
Requestor Location	University of Waterloo 200 University Ave West Waterloo, ON N2L 3G1 Canada Attn: University of Waterloo
Publisher Tax ID	GB 494 6272 12
Total	0.00 USD

License agreement for Figure 3.1

JOHN WILEY AND SONS LICENSE
TERMS AND CONDITIONS

Jun 17, 2024

This Agreement between Shahrzad Ghodrati ("You") and John Wiley and Sons ("John Wiley and Sons") consists of your license details and the terms and conditions provided by John Wiley and Sons and Copyright Clearance Center.

License Number	5811460675012
License date	Jun 17, 2024
Licensed Content Publisher	John Wiley and Sons
Licensed Content Publication	Macromolecular Reaction Engineering
Licensed Content Title	Indium Oxide Doped Polyaniline for Detection of Formaldehyde
Licensed Content Author	Bhoomi Het Mavani, Alexander Penlidis
Licensed Content Date	Jun 21, 2022
Licensed Content Volume	16
Licensed Content Issue	6
Licensed Content Pages	10
Type of use	Dissertation/Thesis
Requestor type	University/Academic

Format	Print and electronic
Portion	Figure/table
Number of figures/tables	1
Will you be translating?	No
Title of new work	Synthesis and Characterization of Polymeric Sensing Materials for Detection of Gases in Energy Storage Devices
Institution name	University of Waterloo
Expected presentation date	Jun 2024
Portions	Figure 1 on Page 3
The Requesting Person / Organization to Appear on the License	Shahrzad Ghodrati
Requestor Location	University of Waterloo 200 University Ave West Waterloo, ON N2L 3G1 Canada Attn: University of Waterloo
Publisher Tax ID	EU826007151
Total	0.00 USD

References

[1] N. E. Galushkin, N. N. Yazvinskaya, and D. N. Galushkin, “Mechanism of Gases Generation during Lithium-Ion Batteries Cycling,” *J Electrochem Soc*, vol. 166, no. 6, pp. A897–A908, 2019, doi: 10.1149/2.0041906jes.

[2] “After subway e-bike blaze, Toronto fire chief shares tips to avoid battery fire,” CBC News. Accessed: Mar. 25, 2024. [Online]. Available: https://www.cbc.ca/news/canada/toronto/toronto-e-bike-battery-fire-1.7072547

[3] N. Williard, W. He, C. Hendricks, and M. Pecht, “Lessons Learned from the 787 Dreamliner Issue on Lithium-Ion Battery Reliability,” vol. 6, pp. 4682–4695, 2013, doi: 10.3390/en6094682.

[4] J. Mitali, S. Dhinakaran, and A. A. Mohamad, “Energy storage systems: a review,” *Energy Storage and Saving*, vol. 1, pp. 166–216, 2022, doi: 10.1016/j.enss.2022.07.002.

[5] B. Rowden and N. Garcia-Araez, “A review of gas evolution in lithium ion batteries,” *Energy Reports*, vol. 6, pp. 10–18, May 2020, doi: 10.1016/J.EGYR.2020.02.022.

[6] M. R. Fuhst and D. J. Siegel, “Gas evolution in Li-ion batteries: Modeling ethylene carbonate decomposition on LiCoO2 in the presence of surface magnetism,” *Journal of Physical Chemistry C*, vol. 124, no. 44, pp. 24097–24104, Nov. 2020, doi: 10.1021/ACS.JPCC.0C07550/ASSET/IMAGES/LARGE/JP0C07550_0006.JPEG.

[7] U. Mattinen, M. Klett, G. Lindbergh, and R. Wreland Lindström, “Gas evolution in commercial Li-ion battery cells measured by on-line mass spectrometry – Effects of C-rate and cell voltage,” *J Power Sources*, vol. 477, p. 228968, Nov. 2020, doi: 10.1016/J.JPOWSOUR.2020.228968.

[8] A. Shakeel, K. Rizwan, U. Farooq, S. Iqbal, and A. A. Altaf, “Advanced polymeric/inorganic nanohybrids: An integrated platform for gas sensing applications,” *Chemosphere*, vol. 294, May 2022, doi: 10.1016/j.chemosphere.2022.133772.

[9] K. Arora and N. K. Puri, “Chemiresistive sensing platform based on PdO-PANI/ITO heterostructure for room temperature hydrogen detection,” *Mater Chem Phys*, vol. 247, Jun. 2020, doi: 10.1016/j.matchemphys.2020.122850.

[10] R. K. Pippara, P. S. Chauhan, A. Yadav, V. Kishnani, and A. Gupta, “Room temperature hydrogen sensing with polyaniline/SnO2/Pd nanocomposites,” *Micro and Nano Engineering*, vol. 12, Aug. 2021, doi: 10.1016/j.mne.2021.100086.

[11] N. D. Sonwane, M. D. Maity, and S. B. Kondawar, “Conducting polyaniline/SnO2 nanocomposite for room temperature hydrogen gas sensing,” *Mater Today Proc*, vol. 15, pp. 447–453, Jan. 2019, doi: 10.1016/J.MATPR.2019.04.106.

[12] H. J. Sharma, N. D. Sonwane, and S. B. Kondawar, “Electrospun SnO2/Polyaniline composite nanofibers based low temperature hydrogen gas sensor,” *Fibers and Polymers*, vol. 16, no. 7, pp. 1527–1532, Jul. 2015, doi: 10.1007/S12221-015-5222-0/METRICS.

[13] S. Nasirian and H. Milani Moghaddam, “Polyaniline assisted by TiO2:SnO2 nanoparticles as a hydrogen gas sensor at environmental conditions,” *Appl Surf Sci*, vol. 328, pp. 395–404, Feb. 2015, doi: 10.1016/J.APSUSC.2014.12.051.

[14] “Best Ethylene Gas Detector (for Fruit Ripening) – Forensics Detectors.” Accessed: Jan. 31, 2023. [Online]. Available: https://www.forensicsdetectors.com/blogs/articles/ethylene-gas-detector-produce

[15] X. Chen, R. Wreyford, and N. Nasiri, “Recent Advances in Ethylene Gas Detection,” *Materials*, vol. 15, no. 17. MDPI, Sep. 01, 2022. doi: 10.3390/ma15175813.

[16] M. Šetka *et al.*, “Love wave sensors based on gold nanoparticle-modified polypyrrole and their properties to ammonia and ethylene,” *Sens Actuators B Chem*, vol. 304, p. 127337, Feb. 2020, doi: 10.1016/j.snb.2019.127337.

[17] M. A. K. P. Tolentino, D. R. B. Albano, and F. B. Sevilla, “Piezoelectric sensor for ethylene based on silver(I)/polymer composite,” *Sens Actuators B Chem*, vol. 254, pp. 299–306, 2018, doi: 10.1016/j.snb.2017.07.015.

[18] A. Husain, S. Ahmad, and F. Mohammad, “Thermally stable and highly sensitive ethene gas sensor based on polythiophene/zirconium oxide nanocomposites,” *Mater Today Commun*, vol. 20, Sep. 2019, doi: 10.1016/J.MTCOMM.2019.100574.

[19] P. Pattananuwat and D. Aht-Ong, “In-Situ Electrochemical Synthesis of Novel Sensitive Layer of Polyaniline/Multiwall Carbon Nanotube/Tin Oxide Hybrid Materials for Ethylene Gas Detection,” *Polymer - Plastics Technology and Engineering*, vol. 52, no. 2, pp. 189–194, Jan. 2013, doi: 10.1080/03602559.2012.735312.

[20] A. Sholehah, K. Karmala, N. Huda, L. Utari, N. L. W. Septiani, and B. Yuliarto, “Structural effect of ZnO-Ag chemoresistive sensor on flexible substrate for ethylene gas detection,” *Sens Actuators A Phys*, vol. 331, p. 112934, Nov. 2021, doi: 10.1016/j.sna.2021.112934.

[21] J. Kathirvelan, R. Vijayaraghavan, and A. Thomas, “Ethylene detection using TiO2-WO3 composite sensor for fruit ripening applications,” *Sensor Review*, vol. 37, no. 2, pp. 147–154, 2017, doi: 10.1108/SR-12-2016-0262.

[22] M. Krivec *et al.*, “Quantitative Ethylene Measurements with MOx Chemiresistive Sensors at Different Relative Air Humidities,” *Sensors*, vol. 15, pp. 28088–28098, 2015, doi: 10.3390/s151128088.

[23] Sultan Adil, Ahmad Sharique, and Mohammad Faiz, “Synthesis, Characterization and Electrical Properties of Polypyrrole/ Zirconia Nanocomposite and its Application as Ethene Gas Sensor,” *Polymers and Polymer Composites*, pp. 695–704, 2017, doi: https://doi.org/10.1177/096739111702500908.

[24] K. C. Hsu, T. H. Fang, I. T. Tang, Y. J. Hsiao, and C. Y. Chen, “Mechanism and characteristics of Au-functionalized SnO2/In2O3 nanofibers for highly sensitive CO detection,” *J Alloys Compd*, vol. 822, May 2020, doi: 10.1016/J.JALLCOM.2019.153475.

[25] M. Onuki *et al.*, “Identification of the Source of Evolved Gas in Li-Ion Batteries Using [sup 13]C-labeled Solvents,” *J Electrochem Soc*, vol. 155, no. 11, p. A794, Sep. 2008, doi: 10.1149/1.2969947/XML.

[26] B. B. Berkes, A. Schiele, H. Sommer, T. Brezesinski, and J. Janek, “On the gassing behavior of lithium-ion batteries with NCM523 cathodes,” *Journal of Solid State*

Electrochemistry, vol. 20, no. 11, pp. 2961–2967, Nov. 2016, doi: 10.1007/S10008-016-3362-9/FIGURES/6.

[27] A. Wuersig, W. Scheifele, and P. Novák, "CO2 Gas Evolution on Cathode Materials for Lithium-Ion Batteries," *J Electrochem Soc*, vol. 154, no. 5, p. A449, Mar. 2007, doi: 10.1149/1.2712138/XML.

[28] C. Aranthady, G. V. Shanbhag, and N. G. Sundaram, "Polyaniline/(Ta2O5 –SnO2) hybrid nanocomposite for efficient room temperature CO gas sensing," *RSC Adv*, vol. 12, no. 25, pp. 15759–15766, May 2022, doi: 10.1039/D2RA00602B.

[29] T. Sen, N. G. Shimpi, and S. Mishra, "Room temperature CO sensing by polyaniline/Co3O4 nanocomposite," *J Appl Polym Sci*, vol. 133, no. 42, p. 44115, Nov. 2016, doi: 10.1002/APP.44115.

[30] V. Kishnani, G. Verma, R. K. Pippara, A. Yadav, P. S. Chauhan, and A. Gupta, "Highly sensitive, ambient temperature CO sensor using tin oxide based composites," *Sens Actuators A Phys*, vol. 332, p. 113111, Dec. 2021, doi: 10.1016/J.SNA.2021.113111.

[31] K.-S. Jian *et al.*, "High Response CO Sensor Based on a Polyaniline/SnO2 Nanocomposite," *Polymers (Basel)*, 2019, doi: 10.3390/polym11010184.

[32] S. Nasirian, "Enhanced carbon dioxide sensing performance of polyaniline/tin dioxide nanocomposite by ultraviolet light illumination," *Appl Surf Sci*, vol. 502, p. 144302, Feb. 2020, doi: 10.1016/J.APSUSC.2019.144302.

[33] R. K. Sonker, S. R. Sabhajeet, and B. C. Yadav, "TiO2–PANI nanocomposite thin film prepared by spin coating technique working as room temperature CO2 gas sensing," *Journal of Materials Science: Materials in Electronics*, vol. 27, no. 11, pp. 11726–11732, Nov. 2016, doi: 10.1007/S10854-016-5310-Y/FIGURES/7.

[34] S. H. Nimkar, S. P. Agrawal, and S. B. Kondawar, "Fabrication of Electrospun Nanofibers of Titanium Dioxide Intercalated Polyaniline Nanocomposites for CO2 Gas Sensor," *Procedia Materials Science*, vol. 10, pp. 572–579, Jan. 2015, doi: 10.1016/J.MSPRO.2015.06.008.

[35] R. V. Barde, “Preparation, characterization and CO2 gas sensitivity of Polyaniline doped with Sodium Superoxide (NaO2),” *Mater Res Bull*, vol. 73, pp. 70–76, Jan. 2016, doi: 10.1016/J.MATERRESBULL.2015.08.026.

[36] S. Pandey, “Highly sensitive and selective chemiresistor gas/vapor sensors based on polyaniline nanocomposite: A comprehensive review,” *Journal of Science: Advanced Materials and Devices*, vol. 1, no. 4. Elsevier B.V., pp. 431–453, Dec. 01, 2016. doi: 10.1016/j.jsamd.2016.10.005.

[37] L. Tirfie Zegebreal, N. A. Tegegne, and F. Gashaw Hone, “Recent progress in hybrid conducting polymers and metal oxide nanocomposite for room-temperature gas sensor applications: A review,” *Sens Actuators A Phys*, vol. 359, p. 114472, 2023, doi: 10.1016/j.sna.2023.114472.

[38] A. Verma, R. Gupta, A. S. Verma, and T. Kumar, “A review of composite conducting polymer-based sensors for detection of industrial waste gases,” *Sensors and Actuators Reports*, vol. 5, p. 100143, Jun. 2023, doi: 10.1016/J.SNR.2023.100143.

[39] B. Arman Kuzubasoglu, “Recent Studies on the Humidity Sensor: A Mini Review,” *ACS Applied Electronic Materials*, vol. 4, no. 10. American Chemical Society, pp. 4797–4807, Oct. 25, 2022. doi: 10.1021/acsaelm.2c00721.

[40] P. Cavallo, D. F. Acevedo, M. C. Fuertes, G. J. A. A. Soler-Illia, and C. A. Barbero, “Understanding the sensing mechanism of polyaniline resistive sensors. Effect of humidity on sensing of organic volatiles,” *Sens Actuators B Chem*, vol. 210, pp. 574–580, 2015, doi: 10.1016/j.snb.2015.01.029.

[41] M. E. Azim-Araghi and M. J. Jafari, “Electrical and gas sensing properties of polyaniline-chloroaluminium phthalocyanine composite thin films,” *Eur. Phys. J. Appl. Phys*, vol. 52, p. 10402, 2010, doi: 10.1051/epjap/2010133.

[42] A. Sanger, A. Kumar, S. Chauhan, Y. K. Gautam, and R. Chandra, “Fast and reversible hydrogen sensing properties of Pd/Mg thin film modified by hydrophobic porous silicon substrate,” *Sens Actuators B Chem*, vol. 213, pp. 252–260, Jul. 2015, doi: 10.1016/J.SNB.2015.02.098.

[43] S. Manjunatha, T. Machappa, Y. T. Ravikiran, B. Chethan, and A. Sunilkumar, "Polyaniline based stable humidity sensor operable at room temperature," *Physica B Condens Matter*, vol. 561, pp. 170–178, May 2019, doi: 10.1016/j.physb.2019.02.063.

[44] S. C. Nagaraju, A. S. Roy, J. B. Prasanna Kumar, K. R. Anilkumar, and G. Ramagopal, "Humidity Sensing Properties of Surface Modified Polyaniline Metal Oxide Composites," 2014, doi: 10.1155/2014/925020.

[45] K. C. Sajjan, • Aashis, S. Roy, A. Parveen, and S. Khasim, "Analysis of DC and AC properties of a humidity sensor based on polyaniline-chromium oxide composites", doi: 10.1007/s10854-014-1715-7.

[46] S. Kotresh, Y. T. Ravikiran, H. G. R. Prakash, and S. C. V. Kumari, "Polyaniline-Titanium dioxide composite as humidity sensor at room temperature," *Nanosystems: Physics, Chemistry, Mathematics*, pp. 732–739, Aug. 2016, doi: 10.17586/2220-8054-2016-7-4-732-739.

[47] T. Machappa and A. Prasad, "Humidity sensing behavior of polyaniline/magnesium chromate (MgCrO4) composite," *Bulletin of Materials Science,* vol. 35, no. 1, pp. 75–81, 2012.

[48] K. Mistry *et al.*, "Highly Sensitive Self-Actuated Zinc Oxide Resonant Microcantilever Humidity Sensor," *Nano Lett*, vol. 22, no. 8, pp. 3196–3203, Apr. 2022, doi: 10.1021/acs.nanolett.1c04378.

[49] A. G. Macdiarmid, J. C. Chiang, A. F. Richter, and A. J. Epstein, "Polyaniline: A New Concept in Conducting Polymers," *Synth Met*, vol. 18, pp. 285–290, 1987.

[50] A. Samadi, M. Xie, J. Li, H. Shon, C. Zheng, and S. Zhao, "Polyaniline-based adsorbents for aqueous pollutants removal: A review," *Chemical Engineering Journal*, vol. 418, p. 129425, Aug. 2021, doi: 10.1016/J.CEJ.2021.129425.

[51] A. Verma, R. Gupta, A. S. Verma, and T. Kumar, "Review—Recent Advances and Challenges of Conducting Polymer-Metal Nanocomposites for the Detection of Industrial Waste Gases," *ECS Journal of Solid State Science and Technology*, vol. 12, no. 4, p. 047002, Apr. 2023, doi: 10.1149/2162-8777/acc75e.

[52] K. M. E. Stewart and A. Penlidis, “Designing polymeric sensing materials: what are we doing wrong?,” *Polym Adv Technol*, pp. 319–344, 2017, doi: 10.1002/pat.3893.

[53] S. R. Jamnani, H. M. Moghaddam, S. G. Leonardi, and G. Neri, “PANI/Sm2O3 nanocomposite sensor for fast hydrogen detection at room temperature,” *Synth Met*, vol. 268, Oct. 2020, doi: 10.1016/j.synthmet.2020.116493.

[54] Y. C. Wong, B. C. Ang, A. S. M. A. Haseeb, A. A. Baharuddin, and Y. H. Wong, “Review—Conducting Polymers as Chemiresistive Gas Sensing Materials: A Review,” *J Electrochem Soc*, vol. 167, no. 3, p. 037503, 2020, doi: 10.1149/2.0032003jes.

[55] S. K. Vashist and H. Holthofer, “Microcantilevers for sensing applications,” *Measurement and Control*, vol. 43, no. 3, pp. 84–88, 2010, doi: 10.1177/002029401004300305.

[56] F. M. Battiston *et al.*, “A chemical sensor based on a microfabricated cantilever array with simultaneous resonance-frequency and bending readout,” *Sensors and Actuators B*, pp. 122–131, 2001.

[57] Chaudhary Monika and Gupta Amita, “Microcantilever-based Sensors,” *Def Sci J*, vol. 59, no. 6, pp. 634–641, 2009.

[58] P. S. Chauhan and S. Bhattacharya, “Hydrogen gas sensing methods, materials, and approach to achieve parts per billion level detection: A review,” *International Journal of Hydrogen Energy*, vol. 44, no. 47. Elsevier Ltd, pp. 26076–26099, Oct. 04, 2019. doi: 10.1016/j.ijhydene.2019.08.052.

[59] K. Stewart and A. Penlidis, “Design of sensitive and selective sensing materials for ethanol detection,” *Trends in Chemical Engineering*, vol. 16, pp. 1–13, 2017.

[60] K. M. E. Stewart and A. Penlidis, “Novel Test System for Gas Sensing Materials and Sensors,” *Macromol Symp*, vol. 324, no. 1, pp. 11–18, Feb. 2013, doi: 10.1002/MASY.201200062.

[61] B. H. Mavani and A. Penlidis, “Indium Oxide Doped Polyaniline for Detection of Formaldehyde,” *Macromol React Eng*, vol. 16, no. 6, p. 2200012, Dec. 2022, doi: 10.1002/MREN.202200012.

[62] J. Stetefeld, S. A. Mckenna, and T. R. Patel, “Dynamic light scattering: a practical guide and applications in biomedical sciences,” *Biophys Rev*, doi: 10.1007/s12551-016-0218-6.

[63] B. H. Mavani, M. Arabi, R. Saritas, A. J. Scott, E. Abdel-Rahman, and A. Penlidis, “Deposition of polymeric sensing materials for gas detection,” *Canadian Journal of Chemical Engineering*, 2023, doi: 10.1002/CJCE.24866.

[64] Y. Shama, “MEMS Sensors For Aqueous Media,” PhD Comprehensive Report, University of Waterloo, Waterloo, 2022.

[65] Y. S. Shama, S. Rahmanian, H. Mouharrar, R. Abdelrahman, A. Elhady, and E. M. Abdel-Rahman, “Unraveling the nature of sensing in electrostatic MEMS gas sensors,” *Microsyst Nanoeng*, vol. 10, no. 56, 2024, doi: 10.1038/s41378-024-00688-3.

[66] B. H. Mavani, “Polymeric Materials for Detection of Chemical Warfare Agents,” MASc Thesis, University of Waterloo, Waterloo, 2021. Accessed: Jan. 24, 2024. [Online]. Available: https://uwspace.uwaterloo.ca/handle/10012/17744

[67] K. G. Kim, “Synthesis and Characterization of Polymeric Gas Sensing Materials for Detection of Agriculture Lagoon Off-Gas,” MASc Thesis, University of Waterloo, Waterloo, 2023. [Online]. Available: https://uwspace.uwaterloo.ca/handle/10012/20014

[68] S. Vladimirova *et al.*, “Co3O4 as p-Type Material for CO Sensing in Humid Air,” *Sensors*, 2017, doi: 10.3390/s17102216.

[69] H. Chai *et al.*, “Stability of Metal Oxide Semiconductor Gas Sensors: A Review,” *IEEE Sensors Journal*, vol. 22, no. 6. Institute of Electrical and Electronics Engineers Inc., pp. 5470–5481, Mar. 15, 2022. doi: 10.1109/JSEN.2022.3148264.

[70] A. J. Scott, “Design of Polymeric Materials: Novel Functionalized Polymers for Enhanced Oil Recovery & Gas Sorption Applications,” University of Waterloo, 2019. Accessed: Nov. 15, 2023. [Online]. Available: https://uwspace.uwaterloo.ca/handle/10012/15270

[71] S. Manjunatha, T. Machappa, A. Sunilkumar, and Y. T. Ravikiran, “Tungsten disulfide: an efficient material in enhancement of AC conductivity and dielectric properties of polyaniline,” vol. 29, pp. 11581–11590, 2018, doi: 10.1007/s10854-018-9255-1.

[72] Y. T. Ravikiran *et al.*, “Synthesis, characterization and low frequency AC conduction of polyaniline/niobium pentoxide composites,” *Synth Met*, vol. 156, pp. 1139–1147, 2006, doi: 10.1016/j.synthmet.2006.08.005.

[73] M. Thommes *et al.*, “Physisorption of gases, with special reference to the evaluation of surface area and pore size distribution (IUPAC Technical Report),” *Pure and Applied Chemistry*, vol. 87, no. 9–10, pp. 1051–1069, Oct. 2015, doi: 10.1515/pac-2014-1117.

[74] B. H. Mavani, “Polymeric Gas Sensing Materials for Detection of Toxic Analytes,” PhD Comprehensive Report, University of Waterloo, Waterloo, 2023.

[75] L. Hlekelele, N. E. Nomadolo, K. Z. Setshedi, L. E. Mofokeng, A. Chetty, and V. P. Chauke, “Synthesis and characterization of polyaniline, polypyrrole and zero-valent iron-based materials for the adsorptive and oxidative removal of bisphenol-A from aqueous solution †,” 2019, doi: 10.1039/c9ra01666j.

[76] L. Wang *et al.*, “In situ preparation of SnO2 @polyaniline nanocomposites and their synergetic structure for high-performance supercapacitors †,” 2014, doi: 10.1039/c3ta15266a.

[77] S. Sonal and B. K. Mishra, “A comprehensive review on the synthesis and performance of different zirconium-based adsorbents for the removal of various water contaminants,” *Chemical Engineering Journal*, vol. 424, p. 130509, 2021, doi: 10.1016/j.cej.2021.130509.

[78] N. Hassanzadeh, H. Omidvar, and S. H. Tabaian, “Chemical synthesis of high density and long polypyrrole nanowire arrays using alumina membrane and their hydrogen

sensing properties," *Superlattices Microstruct*, vol. 51, no. 3, pp. 314–323, Mar. 2012, doi: 10.1016/j.spmi.2011.12.001.

[79] D. Chen, X. Guo, Z. Wang, P. Wang, Y. Chen, and L. Lin, "Polyaniline nanofiber gas sensors by direct-write electrospinning," in *Proceedings of the IEEE International Conference on Micro Electro Mechanical Systems (MEMS)*, 2011, pp. 1369–1372. doi: 10.1109/MEMSYS.2011.5734689.

[80] N. Bafandeh, M. M. Larijani, and A. Shafiekhani, "Investigation on hydrogen sensing property of MWCNT/Pani nanocomposite films," *Polymer Bulletin*, vol. 77, no. 7, pp. 3697–3706, Jul. 2020, doi: 10.1007/S00289-019-02915-8/FIGURES/8.

[81] N. Goel, J. Bera, R. Kumar, S. Sahu, and M. Kumar, "MoS2-PVP Nanocomposites Decorated ZnO Microsheets for Efficient Hydrogen Detection," *IEEE Sens J*, vol. 21, no. 7, pp. 8878–8885, Apr. 2021, doi: 10.1109/JSEN.2021.3054038.

[82] D. Punetha, M. Kar, and S. K. Pandey, "A new type low-cost, flexible and wearable tertiary nanocomposite sensor for room temperature hydrogen gas sensing," *Scientific Reports 2020 10:1*, vol. 10, no. 1, pp. 1–11, Feb. 2020, doi: 10.1038/s41598-020-58965-w.

[83] I. O.¨ Stergren *et al.*, "Highly Permeable Fluorinated Polymer Nanocomposites for Plasmonic Hydrogen Sensing," *ACS Appl. Mater. Interfaces*, vol. 13, 2021, doi: 10.1021/acsami.1c01968.

[84] Y. Zou *et al.*, "Pd-doped TiO2@polypyrrole core-shell composites as hydrogen-sensing materials," *Ceram Int*, vol. 42, no. 7, pp. 8257–8262, May 2016, doi: 10.1016/J.CERAMINT.2016.02.038.

[85] S. Nasirian and H. Milani Moghaddam, "Hydrogen gas sensing based on polyaniline/anatase titania nanocomposite," *Int J Hydrogen Energy*, vol. 39, no. 1, pp. 630–642, Jan. 2014, doi: 10.1016/j.ijhydene.2013.09.152.

[86] H. Milani Moghaddam and S. Nasirian, "Hydrogen gas sensing feature of polyaniline/titania (rutile) nanocomposite at environmental conditions," *Appl Surf Sci*, vol. 317, pp. 117–124, Oct. 2014, doi: 10.1016/J.APSUSC.2014.08.062.

[87] L. Al-Mashat *et al.*, “Graphene/polyaniline nanocomposite for hydrogen sensing,” *Journal of Physical Chemistry C*, vol. 114, no. 39, pp. 16168–16173, Oct. 2010, doi: 10.1021/JP103134U/ASSET/IMAGES/LARGE/JP-2010-03134U_0002.JPEG.

[88] Kondawar S.B., More A.M., Sharma H.J., and Dongre S.P., “Ag-SnO2/Polyaniline composite nanofibers for low operating temperature hydrogen gas sensor,” Journal of Materials NanoScience. Accessed: Jan. 09, 2023. [Online]. Available: https://pubs.thesciencein.org/journal/index.php/jmns/article/view/201/175

[89] Y. Zou *et al.*, “Doping composite of polyaniline and reduced graphene oxide with palladium nanoparticles for room-temperature hydrogen-gas sensing,” *Int J Hydrogen Energy*, vol. 41, no. 11, pp. 5396–5404, Mar. 2016, doi: 10.1016/J.IJHYDENE.2016.02.023.

[90] J. García-Aguilar, I. Miguel-García, Á. Berenguer-Murcia, and D. Cazorla-Amorós, “Single wall carbon nanotubes loaded with Pd and NiPd nanoparticles for H2 sensing at room temperature,” *Carbon N Y*, vol. 66, pp. 599–611, Jan. 2014, doi: 10.1016/J.CARBON.2013.09.047.

[91] S. Dhall, K. Sood, and R. Nathawat, “Room temperature hydrogen gas sensors of functionalized carbon nanotubes based hybrid nanostructure: Role of Pt sputtered nanoparticles,” *Int J Hydrogen Energy*, vol. 42, no. 12, pp. 8392–8398, Mar. 2017, doi: 10.1016/J.IJHYDENE.2017.02.005.

[92] K. S. Choi and S. P. Chang, “Effect of structure morphologies on hydrogen gas sensing by ZnO nanotubes,” *Mater Lett*, vol. 230, pp. 48–52, Nov. 2018, doi: 10.1016/J.MATLET.2018.07.031.

[93] A. Z. Sadek *et al.*, “Nanoporous TiO2 thin film based conductometric H2 sensor,” *Thin Solid Films*, vol. 518, no. 4, pp. 1294–1298, Dec. 2009, doi: 10.1016/J.TSF.2009.02.151.

[94] B. Mondal, B. Basumatari, J. Das, C. Roychaudhury, H. Saha, and N. Mukherjee, “ZnO–SnO2 based composite type gas sensor for selective hydrogen sensing,” *Sens Actuators B Chem*, vol. 194, pp. 389–396, Apr. 2014, doi: 10.1016/J.SNB.2013.12.093.

[95] B. Esser, J. M. Schnorr, and T. M. Swager, “Selective detection of ethylene gas using carbon nanotube-based devices: Utility in determination of fruit ripeness,” *Angewandte Chemie - International Edition*, vol. 51, no. 23, pp. 5752–5756, Jun. 2012, doi: 10.1002/anie.201201042.

[96] A. Manzoli *et al.*, “Low-cost gas sensors produced by the graphite line-patterning technique applied to monitoring banana ripeness,” *Sensors*, vol. 11, no. 6, pp. 6425–6434, Jun. 2011, doi: 10.3390/s110606425.

[97] M. Krivec *et al.*, “Quantitative ethylene measurements with MOx chemiresistive sensors at different relative air humidities,” *Sensors (Switzerland)*, vol. 15, no. 11, pp. 28088–28098, Nov. 2015, doi: 10.3390/s151128088.

[98] O. Green, N. A. Smith, A. B. Ellis, and J. N. Burstyn, “AgBF4-Impregnated Poly(vinyl phenyl ketone): An Ethylene Sensing Film,” *J Am Chem Soc*, vol. 126, no. 19, pp. 5952–5953, May 2004, doi: 10.1021/ja039203o.

[99] M. A. G. Zevenbergen, D. Wouters, V.-A. T. Dam, S. H. Brongersma, and M. Crego-Calama, “Electrochemical Sensing of Ethylene Employing a Thin Ionic-Liquid Layer,” *Anal. Chem*, vol. 83, pp. 6300–6307, 2011, doi: 10.1021/ac2009756.

[100] L.-P. Wang *et al.*, “The detection of ethylene using porous ZnO nanosheets: utility in the determination of fruit ripeness,” *New J. Chem*, vol. 43, p. 3619, 2019, doi: 10.1039/c9nj00031c.

[101] A. A. Alharbi, A. Sackmann, U. Weimar, and N. Bârsan, “A highly selective sensor to acetylene and ethylene based on LaFeO3,” *Sens Actuators B Chem*, vol. 303, p. 127204, Jan. 2020, doi: 10.1016/J.SNB.2019.127204.

[102] A. A. Alharbi, A. Sackmann, U. Weimar, and N. Bârsan, “Acetylene- And Ethylene-Sensing Mechanism for LaFeO3-Based Gas Sensors: Operando Insights,” *Journal of Physical Chemistry C*, vol. 124, no. 13, pp. 7317–7326, Apr. 2020, doi: 10.1021/ACS.JPCC.0C01052/ASSET/IMAGES/LARGE/JP0C01052_0005.JPEG.

[103] D. Fong, S. X. Luo, R. S. Andre, and T. M. Swager, “Trace Ethylene Sensing via Wacker Oxidation,” *ACS Cent Sci*, vol. 6, no. 4, pp. 507–512, Apr. 2020, doi: 10.1021/ACSCENTSCI.0C00022.

[104] M. Agarwal, M. D. Balachandran, S. Shrestha, and K. Varahramyan, “SnO2 nanoparticle-based passive capacitive sensor for ethylene detection,” *J Nanomater*, vol. 2012, 2012, doi: 10.1155/2012/145406.

[105] R. Zhang, M. I. Tejedor, M. A. Anderson, M. Paulose, and C. A. Grimes, “Ethylene Detection Using Nanoporous PtTiO2 Coatings Applied to Magnetoelastic Thick Films,” *Sensors 2002, Vol. 2, Pages 331-338*, vol. 2, no. 8, pp. 331–338, Aug. 2002, doi: 10.3390/S20800331.

[106] S. F. Hashemi Karouei and H. Milani Moghaddam, “P-p heterojunction of polymer/hierarchical mesoporous LaFeO3 microsphere as CO2 gas sensing under high humidity,” *Appl Surf Sci*, vol. 479, pp. 1029–1038, Jun. 2019, doi: 10.1016/J.APSUSC.2019.02.099.

[107] W. C. Oh, K. N. Fatema, Y. Liu, K. Y. Cho, C. H. Jung, and M. R. U. D. Biswas, “Novel designed quaternary CuZnSnSe semiconductor combined graphene-polymer (CuZnSnSe-G-PPy) composites for highly selective gas-sensing properties,” *Journal of Materials Science: Materials in Electronics*, vol. 32, no. 10, pp. 12812–12821, May 2021, doi: 10.1007/S10854-020-03651-W/FIGURES/11.

[108] W. C. Oh, Y. Liu, S. Sagadevan, K. N. Fatema, and M. R. U. D. Biswas, “Polymer bonded Graphene- LaNiSbWO4 nanocomposite (G-LaNiSbWO4-PPy) for CO2 sensing performance under normal temperature condition,” *Inorganic and Nano-Metal Chemistry*, vol. 51, no. 12, pp. 1803–1812, 2021, doi: 10.1080/24701556.2020.1855197/SUPPL_FILE/LSRT_A_1855197_SM7677.DOCX.

[109] U. Kumar, B. C. Yadav, T. Haldar, C. K. Dixit, and P. K. Yadawa, “Synthesis of MWCNT/PPY nanocomposite using oxidation polymerization method and its employment in sensing such as CO2 and humidity,” *J Taiwan Inst Chem Eng*, vol. 113, pp. 419–427, Aug. 2020, doi: 10.1016/J.JTICE.2020.08.026.

[110] S. Riyazi and M. E. Azim Araghi, “Performance of interdigitated capacitive-type CO2 sensor based on polypyrrole/copper phthalocyanine nanocomposite,” *Journal of Materials Science: Materials in Electronics*, vol. 31, no. 4, pp. 3539–3548, Feb. 2020, doi: 10.1007/S10854-020-02902-0/FIGURES/10.

[111] B. M. Mude, K. M. Mude, K. B. Raulkar, R. N. Zade, S. M. Yenorkar, and S. P. Yawale, “Study of CO2 gas detection by multilayer SnO2-ZnO-PPy sensor,” *Applied Nanotechnology and Nanoscience*, 2017, Accessed: Sep. 02, 2023. [Online]. Available: http://www.irjse.in

[112] S. Nasresfahani, Z. Zargarpour, M. H. Sheikhi, and S. F. Nami Ana, “Improvement of the carbon monoxide gas sensing properties of polyaniline in the presence of gold nanoparticles at room temperature,” *Synth Met*, vol. 265, p. 116404, Jul. 2020, doi: 10.1016/J.SYNTHMET.2020.116404.

[113] N. Roy, R. Sinha, T. T. Daniel, H. B. Nemade, and T. K. Mandal, “Highly Sensitive Room Temperature CO Gas Sensor Based on MWCNT-PDDA Composite,” *IEEE Sens J*, vol. 20, no. 22, pp. 13245–13252, Nov. 2020, doi: 10.1109/JSEN.2020.3004994.

[114] Z. Wang, X. Peng, C. Huang, X. Chen, W. Dai, and X. Fu, “CO gas sensitivity and its oxidation over TiO2 modified by PANI under UV irradiation at room temperature,” *Appl Catal B*, vol. 219, pp. 379–390, Dec. 2017, doi: 10.1016/J.APCATB.2017.07.080.

[115] S. Kumar Tripathy and B. P. Hota, “Carbon Monoxide Sensitivity of Tin Oxide Thin Film Synthesized by Sol Gel Method,” *The African Review of Physics*, vol. 7, 2012.

Appendices

Appendix A to Appendix C include summary tables outlining various sensing materials (both polymeric and inorganic) used for detection of different gas analytes (H_2, C_2H_4, CO_2, and CO). These tables provide a summary of information found in the literature for sensing materials. Some papers lack information on certain categories, which are indicated by a (-). Additionally, approximated values from graphs (e.g., values for response and recovery times and sensing response) are indicated by a tilde (~) prefix. In the tables below, RT stands for room temperature. Also, R_a is the resistance in air, while R_g is the resistance in the presence of gas analyte.

Appendix A: Sensing Materials for Detection of Hydrogen

Table A.1: Sensing materials for hydrogen

Sensing Materials and dopants (if applicable)	**Concentration Range/Limit of Detection (LOD)**	**Operating Temperature**	**Response/ Sensitivity**	**Response Time**	**Recovery Time**	**Remarks**	**Ref.**
PPy nanowire arrays	12000 ppm	RT	1.01 (S=Rg/Ra) S (%) = $[(R_0 – R_i)]/R_0$ *100	692 sec	1396 sec		[78]
PANI/ Pd (0.4 wt.%)	100000 ppm (0.3% H_2)	RT	1.17 (S=Rg/Ra)	90 sec	140 sec	Dry air, comparison between film and fiber, high repeatability	[79]

PANI/ SnO_2+Pd	50 ppm 350 ppm	RT	19.2% 353.7%	39 sec 141 sec	53 sec 76 sec	Hydrothermal synthesis technique, highest performance factor	[10]
PANI/ PdO+ITO (Indium Tin Oxide)	10,000 ppm (1% of H_2)	RT (28 ℃)	1.75	3 sec	4 sec	Highly sensitive towards H_2 gas	[9]
PANI/ Sm_2O_3 (Samarium Oxide)	10,000 ppm	RT	394%	3 sec	7 sec	Good repeatability	[53]
PANI/ MWCNTs	4000 ppm	0 ℃	24%	48 sec	55 sec		[80]
PANI/ SnO_2	6000 ppm	30 ℃	42%	11 sec	7 sec		[11]
PVP/ MoS_2 (Molybdenum disulphide) + ZnO	50 ppm	150 ℃	46%	-	-		[81]
PVDP/ SnO_2+rGO	100 ppm	RT	49.2%	34 sec	142 sec	First time ever	[82]
Teflon AF/ Pd	-	RT	-	2.5 sec	-		[83]
PPy/ Pd+TiO_2	10,000 ppm	25 ℃	8.1%	220 sec	100 sec		[84]
PANI (emeraldine)/ Anatase TiO_2	0.8%	RT	1.63	83 sec	130 sec	Good long-term response	[85]
PANI/ Rutile TiO_2	0.8%	27 ℃	1.54	152 sec	170 sec		[86]
PANI/ TiO_2:SnO_2	0.8%	27 ℃	1.25	75 sec	117 sec		[13]
PANI/ Graphene	1% H_2	24 ℃	16.57%	-	-		[87]
PANI/ Ag-SnO_2	500 ppm	42 ℃	1.9	16 sec	24 sec		[88]
PANI/ Pd-rGO	1%	25 ℃	1.25	20 sec	50 sec		[89]
PANI/ SnO_2	1000 ppm	50 ℃	1.5	3 sec	4 sec		[12]
Ni+Pd+SWCNTs		25 ℃	10%	720 sec	60 sec		[90]
MWCNTs+TiO_2+Pd	500 ppm	RT	3.9%	-	-		[91]
ZnO thin film	0.5%	100 ℃	1.48	150 sec	170 sec		[92]
TiO_2 thin film	1%	225 ℃	1.24	250 sec	300 sec		[93]
ZnO-SnO_2 composite	10,000 ppm	150 ℃	1.9	60 sec	75 sec		[94]

Appendix B: Sensing Materials for Detection of Ethylene

Table B.1: Sensing materials for ethylene

Sensing Materials and dopants (if applicable)	Detection Limit	Operating Temperature	Response/ Sensitivity	Response Time	Recovery Time	Sensor Type	Remarks	Ref.
ZnO-Ag layer on a flexible PET-ITO substrate	30, 50, 70, 100 ppm	RT	5.65% (30 ppm) 16.01% (100 ppm)	5 min	10 min (30 ppm) 15 min (100 ppm)	Chemoresistive	PET-ITO serves as a substrate for a more flexible and lighter sensor.	[20]
Polyvinylpyrrolidone (PVP) / $AgBF_4$ (1:4 silver-to-monomer ratio)	420 ppb	30 ℃	51 Hz/ppm	10 min	~ 13 min	QCM	Does not clearly define selectivity. They studied selectivity of ethylene over hexane, ethyl acetate, ethanol, and diethyl ether.	[17]
Single-walled carbon nanotube (SWCNTs) with a copper(I) complex	50 ppm	RT	~1.8% ($\Delta G/G_0$)	~1 min	~1.5 min	Chemoresistive		[95]
PANI/ MWCNT/ SnO_2	10 ppm	RT	2.42% (change in resistance)	-	-	IDE (Interdigitated electrodes)		[19]
PANI/ four different acids		RT				interdigitated graphite electrodes on tracing paper	Non-specific sensor, an overall response profile to spices present in VOCs	[96]

							including ethylene, Global selectivity	
WO_3 (commercial sensor- MiCS-5914)		Does not mention exact temperature but the sensor was equipped with integrated heater		29 sec (Referred to as saturation time)	43 sec (Referred to as desaturation time)	Metal oxide sensor		[97]
SnO_2 (commercial sensor MQ-3)		Does not mention exact temperature but the sensor was equipped with integrated heater		80 sec	165 sec	Metal oxide sensor		[97]
Poly (vinyl phenyl ketone)/ $AgBF_4$						photoluminescence		[98]
BMIM-NTf2 (Ionic Liquid Layer)	760 ppb–10 ppm	22 °C	51 pA/ppm			Amperometric		[99]
Porous ZnO NS (NS= nanosheets)	5-2000 ppm	350–500 °C	0.6 μA/ppm	8 sec	20 sec	Chemiresistive		[100]
$LaFeO_3$ (La= Lanthanum)	25–5000 ppm	20–200 °C	0.4 Ω/ppm		~1 sec	Chemiresistive		[101] [102]
SWCNTs	0.5–50 ppm	3 °C	1.2% (R/ppm)			Chemiresistive		[103]
SnO_2 nanoparticles	20–100 ppm	22 °C	0.0531 (pF/ppm)		~10 sec	Chemicapacitive		[104]
$PtTiO_2$ (platinum titanium-oxide)	0.5–50 ppm	19 °C	8.5 (Hz/ppm)			Magnetoelastic		[105]

Appendix C: Sensing Materials for Detection of Carbon Oxides (CO_2 and CO)

Table C.1: Sensing materials for carbon dioxide (CO_2)

Sensing Materials and dopants (if applicable)	**Detection Limit**	**Operating Temperature**	**Response/ Sensitivity**	**Response Time (s)**	**Recovery Time (s)**	**Remarks**	**Ref.**
PANI-SnO_2 (under UV)	5000 ppm	RT	47.4%	35.1	43.2	Good reproducibility, dependability and selectivity response in multi-cycle towards various CO_2 levels	[32]
PANI-TiO_2 (1% of PANI)	1000 ppm	RT	53%	552	342		[33]
PANI-NaO_2	4000 ppm	RT	60%	900	600		[35]
PANI-$LaFeO_3$	5000 ppm	RT	12.13%	197.82	42.17		[106]
PANI-TiO_2	1000 ppm	48 °C	-	80	100		[34]
CuZnSnSe-G-PPy	1000 ppm	RT	65%	7–15	6–35	Facile and low-cost route	[107]
$LaNiSbWO_4$-G-PPy	1800 ppm	RT	120%	<1	<1	Good repeatability, reproducibility and measurement accuracy	[108]
PPy-MWCNTs	1000 ppm 720 ppm	RT		30	37	Higher accuracy	[109]
PPy-CuPc (copper phthalocyanine)	5000 ppm	RT (27 °C)	175%	34	175	Low-cost, reliable and sensitive towards CO2 gas	[110]
SnO_2-ZnO-PPy	80 ppm	RT	85%	59	101		[111]

Table C.2: Sensing materials for carbon monoxide (CO)

Sensing Materials and dopants (if applicable)	**Detection Limit**	**Operating Temperature**	**Response/ Sensitivity**	**Response Time**	**Recovery Time**	**Remarks**	**Ref.**
PANI/Co_3O_4	75 ppm	RT	81% (Change in current)	40 s 45 s (for 50 ppm)	140 s 90 s (for 50 ppm)	Effect of RH was studied. High selectivity	[29]
PANI/ Au NPs	200-6000 ppm	RT	27% (6000 ppm) 14% (1000 ppm)	180 s	200 s	Low detection limit and good selectivity	[112]
PANI/SnO_2/Pd	50-300 ppm	RT	30–401%	11–88 s	45–62 s		[30]
PANI/SnO_2 (45% PANI/55% SnO_2)	25-200 ppm	30 °C	65% 53% (for 25 ppm)	-	-		[31]
PDDA/MWCNTs Poly (diallyldi-methylammonium chloride)	20 ppm	RT	11.5%	18 s	33 s	Stable for 2 months with excellent reproducibility	[113]
PANI/TiO_2 (under UV) 4 wt% ratio of PANI to TiO_2 (PANI is used as a dopant)	-	RT	40.73%	-	-	The sensing material was mainly composed of TiO_2 and only a small amount of PANI.	[114]
SnO_2	50 ppm	220 °C	~60%	20 s	100 s		[115]

Appendix D: Sensing Materials Tested in Gas Sorption Experiments (GC)

Appendix D provides a summary of polymeric materials tested for their sorption performance towards formaldehyde (see Table D.1). Sorption experiments were performed using a gas chromatograph incorporated in a specialized test system, as explained in section 3.2. Note that sorption measurements were independently replicated at least once for all the materials listed in Table D.1. The sequence of tests performed with the corresponding sample number and name are given in Table D.2. Appendix D also shows the chemical structures of tested materials (see Figure D.1).

Table D.1: List of sensing materials tested for formaldehyde (F) sorption.

Sample No.	Sensing material	Source	Purpose of test
Pristine polymers (no dopants)			
1	Polyaniline (PANI)	F (11.1 ppm)	Sensitivity of F
2	Polypyrrole (PPy)	F (11.1 ppm)	Sensitivity of F
3	polythiophene (PTh)	F (11.1 ppm)	Sensitivity of F
4	polyvinylpyrrolidone (PVP)	F (11.1 ppm)	Sensitivity of F
Doped polymers with metal oxide(s) content ≥ 5%			
5	PANI with 5% TiO_2	F (11.1 ppm)	Sensitivity of F
6	PANI with 5% SnO_2	F (11.1 ppm)	Sensitivity of F
7	PANI with 5% ZnO	F (11.1 ppm)	Sensitivity of F
8	PANI with 5% Co_3O_4	F (11.1 ppm)	Sensitivity of F
9	PANI with (5% TiO_2 + 2.5% SnO_2)	F (11.1 ppm)	Sensitivity of F
10	PANI with (2.5% TiO_2 + 5% SnO_2)	F (11.1 ppm)	Sensitivity of F
11	PANI with 10% SnO_2	F (11.1 ppm)	Sensitivity of F
Doped polymers with metal oxide content ≤ 5%			
12	PANI with 2.5% TiO_2	F (11.1 ppm)	Sensitivity of F
13	PANI with 2.5% SnO_2	F (11.1 ppm)	Sensitivity of F
14	PANI with 2.5% ZnO	F (11.1 ppm)	Sensitivity of F
15	PANI with 2% Co_3O_4	F (11.1 ppm)	Sensitivity of F
16	PANI with 1% Co_3O_4	F (11.1 ppm)	Sensitivity of F

Table D.2: Sample names and their testing sequence for sorption towards formaldehyde.

Sample No.	Sensing material	Source	Purpose of test
Week of May 29, 2023 (June 1)			
1	PANI with 5% SnO_2	F (11.1 ppm)	New sample, Sensitivity of F
2	PANI with 5% TiO_2	F (11.1 ppm)	New sample, Sensitivity of F
3	PANI	F (11.1 ppm)	New sample, Sensitivity of F
4	PANI with 5% SnO_2	F (11.1 ppm)	Replicate for sample#1
Week of September 25, 2023			
5	PANI with (5% TiO_2 + 2.5% SnO_2)	F (11.1 ppm)	New sample, Sensitivity of F
6	PANI with (2.5% TiO_2 + 5% SnO_2)	F (11.1 ppm)	New sample, Sensitivity of F
7	PANI with 5% TiO_2	F (11.1 ppm)	Replicate for sample#2
8	PPy (Sigma)	F (11.1 ppm)	New sample, Sensitivity of F
9	PANI pristine	F (11.1 ppm)	Replicate for sample#3
10	PANI with (2.5% TiO_2 + 5% SnO_2)	F (11.1 ppm)	Replicate for sample#6
11	PANI with (5% TiO_2 + 2.5% SnO_2)	F (11.1 ppm)	Replicate for sample#5
Week of November 6, 2023			
12	PANI with 2.5% ZnO	F (11.1 ppm)	New sample, Sensitivity of F
13	PANI with 5% ZnO	F (11.1 ppm)	New sample, Sensitivity of F
14	PANI with 2% Co_3O_4	F (11.1 ppm)	New sample, Sensitivity of F
15	PANI with 1% Co_3O_4	F (11.1 ppm)	New sample, Sensitivity of F
16	PANI with 2.5% SnO_2	F (11.1 ppm)	New sample, Sensitivity of F
17	PANI with 2.5% TiO_2	F (11.1 ppm)	New sample, Sensitivity of F
18	PVP (Sigma) – film form	F (11.1 ppm)	New sample, Sensitivity of F
19	PTh (Sigma)	F (11.1 ppm)	New sample, Sensitivity of F
20	PANI with 1% Co_3O_4	F (11.1 ppm)	Replicate for sample#15
21	PANI with 2.5% TiO_2	F (11.1 ppm)	Replicate for sample#17
22	PVP (Sigma) – film form	F (11.1 ppm)	Replicate for sample#18
23	PANI with 5% ZnO	F (11.1 ppm)	Replicate for sample#13
24	PTh (Sigma)	F (11.1 ppm)	Replicate for sample#19

25	PANI with 2% Co_3O_4	F (11.1 ppm)	Replicate for sample#14
26	PAN with 2.5% SnO_2	F (11.1 ppm)	Replicate for sample#16
27	PANI with 2.5% ZnO	F (11.1 ppm)	Replicate for sample#12
Week of January 8, 2024			
28	PANI with 5% Co_3O_4	F (11.1 ppm)	New sample, Sensitivity of F
29	PAN with 10% SnO_2	F (11.1 ppm)	New sample, Sensitivity of F
30	PVP (in powder form)	F (11.1 ppm)	New sample, Sensitivity of F
31	PANI with 2.5% ZnO	F (11.1 ppm)	Replicate for sample#12
32	PPy (Sigma)	F (11.1 ppm)	Replicate for sample#8
33	PAN with 2.5% SnO_2	F (11.1 ppm)	Replicate for sample#16
34	PAN with 10% SnO_2	F (11.1 ppm)	Replicate for sample#29
35	PANI with 5% Co_3O_4	F (11.1 ppm)	Replicate for sample#28

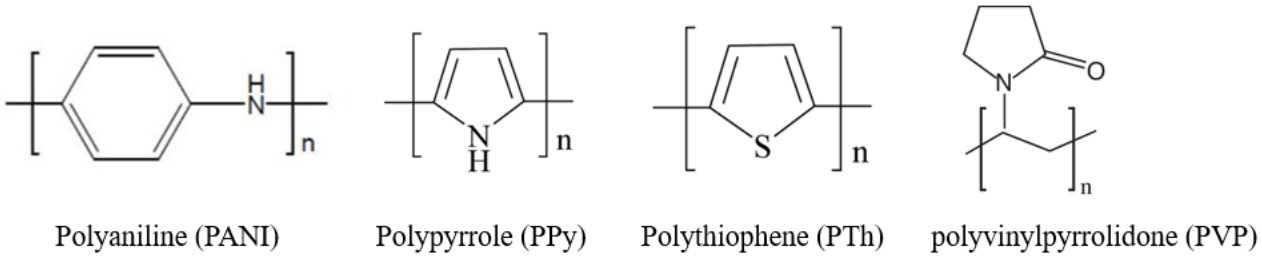

Figure D.1: Chemical structure of different polymers tested in formaldehyde sorption studies (as per Table D.1).

Appendix E: Statistical Analysis

Appendix E contains sample calculations and relevant equations for performing different statistical tests used for data analysis presented in Chapter 4. This appendix has been divided in three subsections (E1, E2, and E3).

E1. Standard Error and Confidence Interval Calculations

Standard error (SE or se) and confidence interval (CI) values for the sorption data presented in this thesis were calculated as per below:

For example, sample calculations for SE and CI values for sorption data of pristine PANI (see Chapter 4, Table 4.1) are shown below:

Table E1.1: Raw data points for PANI sorption

Sorption of PANI (ppm of F)	$x_1 = 1.74$	$x_2 = 1.73$	$x_3 = 1.34$	$x_4 = 1.39$
Total # of observations	$n = 4$			

Average = $\overline{X} = \frac{\sum_{i=1}^{n} x_i}{n}$ = 1.55

Variance (X) = $S^2 = \frac{\sum_{i=1}^{n}(x_i - \overline{X})^2}{n-1}$ = 0.0461

Standard error (SE) = $\sqrt{S^2}$ = 0.2146

Therefore, $Average\ sorption \pm SE = 1.55 \pm 0.215\ ppm\ of\ F$

Given the 4 data points and using the above values for $\overline{X}$ and SE, the 95% confidence interval on average sorption can be constructed using Student's t-distribution (known as 'CONFIDENCE.T' function in Excel):

Confidence interval = $\overline{X} \pm \left(t_{\alpha/2,df}\right)\left(\frac{SE}{\sqrt{n}}\right)$

Where: $\alpha = 0.05$, $df = n - 1 = 4 - 1 = 3$

$t_{\alpha/2,df} = t_{0.025,3} = 3.182$

Therefore, $Average\ sorption \pm 95\%\ CI = 1.55 \pm 0.342\ ppm\ of\ F$

E2. Sample Calculations for Analysis of Variance (ANOVA)

This section shows sample calculations for constructing ANOVA tables based on a typical data set discussed earlier in section 4.4.1. Note that all the ANOVA tables throughout the thesis were constructed using the same procedure described below.

Table E2.1: Raw data points for PANI with 5% SnO2 and its replicate, as presented in Figure 4.9 and Table 4.6.

	Time (min)	12	24	36	48	60	72	84	**Total**
Treatment 1	**Raw data (ppm of F) for PANI with 5% SnO_2 (x_i)**	11.09	9.25	8.94	8.90	8.93	8.99	8.95	**n = 7**
Treatment 2	**Raw data (ppm of F) for PANI with 5% SnO_2 replicate (y_i)**	8.36	9.39	8.92	8.94	8.94			**m = 5**

$$Correction\ for\ the\ mean = \frac{(\sum_{i=1}^{n} x_i + \sum_{i=1}^{m} y_i)^2}{n+m} = \frac{(65.05 + 44.55)^2}{7+5} = 1001.013$$

$Sum\ of\ Squares\ between\ treatments\ (SS_B)$:

$$SS_B = \left(\frac{(\sum_{i=1}^{n} x_i)^2}{n} + \frac{(\sum_{i=1}^{m} y_i)^2}{m}\right) - correction\ for\ the\ mean$$

$$SS_B = \left(\frac{(65.05)^2}{7} + \frac{(44.55)^2}{5}\right) - 1001.013 = 0.42752$$

$Sum\ of\ Squares\ Total\ (SS_T)$:

$$SS_T = \left(\sum_{i=1}^{n} x_i^2 + \sum_{i=1}^{m} y_i^2\right) - correction\ for\ the\ mean$$

$$SS_T = (608.3517 + 397.4753) - 1001.013 = 4.81366$$

$Sum\ of\ Squares\ within\ treatments\ (SS_W)$:

$SS_W = SS_T - SS_B = 4.81366 - 0.4275 = 4.38614$

$Degrees\ of\ freedom\ between\ treatments\ (df_B)$:

$df_B = (Total\ number\ of\ treatments) - 1 = 2 - 1 = 1$

$Degrees\ of\ freedom\ Total\ (df_T)$:

$df_T = (Total\ number\ of\ observations) - 1 = 12 - 1 = 11$

$Degrees\ of\ freedom\ within\ treatments\ (df_W)$:

$df_W = df_T - df_B = 11 - 1 = 10$

$$Mean\ Square\ between\ treatments\ (MS_B) = \frac{SS_B}{df_B} = \frac{0.42752}{1} = 0.42752$$

$$Mean\ Square\ within\ treatments\ (MS_W) = \frac{SS_W}{df_W} = \frac{4.3861}{10} = 0.438614$$

$$F_{observed} = \frac{MS_B}{MS_W} = \frac{0.4275}{0.43861} = 0.9747$$

$$F_{critical\ (tabulated)} = F_{df_B,\, df_W, \alpha} = F_{1,10,0.05} = 4.96$$

Table E2.2: ANOVA table for data sets in Table E2.1.

Source of variation	**SS (Sum of Squares)**	**df (degrees of freedom)**	**MS (Mean Square)**	**Comparison of F values**
Between treatments	0.42752	2-1=1	0.42752	$F_{obs.} = 0.97471474$
Within treatments	4.38614	11-1=10	0.438614	$F_{1,10,0.05} = 4.96$
Total	4.81366	12-1=11		$F_{obs.} < F_{1,10,0.05}$

E3. Fisher's Least Significant Difference (LSD)

This section contains the equations used for performing the LSD analysis, followed by the results of some representative LSD-related calculations performed.

$$c = \frac{k(k-1)}{2}\ , where\ k\ is\ the\ number\ of\ treatments\ (polymers) being\ compared$$

$$\alpha = \frac{0.05}{c}$$

$$s.e. = \sqrt{\frac{2\ MS_w}{n}}$$

Where MS_w is the mean square value for 'within' polymers (i.e., error within treatment) from the ANOVA table, and n is the average value for the number of readings.

$$LSD = (s.e.)(t_{\alpha/2,df_w})$$

Where $t_{\alpha/2,df_w}$ is the t-value from corresponding tables using the degrees of freedom for 'within' polymers from the ANOVA table (df_w, i.e., degrees of freedom for error).

Data analysis for PANI doped with 5% of different metal oxides (Section 4.1.7)

Analysis results for this comparison are presented in the following tables:

Table E3.1: ANOVA comparing formaldehyde sorption on PANI with 5% dopant content.

Source of Variation	**SS**	**df**	**MS**	**$F_{obs.}$**	**$F_{crit.}$ ($F_{3,12,0.05}$)**
Between Polymers	1.8503	4-1= 3	0.6168	40.5605	3.4903
Within Polymers	0.1825	15-3= 12	0.0152		
Total	2.0328	16-1= 15		**$F_{obs.} > F_{crit.}$**	

Table E3.2: Summary of polymer designations, their averages, and standard errors.

	Polymer	# of Readings	Average (ppm)	Standard Deviation
A	PANI 5% TiO_2	4	1.415	0.1330
B	PANI 5% SnO_2	4	2.135	0.0238
C	PANI 5% ZnO	4	1.6875	0.2052
D	PANI 5% Co_3O_4	4	2.26	0.0216

Table E3.3: Multiple comparisons using Fisher's LSD related to Table E3.2.

Mean Comparison	Steps towards LSD Calculation	
A-B= 0.72	[k(k-1)]/2	6
A-C= 0.2725	α	0.0083 (~0.01)
A-D= 0.845	α/2	~0.005
B-C= 0.4475	s.e.	0.0872
B-D= 0.125	t (α/2, df_w)	3.054
C-D= 0.5725	**LSD**	**0.2663**

Note: Highlighted rows indicate polymers that have means significantly different from one another, i.e. differences greater than the LSD value.

Data analysis for PANI doped with 2.5% (or less) of different metal oxides (Section 4.1.8)

Analysis results for this comparison are presented in the following tables:

Table E3.4: ANOVA comparing formaldehyde sorption on PANI with 2.5% dopant content.

Source of Variation	SS	df	MS	$F_{obs.}$	$F_{crit.}$ ($F_{3,16,0.05}$)
Between Polymers	0.9377	4-1= 3	0.3126	6.5409	3.2389
Within Polymers	0.7646	19-3= 16	0.0478		
Total	1.7022	20-1= 19		$F_{obs.} > F_{crit.}$	

Table E3.5: Summary of polymer designations, their averages, and standard errors.

	Polymer	# of Readings	Average (ppm)	Standard Deviation
A	PANI 2.5% TiO_2	4	1.5575	0.1935
B	PANI 2.5% SnO_2	6	1.6683	0.2074
C	PANI 2.5% ZnO	6	2.09	0.2948
D	PANI 2% Co_3O_4	4	1.97	0.0294

Table E3.6: Multiple comparisons using Fisher's LSD related to Table E3.5.

Mean Comparison	Steps towards LSD Calculation	
A-B= 0.1108	[k(k-1)]/2	6
A-C= 0.5325	α	0.0083 (~0.01)
A-D= 0.4125	α/2	~0.005
B-C= 0.4217	s.e.	0.1382
B-D= 0.3017	t (α/2, df_w)	2.921
C-D= 0.12	**LSD**	**0.4038**

Note: Highlighted rows indicate polymers that have means significantly different from one another (larger differences than the LSD).